UKD Universitätsklinikum Düsseldorf

HEINRICH HEINE UNIVERSITÄT DÜSSELDORF

# Analysis of metabolic reprogramming during the enrichment of glioblastoma stem-like cells in glioblastoma via high resolution proton nuclear magnetic resonance (HR $^{1}$H-NMR) spectroscopy

Inaugural Dissertation

zur Erlangung des Doktorgrades der
Mathematisch-Naturwissenschaftlichen Fakultät der
Heinrich-Heine-Universität Düsseldorf

vorgelegt von
**Katharina Koch**
aus Leverkusen

Düsseldorf, Dezember 2017

Die vorliegende Arbeit wurde in der Zeit von Mai 2014 bis
November 2017 unter Leitung von Prof. Dr. Jaroslaw Maciaczyk
in der Klinik für Neurochirurgie des Universitätsklinikums Düsseldorf
angefertigt.

Gedruckt mit der Genehmigung der
Mathematisch-Naturwissenschaftlichen Fakultät der
Heinrich-Heine-Universität Düsseldorf

1. Berichterstatter: Prof. Dr. Jaroslaw Maciaczyk
2. Berichterstatter: Prof. Dr. Dieter Willbold

Tag der mündlichen Prüfung: 18.01.2018

## Eidesstattliche Erklärung

Ich versichere an Eides Statt, dass die Dissertation von mir selbständig und ohne unzulässige fremde Hilfe unter Beachtung der „Grundsätze zur Sicherung guter wissenschaftlicher Praxis an der Heinrich-Heine-Universität Düsseldorf“ erstellt worden ist.

Die Dissertation wurde in der vorgelegten oder in ähnlicher Form noch bei keiner anderen Institution eingereicht. Ich habe bisher keine erfolglosen Promotionsversuche unternommen.

Katharina Koch
Düsseldorf, den 06.12.2017

# Contents

# Summary

Glioblastoma is the most malignant primary brain tumor with limited therapeutic options because standard therapy fails to target the most aggressive subtype of glioblastomas, glioblastoma stem-like cells (GSCs). GSCs are enriched by epithelial-mesenchymal transition (EMT) and responsible for tumor initiation, chemoresistance, and tumor relapse. Substantial progress has been made toward understanding how GSCs drive tumor progression and therapy resistance, however, whether GSC enrichment is linked to metabolic reprogramming remains elusive. In this thesis, HR $^{1}$H NMR spectroscopy of *ex vivo* cellular extracts of glioblastoma cultures is used to investigate whether GSC enrichment is dependent on metabolic reprogramming and cause changes of the tumor's metabolic makeup.

In chapter 2.1 we study the effect of glioblastoma culture conditions on the GSC metabolism. The switch to neurosphere growth dramatically increased the CD133$^{pos}$ GSC population in culture. Furthermore, GSC enrichment modulated several intracellular metabolites including choline, creatine, glycine, and myo-inositol that have been previously identified as potential diagnostic markers in tumors. These findings highlight the critical influence of the culture condition on GSC enrichment and cellular metabolism.

Chapter 2.2 studies how EMT influences the metabolism of glioblastomas. We observed that the expression of EMT activators is directly linked to aberrant choline metabolism. EMT increased the expression of choline kinase alpha (CHK$\alpha$) resulting in elevated intracellular levels of phosphocholine and total choline derivatives, a metabolic phenotype associated with malignancy in cancer. Reciprocally, CHK$\alpha$ inhibition significantly reduced the invasiveness, clonogenicity, and expression of EMT associated genes in glioblastoma cells. Moreover, in some cell lines synergetic cytotoxic effects were observed when combining the standard of care chemotherapeutic temozolomide with the CHK$\alpha$ inhibitor V-11-0711. Therefore, CHK$\alpha$ is a powerful regulator of EMT in glioblastoma. This opens the possibility to target chemo-resistant GSCs through impairing their mesenchymal differentiation. Moreover, the newly identified EMT-oncometabolic network may be helpful to monitor the invasive properties of glioblastomas and surveil the success of anti-EMT therapy.

In chapter 2.3 we investigate in further detail the metabolic consequence of GSC enrichment especially focussing on glutamine metabolism. GSCs accumulated known oncometabolites, thereby contributing to a more aggressive metabolic phenotype. Furthermore, we could stratify our GSC models into two subtypes based on their relative amount of glutamine in relationship to glutamate (Gln/Glu). Gln/Glu$^{High}$ GSCs were resistant to glutamine deprivation whereas Gln/Glu$^{Low}$ GSCs responded with a significant decrease in their clonogenicity. Cellular growth was sustained in all subtypes even though the cells showed a complete lack of intracellular glutamine. Therefore, monitoring the Gln/Glu ratio of glioblastoma has utility in predicting resistance to Gln starvation. Strikingly, growth and clonogenicity of both GSC subtypes were effectively impaired when pharmacologically targeting glutaminase (GLS), making GLS inhibition a possible pan-GSC therapy.

# Zusammenfassung

Das Glioblastom ist der bösartigste primäre Hirntumor mit sehr eingeschränkten therapeutischen Optionen. Grund dafür sind hoch aggressive Glioblastom Stammzellen (GSZs), eine Subpopulation des Tumors, welche nicht durch die Standardtherapie eliminiert werden können. GSZs werden durch die epitheliale-mesenchymale Transformation (EMT) angereichert und sind verantwortlich für die Tumorinitiation, Chemoresistenz und die Bildung des Rezidivs. In diversen Studien wurde analysiert auf welchem Wege GSZs die Tumorprogression und Therapieresistenz beeinflussen, allerdings ist nicht bekannt, inwiefern die Anreicherung von GSZs durch metabolische Reprogrammierung gefördert wird. In dieser kumulativen Dissertation wurde mit Hilfe von hochauflösender Protonen Kernspinresonanzspektroskopie (HR $^{1}$H-NMR) in *ex vivo* Zellextrakten von Glioblastomkulturen untersucht, ob die Anreicherung von GSZs durch metabolische Reprogrammierung reguliert wird.

Kapitel 2.1 befasst sich mit dem Einfluss der Kulturbedingungen von Glioblastomzellen auf den Stoffwechsel und die GSZ Population. Wir konnten zeigen, dass die Umstellung auf das Neurosphärenwachstum zu einer signifikanten Erhöhung von CD133$^{pos}$ GSZs führt. Darüber hinaus wurde die Anreicherung von GSZs von der Regulation mehrerer intrazellulär Metaboliten einschließlich Cholin, Kreatin, Glycin und Myo-Inositol begleitet, welche bereits als potenzielle diagnostische Tumormarker identifiziert werden konnten. Diese Resultate unterstreichen den kritischen Einfluss der Kulturbedingungen auf die GSZ-Anreicherung und den Stoffwechsel von Glioblastomzellen.

Kapitel 2.2 untersucht, inwiefern EMT den Metabolismus von Glioblastomzellen beeinflusst. Die Expression von EMT-Aktivatoren korrelierte direkt mit aberrantem Cholinstoffwechsel. Wir beobachteten, dass EMT die Expression von Cholinkinase alpha (CHK$\alpha$) fördert, was zu einem erhöhten intrazellulären Spiegel an Phosphocholin und Gesamtcholinderivaten führte. Dieser metabolische Phänotyp konnte bereits mit Malignität in verschiedenen Krebserkrankungen korreliert werden. Reziprok führte die Inhibierung von CHK$\alpha$ zu einer signifikant verminderten Invasivität, Klonogenität und Expression von EMT assoziierten Genen. Des Weiteren wurden in einigen Zelllinien synergistische zytotoxische Effekte beobachtet, wenn Glioblastomzellen mit einer Kombination aus dem Standardchemotherapeutikum Temozolomid und dem CHK$\alpha$ Inhibitor V-11-0711 behandelt wurden. Demzufolge möchten wir CHK$\alpha$ als einen vielversprechenden Regulator von EMT im Glioblastom und als möglichen Angriffspunkt in neuen GSZ-spezifischen Therapien hervorheben. Darüber hinaus ist das neu identifizierte EMT-onkometabolische Netzwerk ein vielversprechender diagnostischer Marker um die invasiven Eigenschaften von Glioblastomen und den Erfolg der GSZ-spezifischen Therapie zu überwachen.

Kapitel 2.3 beschäftigt sich mit den metabolischen Veränderungen, welche durch eine GSZ-Anreicherung hervorgerufen werden, und legt besonderen Fokus auf den Glutaminstoffwechsel. GSZs akkumulierten diverse Onkometabolite und trugen dadurch zu einem aggressiveren metabolischen Phänotyp bei. Außerdem konnten wir unsere GSZ-Modelle,

basierend auf ihrer relativen Menge an Glutamin im Verhältnis zu Glutamat (Gln/Glu), in zwei verschiedene Subtypen unterteilen. Gln/Glu$^{Hoch}$ GSZs waren resistent gegenüber Glutaminentzug, wohingegen Gln/Glu$^{Niedrig}$ GSZs mit einer signifikanten Abnahme ihrer Klonogenität reagierten. Trotz Abwesenheit eines intrazellulären Glutaminreservoirs wurde das Zellwachstum in beiden Subtypen durch den Entzug von extrazellulärem Glutamin nicht beeinträchtigt. Die Überwachung des Gln/Glu-Verhältnisses im Glioblastom ist demzufolge hilfreich um eine Vorhersage über die Resistenz gegenüber Glutaminentzug treffen zu können. Sowohl das Wachstum als auch die Klonogenität beider GSZ-Subtypen konnten effizient durch pharmakologische Inhibierung von Glutaminase (GLS) reduziert werden, so dass wir GLS-Inhibierung als eine vielversprechende Pan-GSZ-Therapie hervorheben möchten.

# List of Figures

# 1 Introduction

## 1.1 Tumors of the central nervous system

Central nervous system (CNS) tumors are a highly heterogeneous group of diseases with prognosis and mortality rate drastically depending on the location, invasiveness, and structure of the tumor. Primary brain tumors are thought to derive from neuroglial stem or progenitor cells [1], whereas secondary brain tumors form when metastases from cancers outside the CNS spread to the brain. Brain metastases are 5-10 times more common than primary brain tumors [2]. During the development of brain metastases a cancer cell in the primary organ site undergoes mesenchymal transformation, intravasates into the blood stream, and is transported to the CNS where it can lay dormant for various lengths of time before invading the tissue and forming the secondary tumor [2]. The five most common primary tumors from which brain metastases develop are breast, colorectal, kidney, lung and melanoma [2]. This work will further focus on the pathophysiology of primary CNS tumors.

The median age of diagnosis for primary CNS tumors is 59.0 years [3]. However, incidence rates significantly rise with increasing patient age, ranging from 5.54 per 100.000 population in children (age 0-14) to 40.82 per 100.000 population in patients older than 40 [3].

Overall, the most common tumor site inside the CNS is in the meninges (36.8 %). However, only 1.5 % of malignant but 53.0 % of non-malignant tumors are diagnosed as meningiomas, making meningioma the most common non-malignant (53.0 %) and the overall most common (36.8 %) detected histology in the CNS Fig. 1.1 [3]. The second most detected primary CNS tumors are non-malignant tumors of the pituitary (16.2 %) followed by highly-malignant glioblastomas (14.9 %) Fig. 1.1A [3]. Strikingly, glioblastomas represent 47.1 % of all malignant primary tumors, making them the most common malignant histology in the CNS Fig. 1.1B.

Vast differences in survival rates have been reported for malignant and non-malignant CNS tumors. The median 5-year survival rate is 90.7 % for non-malignant and 34.9 % for malignant tumors, ranging from 99.4 % for nerve sheath tumors to 5.5 % for highly malignant glioblastomas [3]. In general, the survival rate significantly decreases with older age at diagnosis [3].

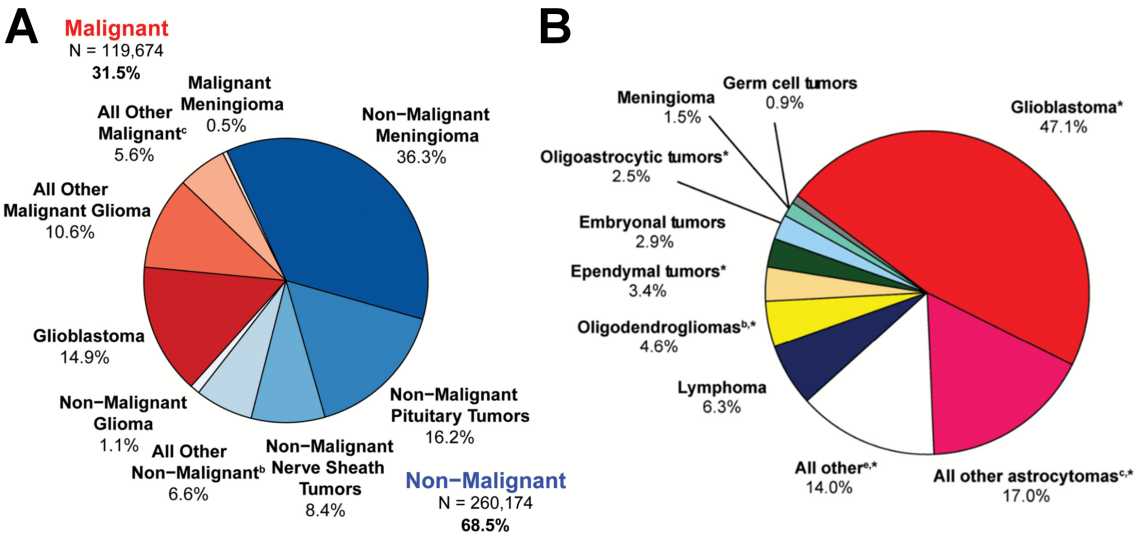


**Figure 1.1: Distribution of malignant and non-malignant tumors of the CNS A.** Distribution of primary CNS tumors by histology grouping and behaviour. **B.** Distribution of malignant primary CNS tumors by histology groupings. The data was aquired from tumors diagnosed in the United States between 2010 and 2014 and analyzed in the CBTRUS Statistical Report 2017 [3]. Modified from Ostrom et al., 2017 [3].

## 1.2 Gliomas

Gliomas represent 74.6 % of all malignant primary brain tumors in adults and the most common gliomas are glioblastomas (56.1 %) (Fig. 1.2) [3]. Although the cause of glioma is unknown, previous exposure to ionizing radiation such as therapeutic radiation (X-rays or CT scans) could be correlated with glioma diagnosis [4]. Furthermore, several epidemiological studies negatively correlated glioma diagnosis with allergy and atopic diseases such as eczema, psoriasis, and asthma [5]. Some rare familial syndromes such as type 1 and type 2 neurofibromatosis, Li Fraumeni syndrome, tuberous sclerosis, Turcot syndrome, and Cowden syndrome could all be positively correlated with glioma occurrence [6]. However, more than 90.0 % of gliomas occur in patients without genetic predisposition, suggesting that unknown environmental factors together with spontaneous genetic mutations cause gliomagenesis in most patients [3].

The first alarming symptoms reported by glioma patients are neurological deficits and seizures. Methods for the detection and classification of gliomas include magnetic resonance imaging (MRI) of the brain with or without contrast enhancement, positron-emission tomography (PET) using radiotracers for tumor grading and surgical planning [7], and histological analysis of biopsy samples and resected tumor material for the final diagnosis [8].

### 1.2.1 Classification of gliomas

Gliomas are subdivided into three specific histological subtypes, astrocytomas, oligodendrogliomas, and ependymomas, based on morphological similarities to the different types of neuroglial cells in the brain [1]. Furthermore, they are graded according to the guidelines of the World Health Organization (WHO) based on the tumor location, differen-

tiation pattern and degree of anaplasia [7]. WHO grade I describes benign, slow growing gliomas, which are well-demarked and rarely evolve into higher-grade lesions [1]. WHO grade II gliomas are still slow growing but increasingly invasive tumors which are hard to resect completely [1]. WHO grade III gliomas are rapidly growing and highly invasive tumors with significant degree of anaplasia, cellular pleomorphism, and worse patient outcome [1]. WHO grade IV is exclusively reserved for glioblastoma, the most invasive form of glioma with microvascular proliferation, necrosis, perinecrotic pseudopallisading of tumor cells, and very poor prognosis for the patient [1].

However, the WHO classification is based on subjective criteria, and therefore imperfect in its reproducibility and ability to predict individual patient outcome [8]. Therefore, vast research efforts have focused on the identification of prognostic biomarkers in order to improve glioma classification. One of the biomarkers which were included in the 2016 WHO Classification of Tumors of the Central Nervous System is a mutation in the enzyme isocitrate dehydrogenase (IDH) [7]. IDH mutations have been found in two-thirds of low-grade (WHO II and II) gliomas, both astrocytomas and oligodendrogliomas, and most secondary glioblastomas, but are very rare in primary glioblastomas (<10 %) [9, 10, 11, 12]. Wild-type IDH catalyzes the oxidative decarboxylation of isocitrate to generate alpha ketoglutarate ($\alpha$-KG), a TCA cycle intermediate, resulting in the production of NADPH from $NAD^+$. On the contrary, mutant IDH converts $\alpha$-KG to (D)-2-hydroxyglutarate (2-HG), thereby consuming NADPH and causing oxidative stress [1, 9, 11]. Furthermore, 2-HG inhibits the activity of $\alpha$-KG-dependent enzymes such as histone demethylases, dioxygenases, and hydrolases [1, 13] , thereby increasing histone methylation and hypermethylation of CpG islands in the DNA. The resulting CpG methylator phenotype is a marker of $IDH^{R132H}$ gliomas [1, 14, 15]. Independent of the histological subtype and grade of the tumor, an IDH mutation is a favorable predictor of prognosis [16].

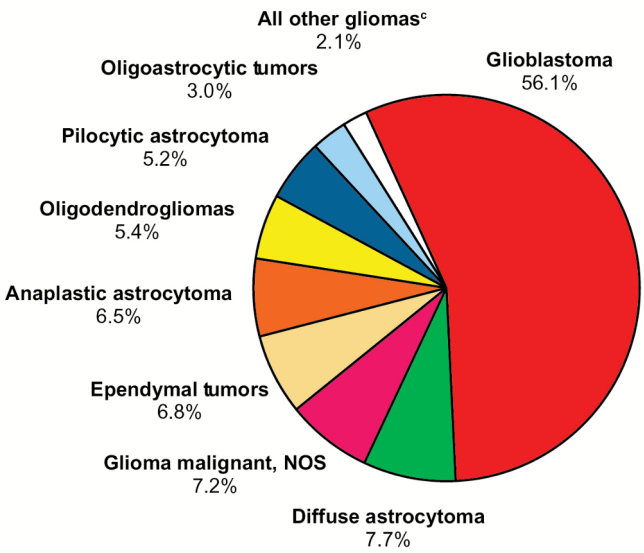


**Figure 1.2: Distribution of primary gliomas in the CNS.** Distribution of primary gliomas by their histological subtype. The data was aquired from tumors diagnosed in the United States between 2010 and 2014 and analyzed in the CBTRUS Statistical Report 2017 [3]. Modified from Ostrom et al., 2017 [3].

Furthermore, 1p/19q co-deletion is an important biomarker of oligodendroglial tumors which are characterized by slow tumor growth and good therapy response [17], whereas TP53 and ATRX mutations often coincide in astrocytic tumors [1]. Methylation of the DNA repair protein O-6-methylguanine-DNA methyltransferase (MGMT) is rare in low-grade

gliomas but frequently in high-grade glioblastomas. MGMT antagonizes the genotoxic effects of alkylating agents. Therefore, transcriptional gene silencing of the MGMT gene due to promoter methylation increases the sensitivity for chemotherapy with alkylating agents and is associated with improved survival [1, 18]. The most common gliomas are glioblastomas (WHO grade IV), representing 55.4 % of all glioma cases and 47.1 % of all malignant CNS tumors [3].

## 1.3 Glioblastoma

Glioblastoma is the most frequent and severe subtype of glioma, the third most frequently reported tumor in the CNS, and the most common malignant brain tumor overall [3]. The state of the art treatment includes maximal possible tumor resection and combination therapy with the alkylating agent Temozolomide (TMZ) and gamma radiation [19, 20, 21]. However, due to drastic recurrence rates, the prognosis is universally very poor. Although treatment of glioblastoma patients with the anti-angiogenic monoclonal antibody bevacizumab (Avastin) improved progression free survival, no significant increase in overall survival could be detected [22].

### 1.3.1 Classification of glioblastoma subtypes

Glioblastomas can be subdivided into primary and secondary tumors. Primary glioblastomas develop *de novo* from transformed neural stem cells or neural progenitor cells and are almost exclusively IDH wildtype. Secondary glioblastomas develop when lower grade lesions such as WHO grade II astrocytomas progress to grade III and finally to grade IV, they are mostly (up to 98 %) IDH mutant [9, 23, 24]. There is a favorable outcome reported for glioblastoma patients with methylated MGMT locus, due to the improved performance of the alkylating agent TMZ when MGMT function is impaired [18].

Based on transcriptomic analyses glioblastomas can be classified into four gene expression clusters: classic, mesenchymal, proneural, and neural [25]. **Classical** glioblastomas are characterized by chromosome 7 amplification, chromosome 10 loss, and high-level EGFR amplification. Deletion in the NF-1 gene predominantly occurs in the **mesenchymal** subtype and the main features of the **proneural** subtype are PDGFRA alteration and IDH1 mutations. The **neural** subtype exhibits expression of neuron markers, such as NEFL, GABRA1, SYT1, and SLC12A5. The most consistent clinical association was observed between the age of the patient and the proneural subtype, with patients in this group tending to be younger [25]. Transcriptomic profiling of tumor samples may be of significant clinical relevance for the planning of therapeutic strategies, since treatment efficiency differed between the glioblastoma subtypes [25].

Recent transcriptomic and epigenetic profiling identified six glioblastoma subgroups, partly supporting, partly further dividing the four gene expression clusters described by Verhaak et al [23, 25]. Tumors of the **IDH** subgroup exhibit global hypermethylation and mutated IDH and TP53. The **K27** group includes mostly pediatric tumors with a K27 mutation in H3F3A and often mutant TP53. The **G34** group often occurs in young adults

and is characterized by widespread hypomethylation, G34 mutation in H3F3A, and mutant TP53. The **RTKI** group exhibits PDGFRA amplification and the **RTKII** group exhibits chromosome 7 gain, chromosome 10 loss, CDKN2A deletion and EGFR amplification. Finally, the **mesenchymal** group exhibits no mutations in IDH1, TP53, EGFR, or H3F3A [23]. Although not considered in the 2016 WHO Classification of Brain and CNS tumors, transcriptomic and epigenetic profiling is a promising way to characterize the individual tumor for tailored therapeutic approaches and the development of new treatment strategies.

## 1.4 Glioblastoma stem-like cells

The poor prognosis of glioblastoma is attributable to the high degree of therapy resistance and tumor recurrence. Several studies identified glioblastoma stem-like cells (GSCs) in glioblastomas, a subpopulation that expresses neural stem cell markers and possesses unlimited self-renewing capability [26, 27]. Upon treatment with TMZ and radiotherapy the majority of the heterogeneous tumor mass is eradicated resulting in tumor shrinkage, however GSCs reside in the tissue, differentiate into tumor cells, and cause tumor recurrence (Fig. 1.3)[19, 20, 21]. The stem cell marker CD133 (prominin-1) is widely used for the identification and isolation of GSCs and $CD133^{pos}$ GSCs exhibit several features found in normal stem cells such as drug resistance, apoptotic resistance, and quiescence [27]. Detailed analysis of the gene expression profile of $CD133^{pos}$ cells revealed enrichment for stem cell markers Nestin, SOX2, Nanog, CD44, Oct4, and Musashi-1 [27, 28]. Furthermore, increased expression of MGMT and BCRP1 in $CD133^{pos}$ cells, both genes involved in drug resistance [18, 29], were associated with resistance against chemotherapeutics TMZ, carboplatin, VP16 and Taxol [27]. $CD133^{pos}$ GSCs further overexpress anti-apoptotic genes, including FLIP, BCL-2 and BCL-xL thereby evidently promoting resistance to chemotherapy [30].

GSCs are located in close proximity to the tumor vasculature, in the perivascular niche [28], and by secreting pro-angiogenic growth factors such as vascular endothelial growth factor (VEGF) they stimulate angiogenesis, necrosis, and hemorrhage *in vivo* [31]. Concisely, treatment with the anti-angiogenic drug bevacizumab reduced stemness and impaired growth of glioblastoma xenografts [28].

Due to rapid tumor expansion and poor vascularization glioblastomas contain regions of severe oxygen deprivation (hypoxia). Hypoxia correlates with poor prognosis since radiotherapy, which is based on the formation of reactive oxygen species (ROS), is less effective in regions with low oxygen. Furthermore, the transcription factor hypoxia-inducible factor (HIF) is stabilized under hypoxic conditions and drives expression of genes involved in cell survival, metabolism, and angiogenesis [28]. GSCs are enriched in hypoxic regions and HIF proteins are highly expressed in GSCs promoting neurosphere formation and proliferation [32]. Due to their tumorigenic capacity and therapy resistance, GSCs provide promising targets in glioblastoma therapy.

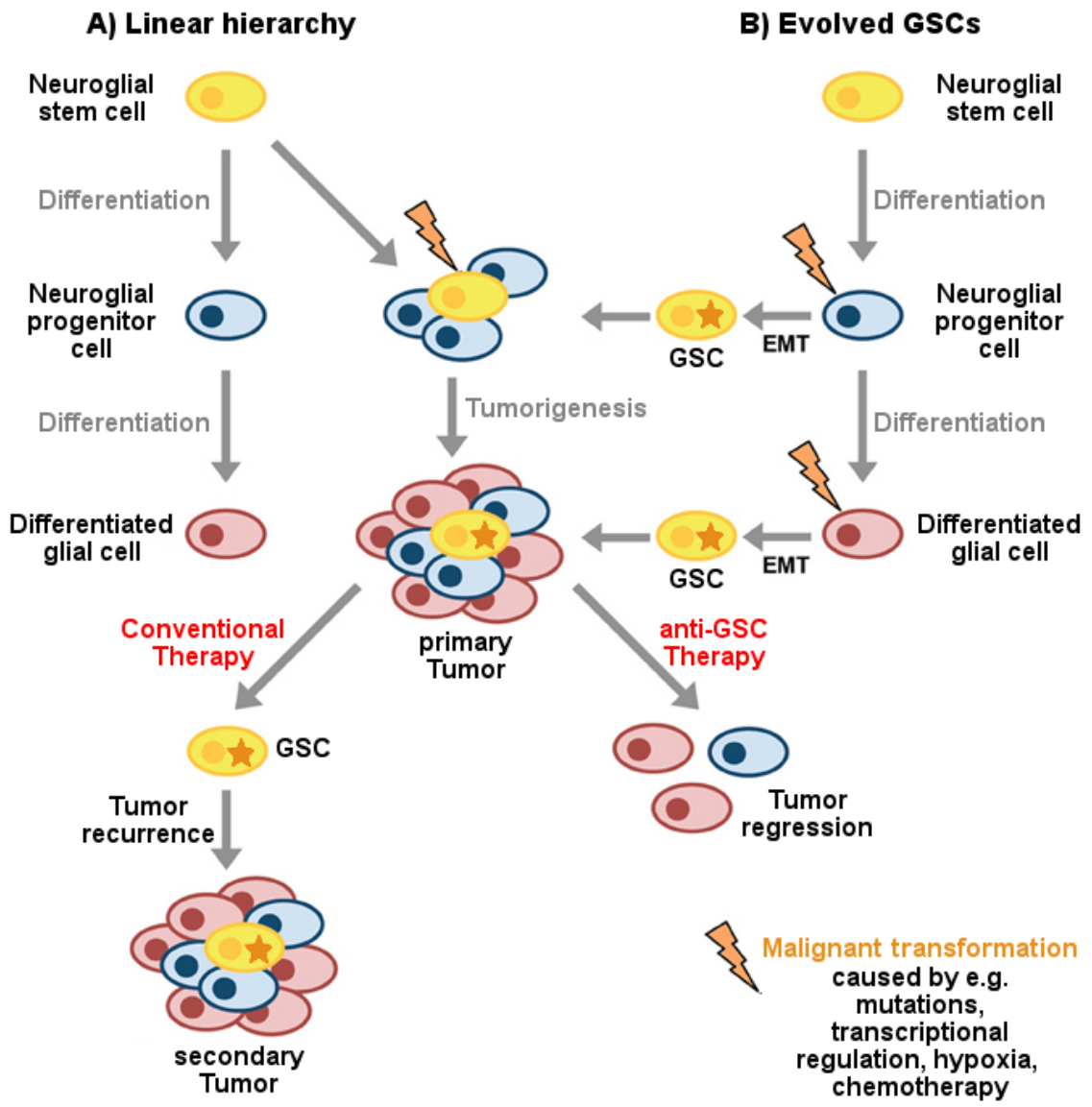


**Figure 1.3: The principles of GSC formation and GSC-mediated chemoresistance.** When neuroglial stem cells differentiate into neuroglial progenitor cells and further into glial cells, they loose their pluripotency. In the hierarchy model of GSC formation (**A**), GSCs are generated due to malignant transformation in neuroglial stem cells. They then give rise to the heterogenous tumor mass comprising GSCs, neural progenitor cells and differentiated cells. In the evolutionary model (**B**), GSCs are described to evolve due to epithelial-mesenchymal transformation of differentiated neuroglial progenitor cells or glial cells. Conventional cancer therapy fails to eradicate GSCs leading to tumor recurrence after initial tumor shrinkage. On the contrary, therapies targeting GSCs lead to tumor regression. Abbreviations: EMT, epithelial-mesenchymal transition; GSC, glioblastoma stem-like cells. Modified from Owens et al., 2013 [33]

## 1.5 Epithelial-mesenchymal-like transition

The formation of GSCs is linked to a key developmental program called epithelial-mesenchymal-like transition (EMT) which has been first described in embryonic development (Fig. 1.3) [34, 35]. The same transcription factors orchestrating EMT in embryogenesis have later been found to promote tumor progression, invasiveness, and therapy resistance in tumors [35, 36]. Initially, EMT has been described for epithelial tumors, however recent studies could link this phenomenon to the enrichment of GSCs in glioblastoma [37, 38, 39, 40]. EMT is precisely orchestrated by transcription factors of the ZEB-, TWIST-, and SNAI-families which induce expression of mesenchymal markers such as Vimentin and N-cadherin [41, 42, 43, 44, 45, 46, 47]. Furthermore, EMT activator expression could directly been linked to chemoresistance and stemness in glioblastoma [39, 48, 49, 50]. The EMT activator ZEB1 has been intensively studied in glioblastoma and described as one of the master regulators of EMT and invasiveness [39, 40, 42, 51]. ZEB1 is preferentially localized in the invasive front of tumor xenografts and glioblastoma patient samples, strongly supporting the idea of an invasive niche harboring GSCs [39, 52]. Both *in vitro* and in patient samples, ZEB1 directly correlates with expression of the GSC markers CD133 and SOX2 and the drug resistance gene MGMT, possibly mediating chemoresistance through transcriptional regulation of MGMT [18, 39]. Concisely, ZEB1 expression in glioblastoma correlates with reduced survival and weak response to TMZ in patients and ZEB1 knockdown has been validated as a robust way to impair EMT both *in vitro* and *in vivo* [39].

## 1.6 Metabolic reprogramming in cancer

Recent studies indicate that GSCs, like tumor cells in general, undergo metabolic reprogramming in order to meet the increased bioenergetic demands of highly proliferating cells and maintain redox balance [53, 54, 55]. Under nutrient-replete conditions cancer cells use anabolic pathways to sustain rapid growth and proliferation, whereas under nutrient deprivation they switch to catabolism in order to ensure survival [54]. Since some metabolic phenotypes correlate with malignancy in several tumor entities, reprogrammed metabolism has been added as a new hallmark of cancer [56]. The metabolism of tumor cells distinguishes them vastly from differentiated, non-proliferating tissues, therefore the identification of key metabolic pathways driving tumorigenesis provides the opportunity to predict therapy outcome by imaging oncometabolite levels in diagnostics and identify metabolic targets that can be used in new therapeutic strategies.

Glucose and glutamine fuel the two main anaplerotic pathways generating intermediates of the tricarboxylic acid cycle (TCA), glycolysis and glutaminolysis, respectively (Fig. 1.4). Pyruvate, the final product of glycolysis, can be metabolized to oxaloacetate instead of acetyl-CoA in order to replenish TCA cycle intermediates used for biosynthetic processes. This carboxylation reaction is catalyzed by pyruvate carboxylase. In the final step of glutaminolysis glutamate is deaminated to generate alpha ketoglutarate. Both

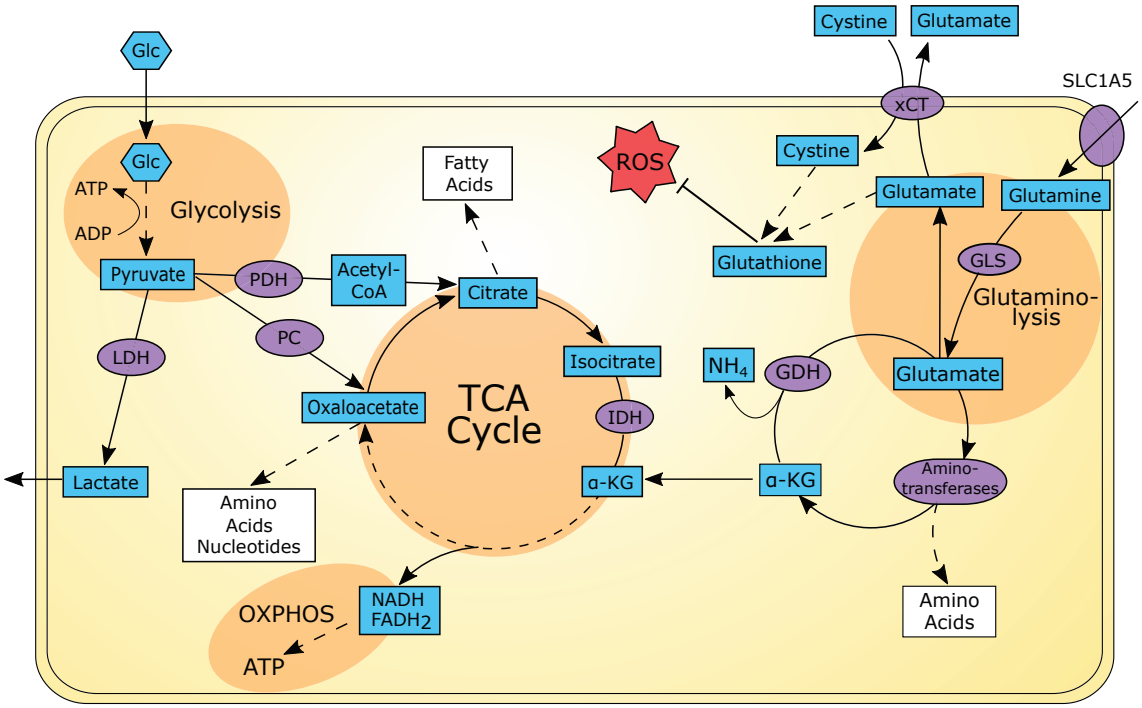


**Figure 1.4: Anaplerotic pathways promoting growth of cancer cells.** The two main anaplerotic pathways fueling the TCA cycle and facilitating high rates of biomolecule synthesis are glycolysis and glutaminolysis. Cancer cells upregulate aerobic glycolysis and metabolize pyruvate to lactate instead of oxaloactetate to accelerate energy production. In order to compensate for the reduced oxaloacetate production and sustain a functional TCA cycle and high rates of proliferation, cancer cells upregulate glutaminolysis. Thereby cancer cells fuel the TCA cycle by massive alpha ketoglutarate production. Enzymes are depicted in purple, metabolites are depicted in blue. Abbreviations: $\alpha$-KG, alpha ketoglutarate; GDH, glutamine dehydrogenase; Glc, glucose; GLS, glutaminase; IDH, isocitrate dehydrogenase; LDH, lactate dehydrogenase; OXPHOS, oxidative carboxylation; PC, pyruvate carboxylase; PDH, pyruvate dehydrogenase complex; ROS, reactive oxygen species; xCT, glutamate/cystine antiporter. Modified from Altman et al., 2016 [57].

pathways are consistently reprogrammed in tumor cells by activation of oncogenes (e.g. c-Myc, KRas), loss of tumor suppressors (e.g. TP53), and up-regulation of signaling pathways (e.g. PI3K pathway) [54, 58, 59, 60]. Cancer cells constitutively take up glucose at higher rates than normal tissues and, regardless of oxygen availability, suppress pyruvate carboxylation and metabolize pyruvate to lactate (Lac) instead of oxaloacetate, a reaction catalyzed by lactate dehydrogenase A (LDH) (Fig. 1.4) [61, 62, 63]. Thereby, cancer cells produce ATP much faster than with conventional oxidative phosphorylation (OXPHOS) in the respiratory chain. Furthermore, aerobic glycolysis causes an accumulation of Lac leading to inflammation and cytokine release further promoting tumor progression [64]. However, to compensate for the reduced oxaloacetate production and maintain a functional TCA cycle for energy production and biosynthetic processes, cancer cells have to increase the rate of glutaminolysis.

## 1.7 Glutaminolysis in cancer

Although the nonessential amino acid glutamine (Gln) can be *de novo* synthesized from glucose-derived carbons and amino acid-derived ammonia, most proliferating cells are

glutamine-addicted and need additional extracellular supply [65]. Due to the suppressed oxidative carboxylation in cancer cells, glutamine serves as a major source of carbon in bioenergetic and biosynthetic processes branching from the TCA cycle, thereby substantially contributing to cell proliferation [63]. Glutaminolysis describes a series of biochemical reactions starting with the initial deamination of glutamine by the enzyme glutaminase (GLS) in the cytosol, yielding glutamate (Glu) and ammonia. Glutamate is transported into the mitochondria where it is converted into $\alpha$-KG, catalyzed either through oxidative deamination by glutamate dehydrogenase (GDH) or by aminotransferases [65]. The $\alpha$-KG directly fuels the TCA cycle leading to NADH/NADPH and ATP production (Fig. 1.4) [66]. Since in highly proliferative cells the TCA cycle is mainly fueled by $\alpha$-KG instead of oxaloacetate, glutamine is the main driver of OXPHOS-derived ATP in cancer [67].

### 1.7.1 Glutamine in the synthesis of biomolecules

Besides energy production, the flux through the TCA cycle drives fatty acid biosynthesis and generates oxaloacetate, a substrates for the biosynthesis of non-essential amino acids (NEAAs), macromolecules, hexosamines and nucleic acids, all required to sustain growth of cancer cells [65, 68]. Interestingly, recent studies revealed that not the generation of ATP via OXPHOS but the uninterrupted flux through the TCA cycle generating oxaloacetate is the major limiting factor for proliferation in cancer cells [69, 70].

Glutamine not only drives the synthesis of NEAAs by fueling the TCA cycle via $\alpha$-KG, it further serves as a nitrogen-donor in several biosynthetic reactions. By transferring nitrogen atoms to aminotransferases, glutamine directly participates in the biosynthesis of alanine, aspartate, serine, glycine and ornithine [65]. The expression of glutamine-dependent aminotransferases has been directly linked to tumor progression, since alanine aminotransferase 2 (GPT2) and aspartate aminotransferase 1 (GOT1) are both upregulated in liver cancer [71]. Furthermore, GPT2 and phosphoserine aminotransferase (PSAT1) could be correlated with tumor progression and chemoresistance in colorectal cancer [72, 73], again elucidating how important glutamine metabolism is for the proliferation of cancer cells.

Apart from participating in energy formation and protein biosynthesis, glutamine is an important nitrogen donor in the synthesis of purine and pyrimidine bases. The synthesis of inosine monophosphate (IMP), precursor of both adenosine monophosphate (AMP) and guanosine monophosphate (GMP), the generation of GMP from IMP, and the synthesis of cytidine triphosphate (CTP) from uridine triphosphate (UTP) require reduced nitrogen atoms derived from glutamine [65].

### 1.7.2 Glutamine in redox homeostasis

Maintaining redox homeostasis is a crucial task for cancer cells since tumor progression and exposure to anti-cancer therapy causes oxidative stress. Cancer cells exhibit elevated levels of reactive oxygen species (ROS) and therefore upregulate anti-oxidative responses [65, 74]. Glutamine-derived glutamate is directly involved in the *de novo* syn-

thesis of the antioxidant glutathione (GSH) (Fig. 1.4). GSH is a tripeptide composed of the amino acids glutamate, glycine, and cysteine [65]. The biosynthesis of GSH is catalyzed by two enzymes: First, glutamate-cysteine ligase (GCL) generates $\gamma$-glutamylcysteine by condensing glutamate with cysteine and second, glutathione synthetase (GTS) ligates glycine with $\gamma$-glutamylcysteine thereby generating GSH [65].

Besides being a direct building block of GSH, glutamine-derived glutamate drives GSH biosynthesis by facilitating the uptake of cystine, the precursor of cysteine. Cystine is imported into the cell via the plasma membrane glutamate/cystine antiporter xCT/SLC7A11 under simultaneous efflux of glutamate (Fig. 1.4). Concisely, glutamine starvation impairs the uptake of cystine via the xCT transporter and pharmacological xCT inhibition causes accumulation of ROS thereby reducing proliferation of tumor cells [65, 75]. Of note, xCT expression is upregulated in breast cancer stem cells and targeting xCT impairs stemness and metastatic progression both *in vitro* and *in vivo* [76]. In glioma cell cultures and xenografts, EGFR expression promotes tumor growth, invasion, and anti-oxidative response by increasing the cell surface expression of xCT [77]. Furthermore, in patients with malignant gliomas, xCT expression correlates with tumor-associated seizures and poor prognosis, making xCT an interesting target in cancer therapy [78].

### 1.7.3 Therapies targeting glutamine metabolism

Due to its importance in energy formation and synthesis of biomolecules, glutamine metabolism is an appealing target in cancer therapy [66]. However, cells vastly differ concerning their need for extracellular glutamine. In glioblastoma, resistance to glutamine starvation correlates with the ability to *de novo* synthesize glutamine from glucose-derived carbon [79], with upregulation of other anaplerotic pathways (e.g. pyruvate carboxylation) [80], and with regulation of enzymes involved in glutaminolysis (e.g. glutamine synthetase) [81].

The use of glutamine mimetic-compounds in cancer therapy has been widely studied. Acivicin, 6-diazo-5-oxo-L-norleucine (L-DON), and azaserine are all L-glutamine analogs which inhibit L-glutamine-dependent enzymes involved in *de novo* purine and pyrimidine synthesis, leading to impaired nucleic acid synthesis and cytotoxicity. All L-glutamine analogs show broad anti-tumor activity [82, 83, 84, 85, 86, 87], however, clinical trials revealed severe side effects including mucositis and toxicity towards the gastrointestinal tract and the CNS [85, 88].

The $Na^+$-dependent neutral amino acid transporter SLC1A5 is the main L-glutamine importer and highly overexpressed in rapidly proliferating cells such as cancer cells (Fig. 1.5). Treatment with the SLC1A5 inhibitor $\gamma$-L-glutamyl-p-nitroanilide (GPNA) impairs tumor growth [89, 90] and stimulates the uptake of the glycolytic inhibitor 3-bromopyruvate by stabilizing monocarboxylate transporter 1 (MCT1), an importer of monocarboxylic-based drugs [91]. Thereby, glutamine deprivation enhances the efficacy of 3-bromopyruvate-dependent glycolysis inhibition in tumor xenografts, disrupting redox homeostasis and causing autophagy [91].

Glutaminase inhibition using small molecule inhibitors C968 and BPTES inhibits transformation of fibroblasts by oncogenic Rho-GTPases and impairs energy formation and proliferation in lymphoma xenografts [92, 93]. Furthermore, C968 effectively inhibits growth and migration in non-small cell lung cancer and causes cell cycle arrest [94, 95]. In gastric cancer, simultaneous inhibition of pyruvate kinase and glutaminase synergistically reduces proliferation of hypoxia-resistant cells [96].

Suppression of $\alpha$-KG synthesis by inhibition of aminotransferase GDH is another approach to interfere with glutamine metabolism. Aminooxyacetate (AOA) is a non-selective inhibitor of aminotransferases and epigallocatechin gallate (EGCG) specifically inhibits GDH [66]. Treatment with AOA showed promising results in breast adenocarcinoma xenografts and both AOA and EGCG suppress growth of neuroblastoma xenografts in mice [66, 97, 98].

## 1.8 Choline metabolism in cancer

Choline is an essential nutrient and the initial precursor for the biosynthesis of the glycerophospholipid phosphatidylcholine (PtdCho) (Fig. 1.5). Up to 95 % of the free choline pool inside mammalian cells is incorporated into PtdCho, the remaining 5 % are metabolized to phosphocholine (PC), glycerophosphocholine (GPC), or acetylcholine [99, 100]. Together with phosphatidylethanolamine (PtdEtn), PtdCho constitutes more than 50 % of the phospholipid bilayer and is therefore crucial for the integrity and structure of eukaryotic membranes [101]. PtdCho is synthesized in three enzymatic reactions termed Kennedy or cytidine diphosphate (CDP)-choline pathway [102].

The CDP-choline pathway starts with the ATP-dependent phosphorylation of choline by choline kinase alpha (CHK$\alpha$), generating PC and ADP. In the second, rate-limiting step, PC and CTP are used to form the high-energy intermediate CDP-choline and pyrophosphate. Finally, CDP-choline and the lipid anchor diacylglycerol (DAG) are joined to form PtdCho under the release of cytidine monophosphate (CMP) [100].

Both the synthesis and breakdown of PtdCho generates second messengers such as PC [103], DAG [104], and arachidonic acid [104], which participate in various signaling pathways regulating cell proliferation and apoptosis [100]. Elevated PC and total choline (tCho = Cho + PC + glycerophosphocholine (GPC)) levels, also called cholinic phenotype, and increased expression of choline metabolizing enzymes were detected in tumor cells, human tumor xenografts, and patient samples [105, 106, 107]. The underlying cause for the increased cholinic phenotype in cancer is upregulation of CHK$\alpha$ by malignant transformation [108, 109]. Concisely, several growth factors (e.g. PDGF) and oncogenes involved in tumor progression (e.g. KRas, HRas, PI3K-Akt) promote choline metabolism and CHK$\alpha$ activity [105].

### 1.8.1 Choline kinase alpha

Choline kinase is a cytoplasmic enzyme encoded by two different genes, CHKA and CHKB. Alternative splicing generates two isoforms, CHK$\alpha$1 and CHK$\alpha$2, from the CHKA

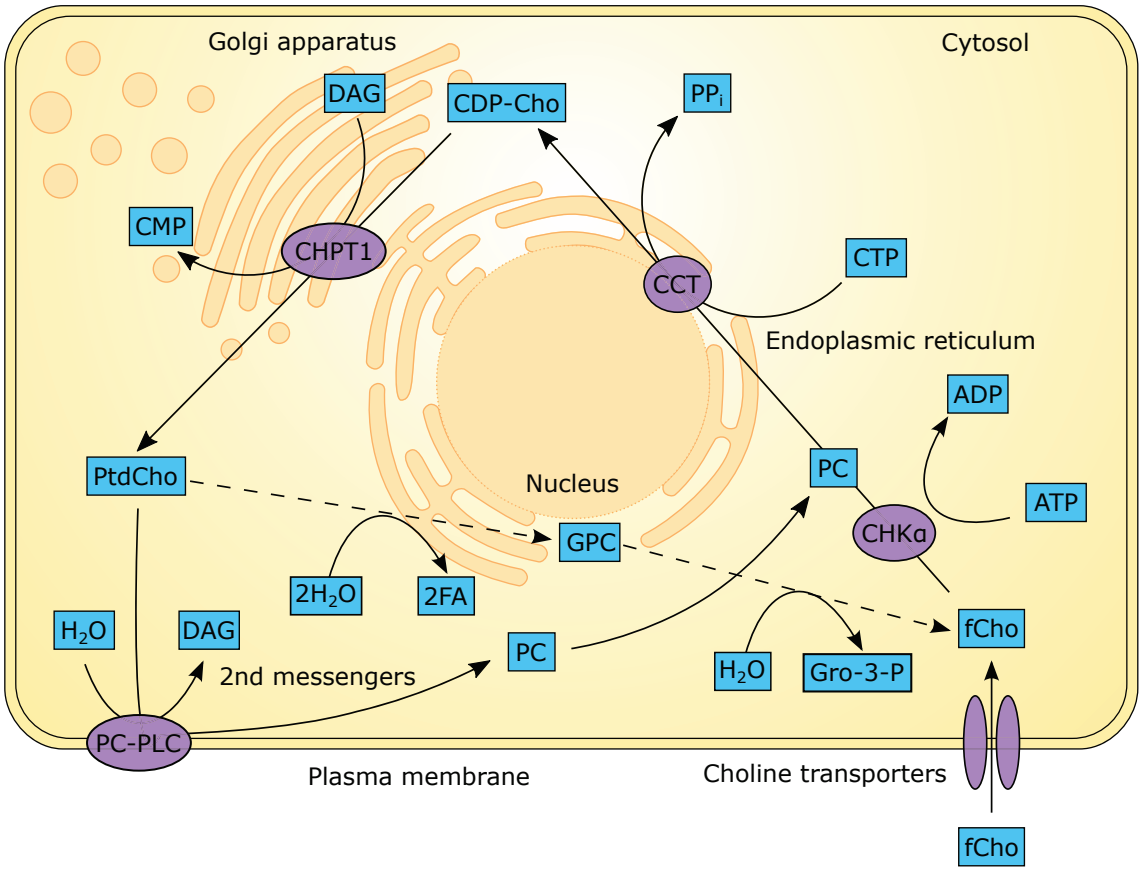


**Figure 1.5: Choline phospholipid metabolism.** The scheme shows the synthesis pathway of phosphatidylcholine, starting with the import of free choline into the cell and ending with the degradation of phosphatidylcholine by phospholipases. Enzymes are depicted in purple, metabolites are depicted in blue. Abbreviations: CCT, CTP:phosphocholine cytidylyltransferase; CDP-Cho, cytidine diphosphate choline; CHK$\alpha$, choline kinase alpha; CHPT1, choline phosphotransferase 1; CMP, cytidine monophosphat; CTP, cytidine triphosphate; DAG, diacylglycerol; FA, fatty acid; fCho, free choline; GPC, glycerophosphocholine; Gro-3-P, glycerol-3-phosphate; PC, phosphocholine; PC-PLC, phosphatidylcholine-specific phospholipase C; $PP_i$, inorganic pyrophosphate; PtdCho, phosphatidylcholine. Modified from Glunde et al., 2011 [105].

gene and a third isoform, CHK$\beta$, from the CHKB gene. CHK monomers are not functionally active, the active CHK enzymes consist of either homo- or hetero-dimers of the different isoforms. Studies with knockout mice highlighted that not CHK$\beta$ but CHK$\alpha$1 and CHK$\alpha$2, further referred to as CHK$\alpha$, are essential for the PtdCho synthesis and proliferation of tumor cells [109, 110]. Concisely, CHK$\alpha$ is overexpressed in several tumor entities including breast, lung, colorectal, and prostate cancer [110, 111, 112, 113, 114, 115]. Furthermore, CHK$\alpha$ activity correlates with advanced histological grade in breast and brain tumors [105, 116, 117] and is a prognostic factor in human lung cancer [118, 119].

CHK$\alpha$ expression is regulated by known oncogenic pathways. Ras transformed cells upregulate CHK$\alpha$ expression via activation of phosphoinositide 3-kinase (PI3K) signaling, thereby increasing choline uptake and intracellular PC and tCho concentrations [105, 120]. Reciprocally, CHK$\alpha$ mediates PI3K signaling and increases cell proliferation [121]. Furthermore, CHK$\alpha$ regulates several genes involved in cell cycle progression thereby facilitating G1-S phase transition [122]. All these observations emphasize the proposed oncogenic function of CHK$\alpha$ in cell proliferation, cell cycle progression, and tumor growth.

CHK$\alpha$ expression is influenced by hypoxic environment since hypoxia response elements (HRE), binding sites for HIF1$\alpha$, are located within the CHK$\alpha$ promoter region. Concisely, both hypoxia and HIF1$\alpha$ overexpression increase PC levels in prostate cancer [111].

### 1.8.2 Clinical implications of choline metabolism

Increased tCho and PC levels indicate for higher aggressiveness in several tumor entities including breast [123], prostate [124], and ovarian cancer [125], therefore, non-invasive monitoring of choline metabolism is used in diagnostics, tumor grading, and monitoring of therapy response. In a study with grade II and III glioma patients increased tCho levels directly correlated with increased cell density and proliferation [126]. A second study identified significantly higher tCho levels in high-grade compared to low-grade gliomas, emphasizing that non-invasive monitoring of choline metabolites can significantly contribute to grading of gliomas and planning of therapy [117].

Furthermore, imaging of choline metabolism can be used to monitor therapy response, since in both preclinical models and human tumors most chemotherapeutic agents decrease tCho levels in responding but not in non-responding tumors [105, 127].

Targeting choline metabolism is a promising approach in cancer therapy and both pharmacological and genetic inhibition of CHK$\alpha$ has been shown to impair tumor growth and induce apoptosis [128, 129, 130]. The highly selective CHK$\alpha$ inhibitor MN58b reduces proliferation of both non-transformed and Ras-transformed cells, but strikingly, non-transformed cells resumed proliferation after drug removal whereas transformed cells were irreversibly affected [131]. Furthermore, CHK$\alpha$ inhibition in combination with chemotherapy of breast cancer cells with 5-fluorouracil has synergistic effects and significantly inhibits proliferation of malignant cells, but has only minor effects on non-malignant cells [105, 132]. The reduced PC and tCho levels resulting from CHK$\alpha$ inhibition can be detected non-invasively with proton nuclear magnetic resonance ($^1$H NMR) spectroscopy and therefore can be used to monitor effective pathway inhibition and therapy response [105, 133].

## 1.9 Imaging of cancer metabolism

Cancer diagnostics, tumor grading and monitoring of treatment response require sophisticated imaging techniques capable of delineating the exact tumor volume and assessing specific tumor characteristics. Computed tomography and magnetic resonance imaging provide information about the anatomy of the lesion, but are not able to differentiate between recurrent tumor and radionecrosis [134]. Imaging of tumor metabolism using non-invasive NMR spectroscopy and PET with radiotracers exploits the fact that tumors exhibit vast metabolic differences compared to normal tissues [135, 136, 137]. With *ex vivo* high resolution (HR) NMR spectroscopy oncometabolites in biological samples such as cellular extracts can be characterized and quantified, a field termed metabolomics. The clinical application of this technique is limited by the field strength of spectrometers

applicable for *in vivo* imaging of cells and solid tumors in living organisms. $^{1}$H NMR spectroscopy of the brain using a 7 T spectrometer can detect oncometabolites such as Lac, glycine (Gly), Gln, Glu and GSH, but is not able to differentiate between PC, GPC and free Cho (fCho) [138]. Nevertheless, monitoring of therapy response by assessing pre- and post-therapeutic tCho levels has been validated in various cancers including in the brain [139].

Metabolic flux analyses are used to monitor the activities of metabolic pathways. In *in vitro* studies the nutrient of interest (e.g. glucose, glutamine) is labelled with NMR active tracer isotopes (e.g. $^{13}$C, $^{15}$N, $^{31}$P), added to the culture medium of cancer cells, and the metabolites of cellular extracts are analyzed with NMR spectroscopy for isotope enrichment. The extent and the distribution of the isotope labelling elucidate which pathways have been involved in the metabolization of the nutrient. Metabolic flux analyses *in vivo* are executed by systemic administration of $^{13}$C- or $^{15}$N-labelled nutrients via boluses or infusions in humans and animals [54]. Studies in cancer patients and mice bearing tumor xenografts not only show substantial labeling of several oncometabolites involved in glycolysis, glutaminolysis and the TCA cycle, they further provide information about the activity of enzymes involved in tumor progression [54, 79, 140, 141].

Positron emission tomography is another technique used to image the structure of neoplasms based on their reprogrammed metabolism [135]. Imaging of glucose accumulation using the radiotracer $^{18}$F-Fluorodeoxyglucose (FDG) exploits the fact that tumors upregulate glucose consumption and is widely used in diagnostics and monitoring of therapy response. Furthermore, since high-grade lesions are more metabolically active than low-grade lesions, FDG PET is used to assess the degree of malignancy at the time of diagnosis [134, 135]. However, in tumors with low glucose consumption rates, in tumors adjacent to tissues with high glucose consumption rates (e.g. heart, brain), or in patients treated with glucose inhibitors, FDG PET can lead to unsatisfying results. In this case $^{11}$C-, $^{13}$N, or $\gamma$-fluorinated $^{18}$F-labelled glutamine can be used as an alternative radiotracer [137]. Glutamine consumption is highly selective for tumor tissue and correlates with increased expression of the Gln importer SLC1A5 in gliomas [142].

## 1.10 Aim of this work

Substantial progress has been made toward understanding how glioma stem-like cells drive tumor progression and therapy resistance in glioblastoma. However, whether the formation and tumorigenicity of GSCs is accompanied by metabolic reprogramming remains elusive. It is known that metabolic reprogramming substantially contributes to tumor aggressiveness and therapy resistance in various tumor entities [53, 54, 143]. In this respect it is crucial to study whether the formation of GSCs is driven by changes in the cellular metabolome. The identification of oncometabolites accumulating as a consequence of GSC enrichment could be used for diagnostic purposes, to predict therapy outcome, and to monitor anti-GSC therapy response. Furthermore, metabolic enzymes involved in GSC enrichment present interesting candidates for novel therapies specifically targeting GSCs. In this work, HR $^{1}$H-NMR spectroscopy of *ex vivo* cellular extracts of glioblastoma cultures is used to investigate metabolic reprogramming occurring during the enrichment of GSCs. Therefore, glioblastoma cultures are modified in three different ways in order to enrich or decrease the GSCs population: 1) Propagation of adherent glioblastoma cultures to neurosphere growth to increase the GSC fraction, 2) impairment of epithelial-mesenchymal transition by knockdown of ZEB1, and 3) targeted glial differentiation of GSC cultures using bone morphogenic protein 4 (BMP4) to decrease the GSC fraction. Furthermore, this thesis comprises studies using genetic and pharmacological inhibition of key metabolic pathways to identify targets for novel anti-GSC therapies based on tumor metabolism. This work is a cumulative thesis and comprises three chapters studying the metabolism of GSCs in three publications.

Section 2.1 studies the effect of culture conditions on the cellular metabolism of glioblastoma cells. Using HR $^{1}$H-NMR spectroscopy, recently described metabolite ratios correlating with tumorigenicity are analyzed both in adherent cells and glioblastoma neurospheres. Furthermore, this work elucidates that propagation to neurosphere growth significantly increases the GSC pool in glioblastoma cultures.

Section 2.2 investigates the role of EMT on the glioblastoma metabolome. EMT is a developmental program significantly enriching the population of GSCs by transcriptional reprogramming [35]. The transcription factor ZEB1 has been described as a master regulator of EMT efficiently promoting invasiveness, therapy resistance and tumor aggressiveness [39, 144]. This chapter includes detailed metabolic analysis of *ex vivo* glioblastoma cell extracts with impaired ZEB1 expression. Furthermore, it highlights that EMT significantly promotes the activity of choline kinase $\alpha$, an enzyme linked to tumor progression in several tumors [112, 114, 130]. Finally, this chapter investigates the efficacy of genetic and pharmacological CHK$\alpha$ suppression as a tool to inhibit EMT and reduce the GSC fraction in glioblastoma cultures.

Section 2.3 includes detailed metabolomic analysis of glioblastoma cultures with different degrees of stemness. Therefore, stemness of GSC neurosphere cultures is reduced using 1) spontaneous differentiation by cultivation as adherent cells and 2) targeted glial differentiation by BMP4 treatment. BMP4 has been described to effectively decrease the GSC pool in glioblastoma cultures [145]. Furthermore, this chapter includes studies on

the effect of glutamine deprivation and glutaminase inhibition on the fraction of GSCs in glioblastoma cultures.

# 2 Publications

## 2.1 The effect of neurosphere culture conditions on the cellular metabolism of glioma cells

### 2.1.1 General Information

**Title: The effect of neurosphere culture conditions on the cellular metabolism of glioma cells**

Ulf D. Kahlert[1,2], Katharina Koch[2], Abigail K. Suwala[2], Rudolf Hartmann[3], Menglin Cheng[4], Donata Maciaczyk[2], Dieter Willbold[3,5], Charles G. Eberhart[1], Kristine Glunde[4], and Jaroslaw Maciaczyk[2,*]

[1]Department of Pathology, Division of Neuropathology, Johns Hopkins Hospital, Baltimore, USA
[2] Department of Neurosurgery, University Medical Center Düsseldorf, Düsseldorf, Germany
[3] Institute of Complex Systems ICS-6, Research Center Jülich, Jülich, Germany
[4] Division of Cancer Imaging Research, Russell H. Morgan Department of Radiology and Radiological Science, Johns Hopkins Hospital, Baltimore, USA
[5] Institute of Physical Biology, Heinrich-Heine-University Düsseldorf, Düsseldorf, Germany
[*] corresponding author, Jaroslaw.Maciaczyk@med.uni-duesseldorf.de

Published in: **Folia Neuropathologica**, Vol. 53, Issue 3, pp. 219-225, 2015 [146]
DOI: 10.5114/fn.2015.54422
Journal Impact Factor (2015): 1.233
Contribution: 30 %. Katharina Koch was responsible for the culture and $^{1}$H-NMR metabolic analysis of U87 adherent cells and evaluated the data. For further details see the Declaration of Author's Contribution.

### 2.1.2 Abstract

Malignant gliomas, with an average survival time of 16-19 months after initial diagnosis, account for one of the most lethal tumors overall. Current standards in patient care provide only unsatisfying strategies in diagnostic and treatment for high-grade gliomas. Here we describe metabolic phenomena in the choline and glycine network associated with stem cell culture conditions in the classical glioma cell line U87. Using high resolution proton magnetic resonance spectroscopy of cell culture metabolic extracts we compare the metabolic composition of U87 chronically propagated as adherent culture in medium supplemented with serum to serum-free neurosphere growth. We found that the switch to neurosphere growth, besides the increase of cells expressing the putative glioma stem cell marker CD133, modulated a number of intracellular metabolites including choline, creatine, glycine, and myo-inositol that have been previously reported as potential diagnostic markers in various tumors.

These findings highlight the critical influence of culture conditions on glioma cell metabolism and therefore particular caution should be drawn to the use of *in vitro* system research in order to investigate cancer metabolism.

### 2.1.3 Introduction

Glioblastoma (GBM) is the most common and lethal adult glial brain tumor, with a mean overall survival of 16-19 months after primary diagnosis under the current standard-of-care treatment scheme [19]. Despite enormous research efforts towards early diagnosis and more efficient treatment, the prognosis of GBMs remains dismal. The influence of culture conditions has been widely investigated in the field of glioma research, suggesting that neurosphere cultures, compared to adherent growth, more closely resemble the original patient's tumor [147] showing high stem cell compartment [148] and therefore are more suitable for testing of novel therapeutic approaches [149]. In this report we describe altered relative concentrations of the cholines, creatine, myo-inositol and glycine in the human GBM cell line U87 propagated under stem cell conditions as compared to classical monolayer culture. Furthermore, U87 neurospheres showed significant higher levels of the putative GBM stem cell marker CD133 as their serum-propagated counterparts. Detection and targeting of miss-regulated choline-, myo-inositol-, creatine- and glycine-metabolism has been described to have potential utility in the diagnosis and treatment of malignant gliomas [150, 151, 152, 153, 154, 155].

This is to our knowledge the hitherto first link of changes in those onco-metabolites [152, 156] to variations in cell culture conditions of glioma cells. Inter-spectral co-analysis of metabolite concentrations under the two propagation conditions identified reductions in ratios of phosphocholine to glycerophosphocholine (PC/GPC) and glycine to total choline (Gly/tCho) but increases in the quotient of total choline to total creatine (tCho/tCre) and PC/tCre, as well as Gly/myo-inositol (Gly/myo). This work should draw the attention of the scientific community on possible *in vitro* artefacts and on the need for appropriate models most closely resembling the *in vivo* biology of investigated tumors.

### 2.1.4 Results

**Modification of the culture condition alters the relative concentration of choline, creatine, glycine, and myo-inositol in U87 glioma cells**

High-resolution $^{1}$H-NMR spectra where obtained as described above and a representative spectrum is shown in figure 2.1A. The most prominent metabolites were annotated and quantified, including adenine (Ade), myo-inositol (myo), glycine (Gly), phosphocholine (PC), glycerophosphocholine (GPC), free choline (fCho), total choline (tCho=fCho+PC+GPC), total creatine (tCre), glutathione (GSH), glutamine (Gln), glutamate (Glu), N-acetylaspartylglutamate (NAAG), alanine (Ala), lactate (Lac), threonine (Thr), and valine/isoleucine (Val/Iso). Due to the previously described importance in glioma biology we focused our quantitative analysis on choline, creatine, glycine, and myo-inositol ratios (Fig. 2.1B).

The switch to neurosphere media decreased the ratio of PC/GPC (40 %) and significantly diminished the Gly/tCho concentration (70 %). In contrast, we could detect an increase in the ratios of Gly/myo (65 %), tCho/tCre (300 %), and PC/tCre (280 %) reaching statistical significance for the latter two.

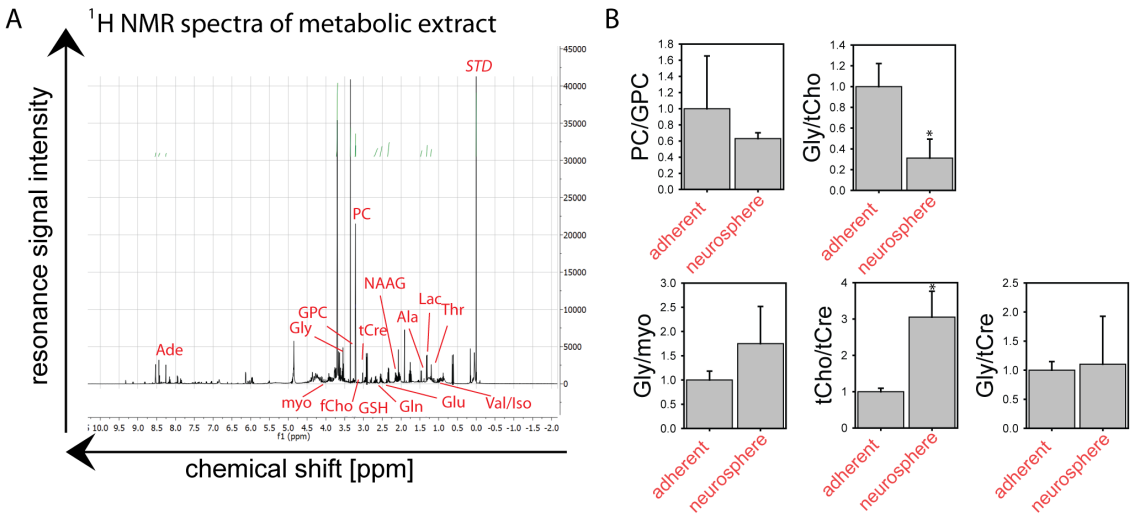


**Figure 2.1: Global metabolic profiling of U87 glioma cells under adherent and suspension growth.** Representative $^{1}$H-NMR spectra of the intracellular metabolites of U87 glioma cells with annotated adenine (Ade), myo-inositol (myo), glycine (Gly), phosphocholine (PC), glycerophosphocholine (GPC), free choline (fCho), total choline (tCho = fCho + PC + GPC), total creatine (tCre), glutathione (GSH), glutamine (Gln), glutamate (Glu), N-acetylaspartylglutamate (NAAG), alanine (Ala), lactate (Lac), threonine (Thr) as well as valine/isoleucine (Val/Iso) plus internal concentration standard (STD) (**A**). Relative quantification of phosphocholine, glycerophosphocholine, glycine, creatine, and myo-inositol revealed altered metabolism after transfer of U87 cells into neurosphere growth conditions: Reduction of PC/GPC and Gly/tCho whereas Gly/myo and tCho/tCre ratios were increased (**B**), p = 0.05.

### Neurosphere assay condition increases the expression of cell surface marker CD133

U87 culture in classical serum-containing growth medium did express very low levels of $CD133^{pos}$ cells (about the amount of the negative control, 1 % $CD133^{pos}$ cells on average). Following their transfer into stem cell conditions, the $CD133^{pos}$ population was increased to 18.5 % (p-value <0.001, Fig. 2.2A). Similar results of $CD133^{pos}$ U87 cells in free-floating culture conditions have been published previously [157, 158].

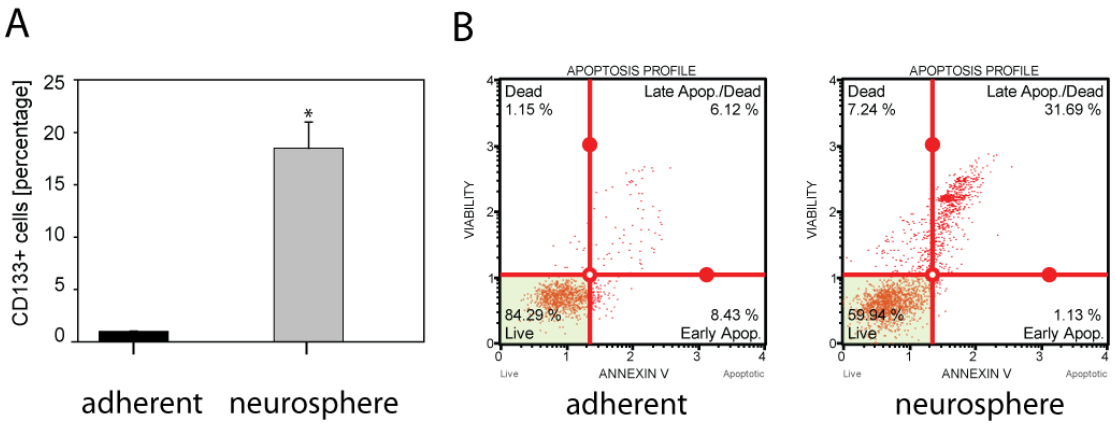


**Figure 2.2:** U87 neurosphere cells compared to monolayer cells show an increased population of cells expressing the cell surface marker CD133. (**A**, p-value < 0.001) and are characterized by a higher number of apoptotic cells (**B**).

.

### U87 neurosphere cultures exhibit a higher fraction of apoptotic cells

We identified increased levels of apoptosis and cell death in cells propagated under neurosphere growth conditions compared to their adherent counterparts as assessed by AnnexinV/Propidium iodide–based quantification (Fig. 2.2B).

## 2.1.5 Discussion

In this work we analyzed the changes of U87 cell metabolism depending on whether a monolayer or 3D *in vitro* propagation has been applied. Our study of this human glioma cell line confirms the accumulation or preferential selection of $CD133^{pos}$ cells, a putative brain tumor stem cell marker [159], under prolonged stem cell culture conditions compared to propagation in serum-containing media. Recent studies addressing the effect of different culture conditions in *in vitro* mouse models of GBM described the robust enhancement of stem cell marker expression and self-renewal capacity of cells transferred

from adherent growth to spheroid culture [148]. Moreover, neurosphere cultures are suggested to more closely resemble the original patient's tumor [147] and therefore are more suitable for testing novel therapeutic approaches [149].

Using high resolution magnetic resonance spectroscopy ($^1$H-NMR) in extracts of cells chronically propagated under serum-free neurosphere growth, we identified several alterations in metabolite concentrations with proposed diagnostic utility as a response to changed growth stimuli.

Phosphocholine (PC), glycerophosphocholine (GPC) and free choline (fCho) all play an important role in membrane phospholipid household that accompanies cell cycle progression [160]. Moreover, miss-regulated choline metabolism has already been proposed as an underlying molecular event during cancerous malformation in a variety of cancers [109] including GBM [150]. Interestingly, we found that U87 glioma neurospheres exhibit a reduced PC/GPC ratio although it is not statistically significant. The PC/GPC ratio has been shown to be elevated in aggressive breast cancer cells [109], however, the diagnostic impact of this parameter in brain cancers has been challenged [161]. The tCho/tCre quotient is a historically established diagnostic biomarker in brain tumors, which increases with progression of malignancy [162, 163, 164]. Concordant with this data we revealed that the tCho/tCre ratio is significantly increased in cells cultivated as neurospheres.

Glycine (Gly), a currently intensively studied metabolite with oncogenic potential has been reported to be directly correlated with glioma malignancy [152]. Hypoxic glioma cells, which are known to contain a population of cells with high stem-like signature [165], are highly susceptible to glycine metabolism [153]. In addition, efforts using $^1$H-NMR-spectroscopy to grade brain tumor malignancy based on their cellular metabolism suggested glycine as a negative prognostic biomarker [166, 167, 168]. The Gly/tCre ratio is thought to be a suitable parameter for grading of gliomas and for their distinction from brain metastasis [169]. Interestingly, we did not notice differences in Gly/tCre between the two growth conditions. Therefore we performed co-analyses with additional metabolites, including myo-inositol (myo) - a metabolite reported to be reduced in high-grade as compared to low-grade brain tumors [151, 155]. We could detect that the Gly/myo ratio, reported to be a valid marker for high-grade gliomas including GBM [168], is increased in suspension cells, indicating either the increase of Gly or the reduction of myo in neurospheres, as compared to adherent cells. An important route for the synthesis of glycine involves the degradation of choline [170]. We therefore sought to compare their relative concentrations in the two culture conditions and found the Gly/tCho ratio significantly diminished (about 75 % decrease) in neurosphere cells. The reduction of Gly/tCho could potentially be due to elevated concentrations of tCho in stem-like neurospheres, as increased levels of tCho is an accepted marker for high-grade brain tumor malignancy [171].

In summary we conclude that switching the cell culture conditions for U87 cells effectively alters their cellular metabolism, influencing a variety of metabolites with reported importance in glioma and glioma stem cell progression. Cells propagated in suspension and adherent growth can dramatically alter their cellular proliferation and apoptosis rate

due to alterations in environmental stimuli. We confirm increased apoptosis in U87 neurosphere cells compared to cells grown as monolayer. We cannot preclude, that the described metabolic differences might, at least partially, be due to the increased cell death.

Therefore, particular caution has to be used interpreting the results of studies on cancer metabolism in the context of the *in vitro* model. As reported here, substantial variations in intracellular levels of metabolites might be a consequence of different culture conditions, precluding the formulation of general conclusions.

### 2.1.6 Methods

#### Cell culture

U87 cell line was purchased from American Type Cell Culture bank (www.ATCC.com) and propagated either as adherent culture in Dulbecco's modified Eagle's medium (DMEM, Life Technologies) containing 20 % fetal calf serum or as neurospheres (stem cell culture) in DMEM/F12 (3:1, both Life Technologies) medium supplemented with B27 (Life Technologies), 20 ng/ml recombinant human basic fibroblast growth factor (bFGF, Peprotech), 20 ng/ml recombinant human epidermal growth factor (EGF, Peprotech), Anti-Anti (Life Technologies) and 5 µg/ml heparin (Sigma–Aldrich) as described before [40]. Cells were passaged at least eight times in each culture condition before they were subjected to experimental analysis.

Cell line identity was confirmed by analysis of nine tandem repeats plus a gender-determining marker, Amelogenin, using the StemElite kit (Promega, Table 2.1).

#### Metabolic extractions of *in vitro* cultures, proton nuclear magnetic resonance spectroscopy ($^1$H-NMR) and metabolite quantification

A minimum of 7*$10^6$ cells were collected for each extraction (each condition n=3). A methanol-chloroform-water (1/1/1, v/v/v) dual phase cell lysis protocol was applied to extract water- and lipid-soluble metabolites as described before [111]. In this study we only assessed the content of the water-soluble extracts. The lyophilized water-soluble extracts were resolved in 20 mM phosphate buffer pH 7.0 (10 % v/v $D_2O$, Sigma- Aldrich, MO, USA) and supplemented with 2,2-dimethyl-2-silapentane-5-sulfonate sodium salt (DSS; Euriso-top, internal NMR-standard, STD) for the scans at Research Center Jülich (Germany) and in $D_2O$ containing 0.24 µM 3-(trimethylsilyl)propionic-2,2,3,3-d4 acid (TSP; Sigma-Aldrich, internal concentration standard, STD) at John Hopkins Hospital. The spectras were acquired at 25 ℃ on a Bruker Avance 500 spectrometer operating at 11.7 T using a 5-mm HX inverse probe as previously described [111] at the Department of Radiology in the Johns Hopkins Hospital and a Bruker Avance III HD 600 spectrometer operating at 14.1 T using a 5-mm TXI cryo-probe at the Institute of Complex Systems (ICS-6) in the Research Center Jülich (Germany). Water suppression was achieved by applying a pulse-sequence using excitation-sculpting with gradients. The fully relaxed $^1$H-NMR data were processed, and the signal integrals listed below were measured us-

ing Mestrenova V10 software (Mestrelab). All metabolite concentrations were quantified through peak integration after standardized performed phase correction and baseline fitting. The respective concentration standard served as intra-spectral normalization for each $^{1}$H-NMR spectra, and metabolite concentrations within the same spectra were co-analysed and presented as means plus SDs.

**FACS-based assessment of CD133+ cell population**

Cells were stained for cell surface antigen CD133 (AC133-PE, #130-098-826, Miltenyi Biotec) according to manufacturer's protocols, as described before [165]. AC133-antibody without a fluorescent dye (AC133-pure, #130-090-422, Miltenyi Biotec) was used as control. Fluorescence activated cell sorting (FACS) was performed on an Accuri C6 cytometer (BD Biosciences, Franklin Lakes, NJ) whereas for post-processing data analysis FlowJo v10 software (FlowJo, Tree Star Inc, Ashland, OR) was applied.

**Cell Apoptosis assays**

Cultures were dissociated to single cell suspension and viable cells were quantified using the MUSE Count & Viability Assay Kit (#MCH100102, Merck KGaA) on a Muse Cell Analyzer (#0500-3115, Merck KGaA). Apoptotic cells were quantified using the AnnexinV & Dead Cell Kit (#MCH100105, Merck KGaA) on the Muse Cell Analyzer according to the manufacturer's protocol. A minimum of 2000 gated events were acquired.

**Statistical evaluation**

Statistical evaluation was performed using Students t-test in Statistica (Statsoft, OK, USA) and presented as mean plus respective standard deviations.

**Acknowledgements**

UDK is supported by the Dr. Mildred Scheel fellowship by the Deutsche Krebshilfe.
The work has been co-financed by the SFF Grant of the HHU University, Düsseldorf, Germany, awarded to JM. AKS is supported by the Friedrich-Ebert Stiftung. KK is a fellow of Düsseldorf School of Oncology (DSO) of HHU University.

### 2.1.7 Supplement

**Table 2.1:** STR analysis U87

| **Loci** | |
|---|---|
| AMEL | X |
| CSFIPO | 10,11 |
| D13S317 | 8,11 |
| D16S539 | 12 |
| D21S11 | 28,32.2 |
| D5S818 | 11,12 |
| D7S820 | 8,9 |
| TH01 | 9.3 |
| TPOX | 8 |
| vWA | 15,17 |

## 2.2 Reciprocal regulation of the cholinic phenotype and epithelial-mesenchymal transition in glioblastoma cells

### 2.2.1 General Information

**Title: Reciprocal regulation of the cholinic phenotype and epithelial-mesenchymal transition in glioblastoma cells**

Katharina Koch[1], Rudolf Hartmann[2], Friederike Schröter[3], Abigail K. Suwala[1], Donata Maciaczyk[1], Andrea C. Krüger[1], Dieter Willbold[2,3], Ulf D. Kahlert[1], and Jaroslaw Maciaczyk[1,*]

[1] Department of Neurosurgery, University Hospital Düsseldorf, Düsseldorf, Germany

[2] Institute of Complex Systems ICS-6, Research Center Jülich, Jülich, Germany

[3] Institute for Stem Cell Research and Regenerative Medicine, Medical Faculty, Heinrich-Heine-University Düsseldorf, Düsseldorf, Germany

[4] Institute fuer Physikalische Biology, Heinrich-Heine-University Düsseldorf, Düsseldorf, Germany

[*] corresponding author, Jaroslaw.Maciaczyk@med.uni-duesseldorf.de

Published in: **Oncotarget**, Vol. 7, Issue 45, pp. 73414-73431, 2016 [172]
DOI: 10.18632/oncotarget.12337
Journal Impact Factor (2016): 5.17
Contribution: 75 %. Katharina Koch performed the experiments, evaluated the data and wrote the manuscript. For further details see the Declaration of Author's Contribution.

### 2.2.2 Abstract

Glioblastoma (GBM) is the most malignant brain tumor with very limited therapeutic options. Standard multimodal treatments, including surgical resection and combined radiochemotherapy do not target the most aggressive subtype of glioma cells, brain tumor stem cells (BTSCs). BTSCs are thought to be responsible for tumor initiation, progression, and relapse. Furthermore, they have been associated with the expression of mesenchymal features as a result of epithelial-mesenchymal transition (EMT) thereby inducing tumor dissemination and chemo resistance. Using high resolution proton nuclear magnetic resonance spectroscopy ($^1$H-NMR) on GBM cell cultures we provide evidence that the expression of well-known EMT activators of the ZEB, TWIST and SNAI families and EMT target genes N-cadherin and VIMENTIN is associated with aberrant choline metabolism. The cholinic phenotype is characterized by high intracellular levels of phosphocholine and total choline derivatives and was associated with malignancy in various cancers. Both genetic and pharmacological inhibition of the cardinal choline metabolism regulator choline kinase alpha (CHK$\alpha$) significantly reduces the cell viability, invasiveness, clonogenicity, and expression of EMT associated genes in GBM cells. Moreover, in some cell lines synergetic cytotoxic effects were observed when combining the standard of care chemother-

apeutic temozolomide with the CHK$\alpha$ inhibitor V-11-0711. Taken together, specific inhibition of the enzymatic activity of CHK$\alpha$ is a powerful strategy to suppress EMT which opens the possibility to target chemo-resistant BTSCs through impairing their mesenchymal transdifferentiation. Moreover, the newly identified EMT-oncometabolic network may be helpful to monitor the invasive properties of glioblastomas and the success of anti-EMT therapy.

### 2.2.3 Introduction

Glioblastoma (GBM) is the most prevalent primary malignant brain tumor with a median survival of less than two years. High levels of therapy resistance, strong cellular invasiveness and rapid cell growth demand aggressive multimodal therapies involving resection followed by radio-chemotherapy [21, 173, 174].

Recent evidence has pointed to the existence of brain tumor initiating cells in GBMs, so called brain tumor stem cells (BTSCs). This subpopulation of GBM cells with stem cell properties are considered to be the main cause of tumor development, progression and chemo-resistance also in malignant gliomas [27, 175, 176, 177]. Recent studies described an important link between stem-like properties and the cells capacity to invade and disseminate into the microenvironment. This molecular switch called epithelial-mesenchymal transition (EMT) enables cell autonomous movement and extracellular matrix digestion, both cardinal features of tumor stem cells [35, 36]. EMT has been first described in epithelial tumors, but recent studies could link this phenomenon to tumor progression, invasion and therapy-resistance in GBM [39, 40]. EMT is precisely orchestrated by transcriptional modulators of the ZEB-, TWIST- and SNAI-families and results in expression of the mesenchymal markers N-cadherin and VIMENTIN [42, 178, 179, 180, 181, 182].

Most recently EMT activation could be associated with aberrant lipid metabolism [183], elucidating the importance of metabolic reprogramming for mesenchymal transformation. Multiple genetic and metabolic pathways are altered during malignant transformation, leading to extensive cellular growth and stress resistance. Thus, targeting onco-metabolic networks might be regarded as an innovative strategy to develop personalized cancer therapies [143, 184].

As such, cancer cells favor to generate ATP more rapidly through upregulation of glycolysis instead of oxidative phosphorylation. This so called Warburg effect is the best characterized metabolic phenotype in cancer [62]. Furthermore, cancer cells have been described to increase choline metabolism, detected by elevated intracellular levels of phosphocholine (PC) and total choline derivatives [tCho, glycerophosphocholine (GPC) + PC + free choline (fCho)]. The cardinal enzyme of choline metabolism, choline kinase alpha (CHK$\alpha$), has been described as the main regulator of the cholinic phenotype and could be associated with tumor progression in various cancers [109, 112, 113, 114].

Induction of the cholinic phenotype has been linked to malignant progression and aggressiveness in several cancers [105, 108, 139]. Here we suppressed EMT by blocking the potent EMT activator ZEB1 and analyzed the effect on the cellular metabolism of

GBM cells using high resolution proton magnetic resonance spectroscopy ($^1$H-NMR). We identified a bidirectional link between EMT and choline metabolism and revealed that targeting CHK$\alpha$ is a powerful strategy to suppress EMT status and BTSC properties of GBM cells. Moreover, metabolites that are connected to EMT progression can be monitored with *ex vivo* imaging technology and therefore have strong potential for rapid clinical translation in tumor diagnostics and surveillance.

### 2.2.4 Results

#### ZEB1 knockdown reduces the viability of GBM cells

In order to analyze whether epithelial to mesenchymal transition (EMT) affects metabolic pathways in GBMs, we established stable tumor models with suppressed expression of the core EMT activator ZEB1 in three GBM cell lines (LN229, GBM1 and JHH520) through RNA interference technology. The knockdown efficiency was confirmed on mRNA and protein level. RT qPCR results showed that transduction with either shZEB1#1 or shZEB1#5 resulted in a significant reduction of *ZEB1* mRNA by 60 % – 80 % (Fig. 2.3A, shown for shZEB1#1). Western blotting confirmed the efficacy of both shZEB1 shRNAs, leading to a distinctive reduction of ZEB1 protein levels (Fig. 2.3B). Previous research of our group revealed the role of ZEB1 in invasion of GBM cells [40, 42]. To further investigate the phenotype of ZEB1 depletion, we analyzed the cell viability after transduction with shZEB1#1 or control vector. Therefore, we performed the TiterBlue® viability assay with LN229, GBM1, and JHH520 shZEB1#1 or control cells over five consecutive days. Figure 2.3C shows that ZEB1 knockdown decreases the viability of all three tested GBM cell lines.

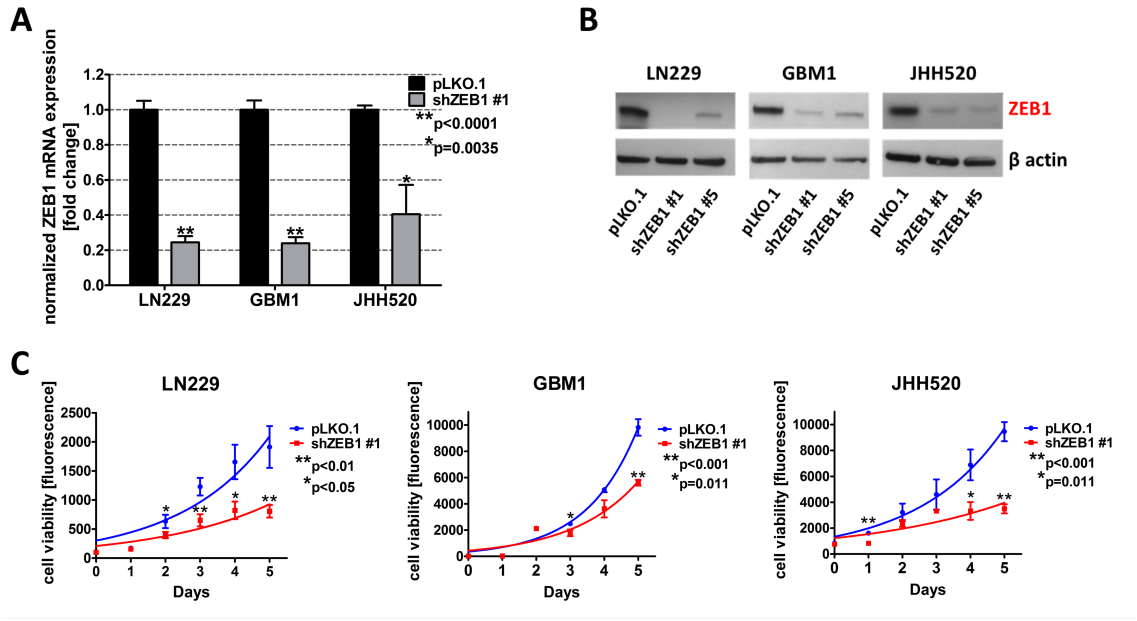


**Figure 2.3: ZEB1 knockdown reduces the cell viability.** GBM cell lines (LN229, GBM1 and JHH520) were transduced with lentiviral particles containing shZEB1 plasmids and knockdown efficiency was confirmed using RT qPCR (**A**) and Western blotting (**B**). **C.** The cell viability of ZEB1 knockdown cells was reduced as compared to control (pLKO.1) cells. Exponential growth curves were calculated for each condition and displayed in the graphs. The data is represented as mean ± SD (n = 3).

### ZEB1 knockdown alters the cellular metabolism of GBM cells

In order to assess whether the reduction of EMT influences the metabolism of GBM cells, we extracted water-soluble metabolites from cells with ZEB1 suppression and control cells. The extracts were analyzed via $^{1}$H-NMR spectroscopy and differences in the relative metabolite concentrations of both conditions were calculated. Figure 2.4A shows a typical spectrum of GBM cell metabolic extracts with the most prominent peaks representing lactate (Lac), alanine (Ala), acetate (Ac), glutamate (Glu), glutamine (Gln), glutathione (GSH), creatine (Cre), phosphocreatine (PCre), free choline (fCho), phosphocholine (PC), glycerophosphocholine (GPC), total choline (tCho; comprising fCho, PC and GPC), myo-inositol (myo), and glycine (Gly). ZEB1 knockdown significantly ($p < 0.05$) alters the intracellular levels of multiple metabolites belonging to various metabolic networks including Glu, GSH, Cre, PC, tCho, and Gly (Suppl.Fig. 2.12). Given the importance of choline metabolism in malignant transformation and its utility for clinical brain tumor diagnostics [185] we decided to focus our studies on alterations in choline derivatives.

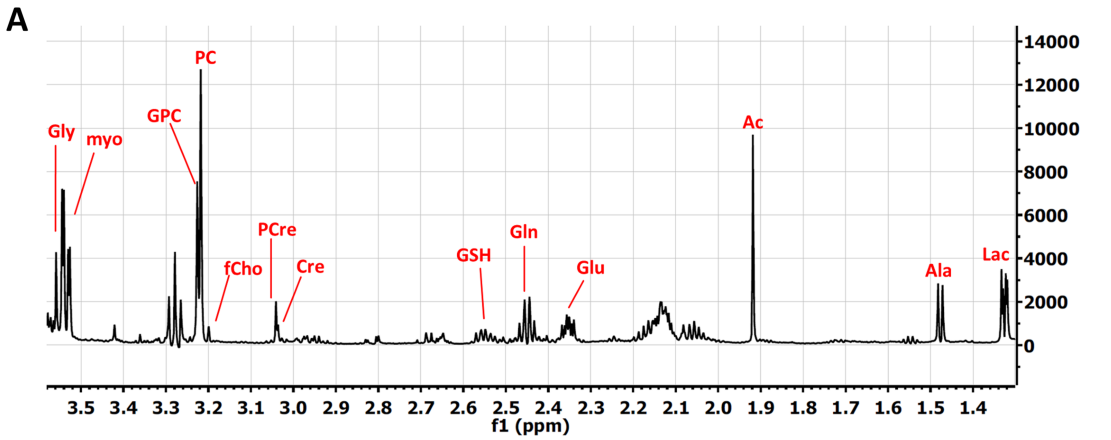


***Water soluble metabolites:*** *lactate (Lac), alanine (Ala), acetate (AC), glutamate (Glu), glutamine (Gln), glutathione (GSH), creatine (Cre), phosphocreatine (PCre), total choline (tCho) consisting of free choline (fCho) + phosphocholine (PC) + glycerophosphocholine (GPC), myo-inositol (myo) and glycine (Gly)*

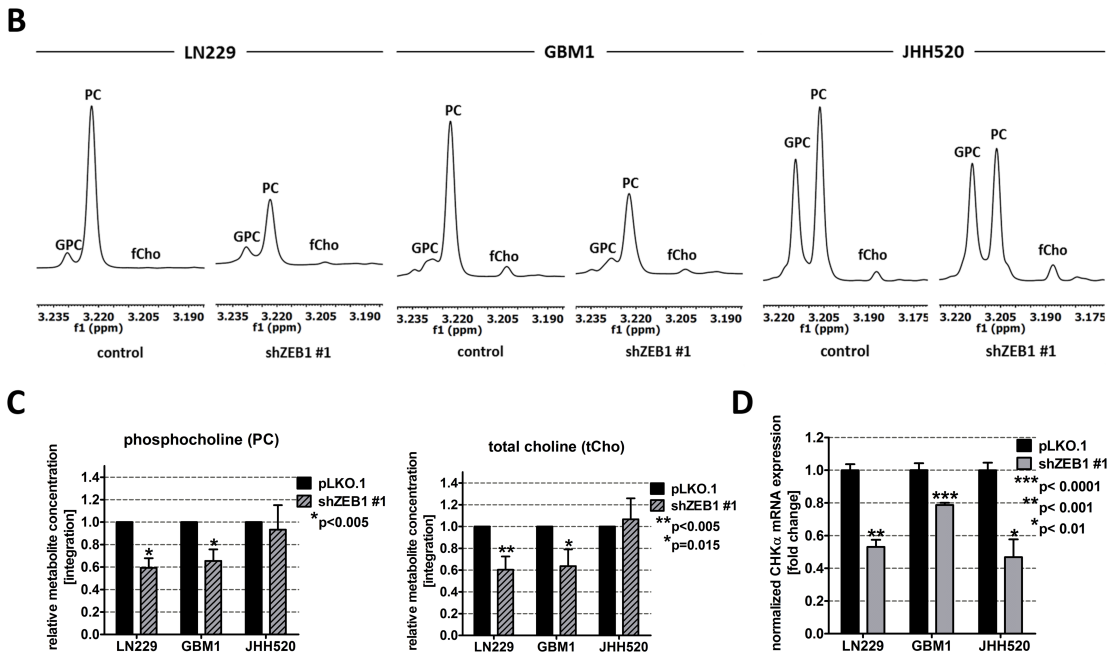


**Figure 2.4: EMT reduction by ZEB1 knockdown alters choline metabolism. A.** Overview of a $^{1}$H-NMR spectrum of metabolic extracts of GBM cells. **B.** Expanded regions of $^{1}$H-NMR spectra of control and shZEB1 transduced cells showing the main choline metabolites. **C.** Quantitation of $^{1}$H-NMR spectra for PC and tCho from metabolic extracts of ZEB1 knockdown and control cells. **D.** Expression of CHKA mRNA in ZEB1 knockdown cells was measured using RT qPCR and compared to control transduced cells. Abbreviations: ppm, parts per million. The data is represented as mean ± SD (n = 3).

### The EMT activator ZEB1 alters choline metabolism by regulating choline kinase alpha (CHK$\alpha$)

ZEB1 depletion reduced the cholinic phenotype, since we detected decreased amounts of the choline metabolites PC and tCho in ZEB1 knockdown cells. Representative choline metabolite peaks of $^{1}$H-NMR spectra and corresponding relative quantifications are shown in Figure 2.4B and 2.4C, respectively. ZEB1 knockdown led to a significant reduction of PC in LN229 ($p < 0.01$) and GBM1 cells ($p < 0.01$). Furthermore, we could detect a significant reduction of tCho ($p < 0.01$ for LN229 and $p = 0.015$ for GBM1) concentrations. In JHH520 GBM cells, ZEB1 depletion did not significantly change PC or tCho concentrations. Next we wanted to investigate which metabolic regulator might account for the ZEB1-mediated alterations in choline metabolism and investigated the expression of the cardinal choline metabolism regulating enzyme CHK$\alpha$. Strikingly, ZEB1 inhibition resulted in suppressed *CHKA* mRNA expression in all tested cell lines ($p < 0.001$ for LN229, $p < 0.0001$ for GBM1, and $p < 0.01$ for JHH520 cells) (Figure 2.4D). As CHK$\alpha$ phosphorylates free choline to generate PC, we speculate that a reduction of CHK$\alpha$ activity most likely causes the decrease of PC and tCho that we observed after ZEB1 knockdown. This initial observation of a putative ZEB1-CHK$\alpha$ link let us investigate whether it is a bidirectionally regulated loop and if targeted CHK$\alpha$ inhibition may impact the EMT properties of GBM cells.

### CHKA knockdown alters choline metabolism similar to ZEB1 suppression

In order to test the influence of CHK$\alpha$ inhibition on EMT in GBM cells, we performed a genetic CHK$\alpha$ knockdown using short hairpin interference technology (shRNAs). RT qPCR analysis revealed a significant ($p < 0.0003$) reduction of CHK$\alpha$ gene expression of up to 75 % (Fig. 2.5A). $^{1}$H-NMR analysis of metabolic extracts showed alterations in relative choline metabolite concentrations in shCHK$\alpha$ cells similar to those found after ZEB1 knockdown. In concordance, the PC signal at 3.22 ppm was highly reduced after CHK$\alpha$ depletion (Fig. 2.5B). Further statistical analysis highlighted a significant reduction of PC ($p < 0.05$) and tCho ($p < 0.05$) in CHK$\alpha$ knockdown cells as compared to control vector transduced cells (Fig. 2.5C). In addition, CHK$\alpha$ knockdown significantly ($p < 0.05$) decreased the product (PC) to educt (fCho) ratio of CHK$\alpha$, suggesting that the reduced amount of PC results from CHK$\alpha$ suppression (Fig. 2.5D). We also noticed alterations in intracellular concentrations of other metabolites after CHK$\alpha$ depletion as presented in supplementary figure 2.13A. CHK$\alpha$ knockdown significantly increased Cre ($p < 0.05$) and GPC ($p < 0.05$) and decreased Lac ($p < 0.05$). We further detected a significant increase of the Cre/PCre ratio in both LN229 ($p < 0.05$) and GBM1 ($p < 0.05$) shCHK$\alpha$ cells (Suppl. Fig. 2.13B), indicating reduced phosphorylation of Cre by creatine kinase brain-type (CKB). Indeed, we could confirm decreased expression of *CKB* in LN229 ($p < 0.05$) and GBM1 ($p > 0.05$) shCHK$\alpha$ cells (Suppl. Fig. 2.13C).

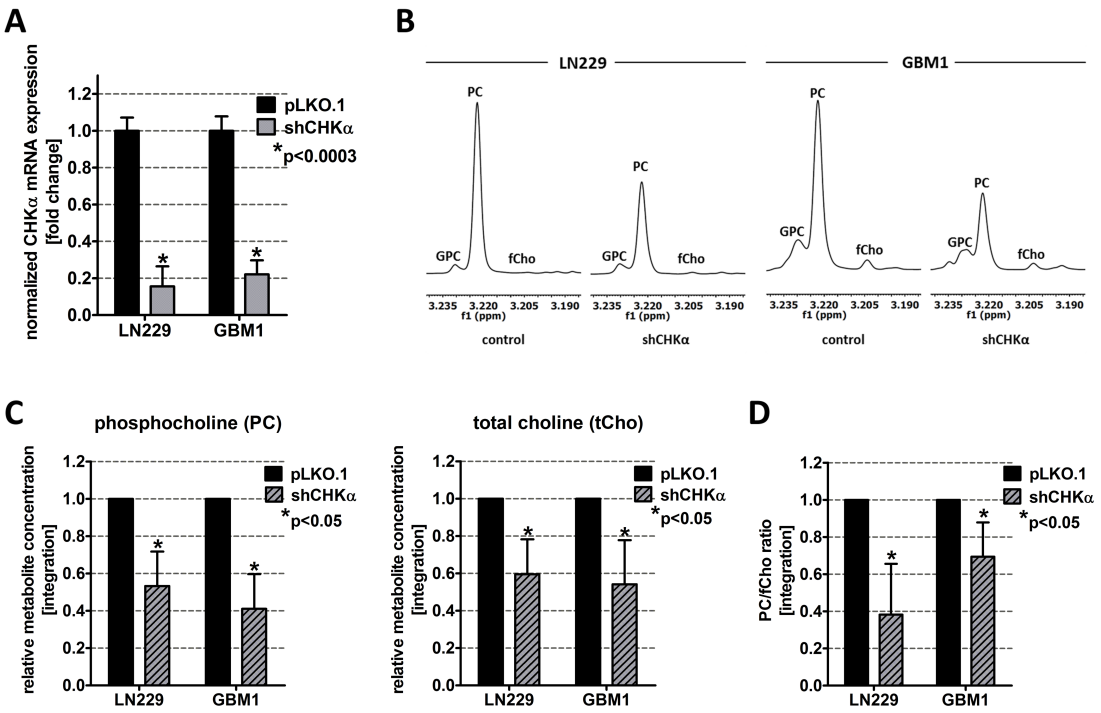


**Figure 2.5: Choline Kinase alpha (CHK$\alpha$) knockdown leads to similar alterations in choline metabolism as ZEB1 knockdown. A.** CHK$\alpha$ suppression was confirmed on mRNA level by RT qPCR. **B.** Expanded regions of $^{1}$H-NMR spectra of control and shCHK$\alpha$ transduced LN229 and GBM1 cells showing the main choline metabolites. **C.** Quantitation of $^{1}$H-NMR spectra for PC and tCho from metabolic extracts of CHK$\alpha$ knockdown and control cells. **D.** Ratio of phosphocholine and free choline (product and educt of CHK$\alpha$). The data is represented as mean ± SD (n = 3).

### Cells that express CHK$\alpha$ are positive for the stem cell marker SOX2 and the mesenchymal marker VIMENTIN

As we found a link between CHK$\alpha$ and the EMT activator ZEB1, we further analyzed if cells with CHK$\alpha$ also express other EMT/BTSC markers. We therefore performed fluorescence microscopy on all analyzed cell lines and stained for the mesenchymal marker VIMENTIN and the stem cell marker SOX2 in combination with CHK$\alpha$ (Fig. 2.6). CHK$\alpha$ staining could be detected in the cytoplasm as well as in the nucleus of the whole cell population, although the expression level differed between cells. The transcription factor SOX2 was expressed in the nucleus of all cells, elucidating the immature character of GBM cells. VIMENTIN could be detected predominantly in the cytoplasm and the expression level differed between the cells. Most interestingly, cells with more VIMENTIN staining tend to have higher expression of CHK$\alpha$. In the co-staining for SOX2 and CHK$\alpha$ we could not detect coherences, as all cells exhibit a strong SOX2 staining. Of note, especially in LN229 cells CHK$\alpha$ tends to accumulate in an area close to the nucleus in a puncta-like structure, presumably in cells undergoing cell division (Fig. 2.6A). In the past, several publications could correlate CHK$\alpha$ expression with cell cycle regulation and mitosis in different tumor entities [122, 186]. Our results now suggest that there could be a correlation between cell division and CHK$\alpha$ expression in GBM as well.

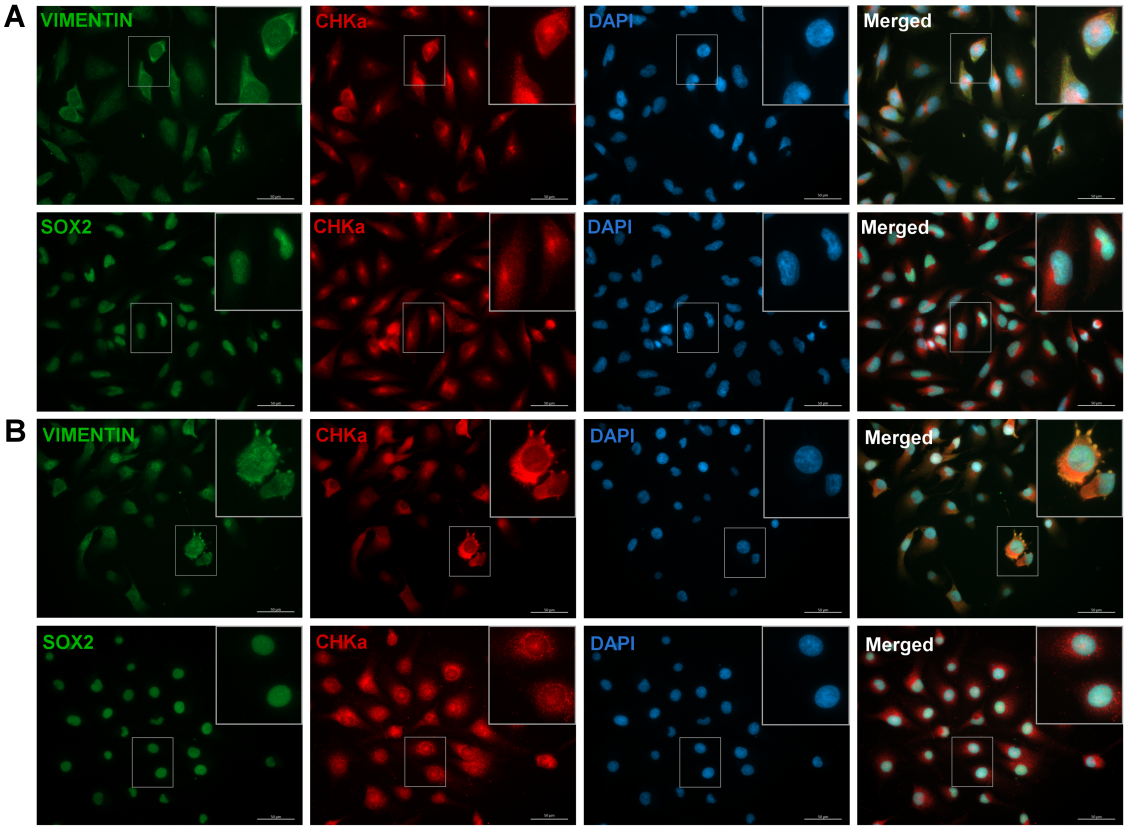


**Figure 2.6: CHK$\alpha$ is co-expressed with the mesenchymal marker VIMENTIN in GBM cells.** Immunocytochemical staining was performed for CHK$\alpha$ (red), VIMENTIN (green), SOX2 (green), and DAPI (blue) in LN229 (**A**) and JHH520 (**B**) cells. All cells were stained positive for the three tested proteins. VIMENTIN/CHK$\alpha$/DAPI and SOX2/CHK$\alpha$/DAPI co-stainings revealed that CHK$\alpha$ expression correlates with the expression of VIMENTIN but not with SOX2 in all tested cell lines. Scale bar: 50 µm; GBM1 not shown.

### Choline kinase alpha knockdown reduces the expression of EMT activators and neural stem cell markers

Given our results of a putative EMT-choline metabolism loop and the co-expression of CHK$\alpha$ and the mesenchymal marker VIMENTIN, we tested the influence of CHK$\alpha$ suppression on the expression of EMT associated genes. We found that suppression of CHK$\alpha$ caused a strong reduction of ZEB1, ZEB2, TWIST 1, SNAI1, and SNAI2. Quantification of RT qPCR results revealed a 66 % reduction of *ZEB1* ($p<0.001$), 62 % reduction of *TWIST1* ($p=0.0014$) and a 53 % reduction of *SNAI1* ($p<0.001$) in LN229 and a 77 % reduction of *ZEB1* ($p<0.0001$), a 63 % reduction of *ZEB2* ($p<0.0001$), a 47 % reduction of *SNAI1* ($p=0.002$), and a 78 % reduction of *SNAI2* in GBM1 cells (Fig. 2.7A). ZEB1 suppression was further confirmed on protein level with up to 57 % reduction in LN229 and 21 % reduction in GBM1 cells (Fig. 2.7B). CHK$\alpha$ depletion in JHH520 cells suppressed *SNAI2* mRNA expression by 76 %, *TWIST1* mRNA expression by 96 % ($p < 0.0001$) and TWIST1 protein expression by up to 73 % but had no effect on ZEB expression. TWIST1 baseline protein expression in LN229 and GBM1 was too low to be detected. Furthermore, we assessed the influence of CHK$\alpha$ on the expression of known EMT target genes and found that CHK$\alpha$ depletion reduced the expression of N-cadherin

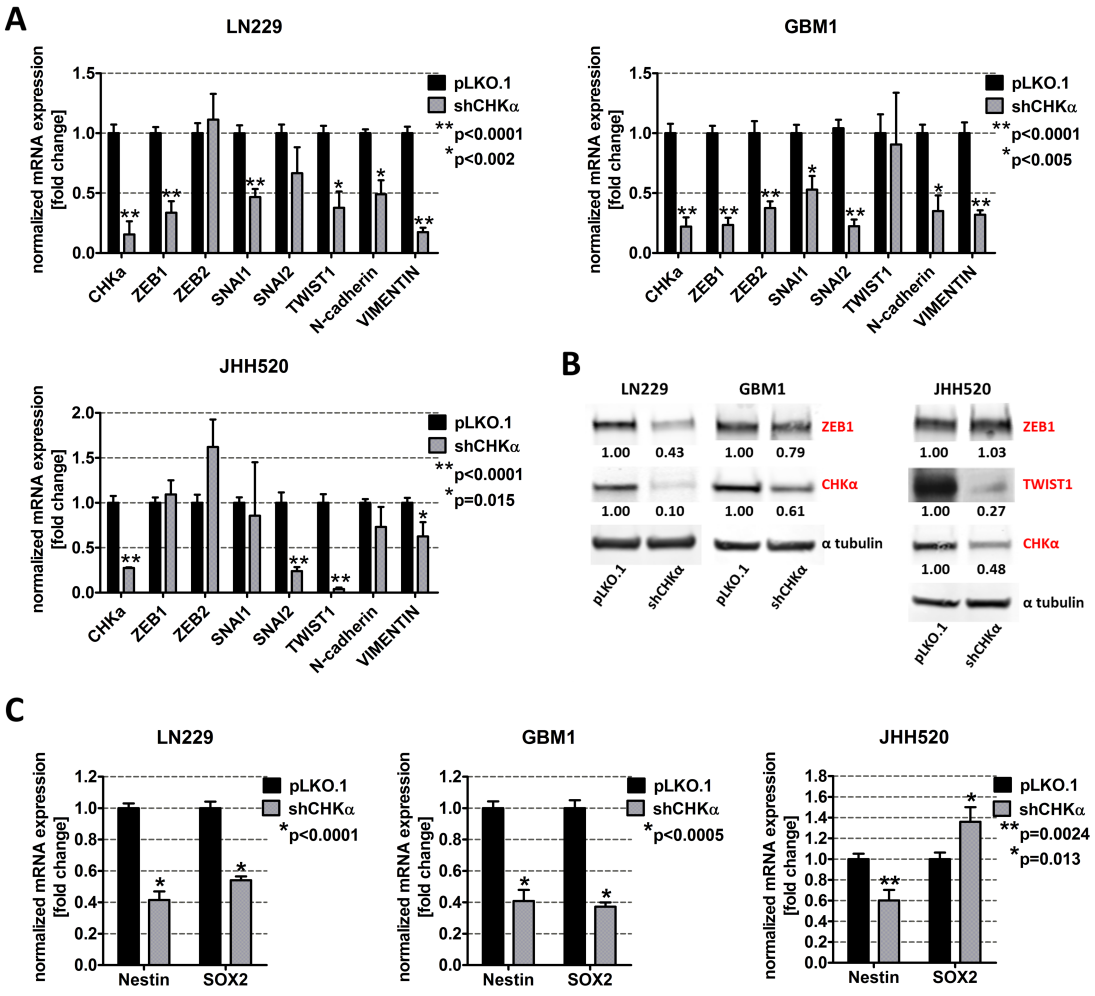


**Figure 2.7: Suppression of CHK$\alpha$ reduces the expression of EMT-associated genes and neural stem cell markers. A.** ZEB1, ZEB2, SNAI1, SNAI2, TWIST1, N-cadherin, and VIMENTIN mRNA levels were analyzed by RT qPCR in shCHK$\alpha$ cells and compared to controls. **B.** ZEB1, TWIST1, and CHK$\alpha$ protein expression levels were detected using immunoblotting in shCHK$\alpha$ and control cells. **C.** Nestin and SOX2 mRNA expression levels in shCHK$\alpha$ cells were analyzed by RT qPCR and compared to control cells. The data is represented as mean ± SD (n = 3).

by 50 % in LN229 ($p < 0.02$) and by 65 % in GBM1 ($p < 0.05$) cells. The expression of VIMENTIN was reduced by 83 % in LN229 ($p < 0.0001$), by 68 % in GBM1 ($p < 0.0001$), and by 38 % in JHH520 ($p < 0.02$) cells with CHK$\alpha$ knockdown, which is in concordance with our immunofluorescence data. As mesenchymal cells are characterized by high levels of stem cells markers, we analyzed the expression of the neural stem cell markers Nestin and SOX2 in shCHK$\alpha$ and control cells. CHK$\alpha$ suppression significantly reduced the expression of *NESTIN* in LN229 ($p<0.0001$), GBM1 ($p<0.0001$) and JHH520 ($p=0.0024$) cells and *SOX2* in LN229 ($p<0.0001$) and GBM1 ($p<0.0001$) cells (Fig. 2.7C). Together these results provide important insight into the ability of CHK$\alpha$ to regulate the activation of EMT and the stem cell character of GBM cells.

### Knockdown of choline kinase alpha reduces the cellular viability, invasiveness and clonogenicity

Next we investigated if CHK$\alpha$ suppression is able to reduce the mesenchymal phenotype of GBM cells. Compared to their control counterparts, CHK$\alpha$ knockdown cells exhibit significantly reduced viability (Fig. 2.8A). Furthermore, we assessed the invasive behavior after CHK$\alpha$ inhibition with modified Boyden chamber assays and found a 48 % decrease in invading cells for LN229 ($p = 0.011$) and a 42 % decrease for GBM1 ($p = 0.0082$) cells (Fig. 2.8B). Moreover, depletion of CHK$\alpha$ significantly diminished the anchorage independent *in vitro* clonogenicity of our tested neurospheres lines (by 90 % in JHH520, $p < 0.0001$ and by 80 % in GBM1, $p < 0.05$). Taken together, shCHK$\alpha$ cells exhibit fewer properties of mesenchymal cells than control vector transduced cells. Furthermore, we looked at RNA sequencing data of different tumor compartments which were identified in the Anatomic Structures ISH Survey and isolated by laser microdissection. Increased expression of CHK$\alpha$ could be found in the infiltrative region and the leading tumor edge of GBMs (Suppl. Fig. 2.14).

### Pharmacological inhibition of choline kinase alpha reduces the expression of the EMT activators ZEB1 and TWIST1 in GBM cells

Targeted suppression of EMT in cancer cells is of highest clinical interest as successful mesenchymal reprogramming appears to be crucial for the invasive properties of a majority of malignant cells. In a translational approach, we applied the CHK$\alpha$-inhibitor V-11-0711 (Vertex Pharmaceuticals Incorporated) on GBM cells and tested subsequent alterations in geno- and phenotype. V-11-0711 has been shown to specifically suppress CHK$\alpha$ catalytic activity in breast cancer and HeLa cells [115, 187]. GBM1 and JHH520 neurospheres were treated with DMSO, 0.1 µM V-11-0711 or 1 µM V-11-0711 for 48 h and metabolic extracts were analyzed by $^1$H-NMR spectroscopy. As the PC signal at 3.22 ppm was highly reduced in the drug treated cells we confirmed the ability of V-11-0711 to inhibit the enzymatic activity of CHK$\alpha$ in GBM cells (Fig. 2.9A). Strikingly, pharmacological suppression of CHK$\alpha$ further led to a dose dependent reduction of ZEB1 protein in GBM1 and both ZEB1 and TWIST1 protein in JHH520 cells (Fig. 2.9B). Additionally, V-11-0711 induced a dose dependent increase of CHK$\alpha$ protein in GBM1 but not in JHH520 cell line.

### Pharmacological inhibition of choline kinase alpha reduces the viability, invasiveness and clonogenicity of GBM cells

Next we wanted to prove that pharmacological inhibition of CHK$\alpha$ can resemble the effect of our genetic inhibition model. Strikingly, treatment with 1 µM or 10 µM V-11-0711 for 48 h drastically reduced the cell viability of GBM1 and JHH520 cells (Fig. 2.10A) which we could associate with dose-dependent induction of apoptosis (Fig. 2.10B). For the following *in vitro* invasion and clonogenicity assays we therefore used V-11-0711 concentrations which induce no (0.47 µM for GBM1) or only mild apoptosis (0.2 µM for JHH520).

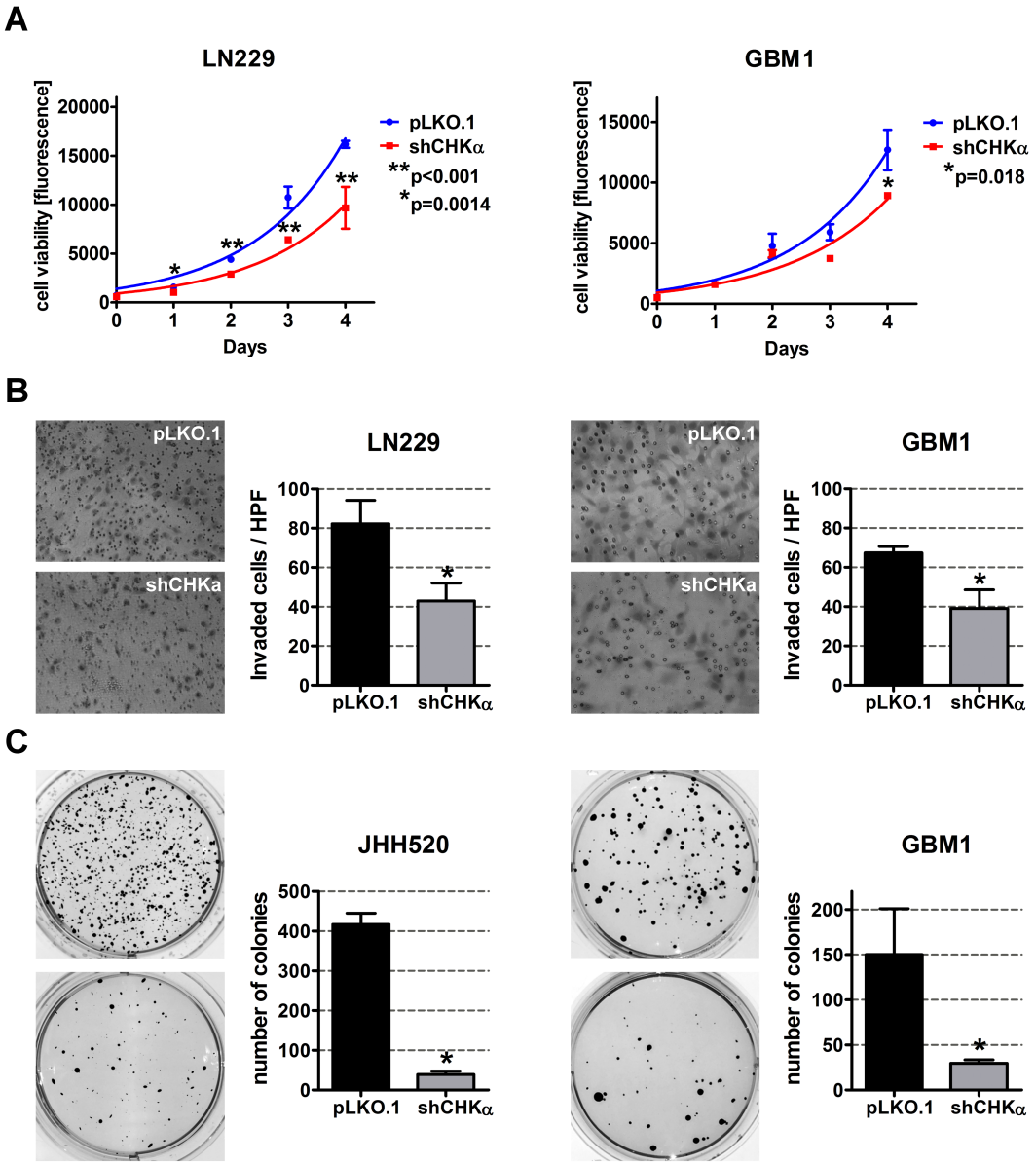


**Figure 2.8: CHKα knockdown reduces the viability, invasiveness and clonogenicity of GBM cells.** **A.** Knockdown of CHKα reduces the viability of LN229 and GBM1 cells. Exponential growth curves were calculated for each condition and displayed in the graphs. **B.** Cells with impaired CHKα expression are less invasive as assessed with modified Boyden chamber assays for 24 h. Representative pictures of hematoxylin stained invaded cells and quantifications of three Boyden chamber experiments are shown (*p < 0.05). **C.** CHKα suppression reduces the clonogenicity of JHH520 and GBM1 cells as assessed by soft agar assays. Representative pictures of NBT stained colonies and quantifications of three colony forming assays are shown (*p < 0.05). Abbreviations: HPF, high power field; NBT, 4-Nitro blue tetrazolium chloride. The data is represented as mean ± SD (n = 3).

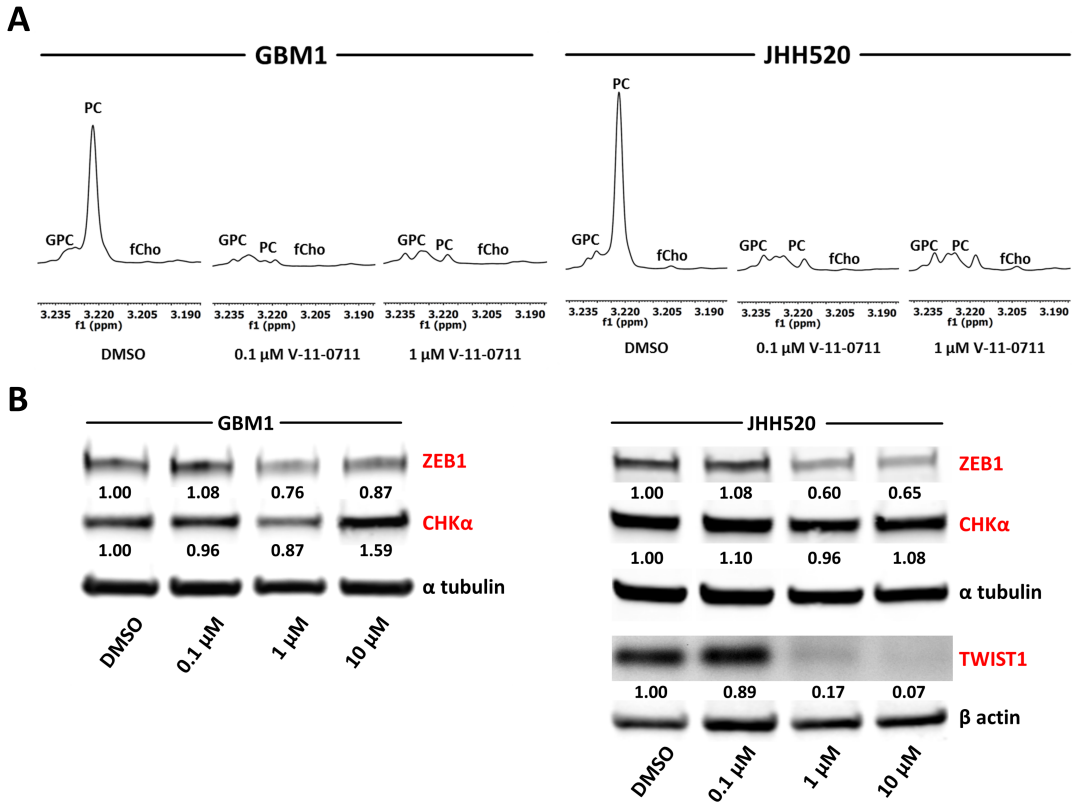


**Figure 2.9: Treatment with the choline kinase inhibitor V-11-0711 alters choline metabolism and reduces the expression of the EMT activators ZEB1 and TWIST1 in GBM cells. A.** Expanded regions of $^{1}$H-NMR spectra for the main choline metabolites of DMSO and V-11-0711 treated cells show the effectiveness of V-11-0711 treatment **B.** V-11-0711 treatment led to a suppression of ZEB1 and induction of CHK$\alpha$ protein in GBM1 and a suppression of both ZEB1 and TWIST1 protein in JHH520 cells as measured by immunoblotting. $\alpha$-tubulin and $\beta$-actin immunoblotting were used as loading controls. Abbreviations: DMSO, dimethyl sulfoxide. The data is represented as mean ± SD (n = 3).

We performed modified Boyden chamber transwell assays for 24 h in the presence of either V-11-0711 or DMSO. The cells were preincubated with indicated concentrations of the drug for 24 h. Two representative pictures and statistical analysis of three Boyden chamber assays are shown in figure 2.10C. We could detect a 66.5 % decrease of invading cells in GBM1 ($p = 0.0018$) and a 44.3 % decrease in JHH520 ($p = 0.027$) cells after drug exposure as compared to controls. Moreover, the capacity of the cells to form colonies was reduced significantly by 90 % in GBM1 ($p < 0.0001$) and by 88 % in JHH520 ($p < 0.005$) cells following treatment with V 11-0711 (Fig. 2.10D). In summary, our results unequivocally prove the potential of CHK$\alpha$ inhibition to precisely target the invasive and clonogenic population of GBM cells by suppressing key EMT activators and EMT target genes.

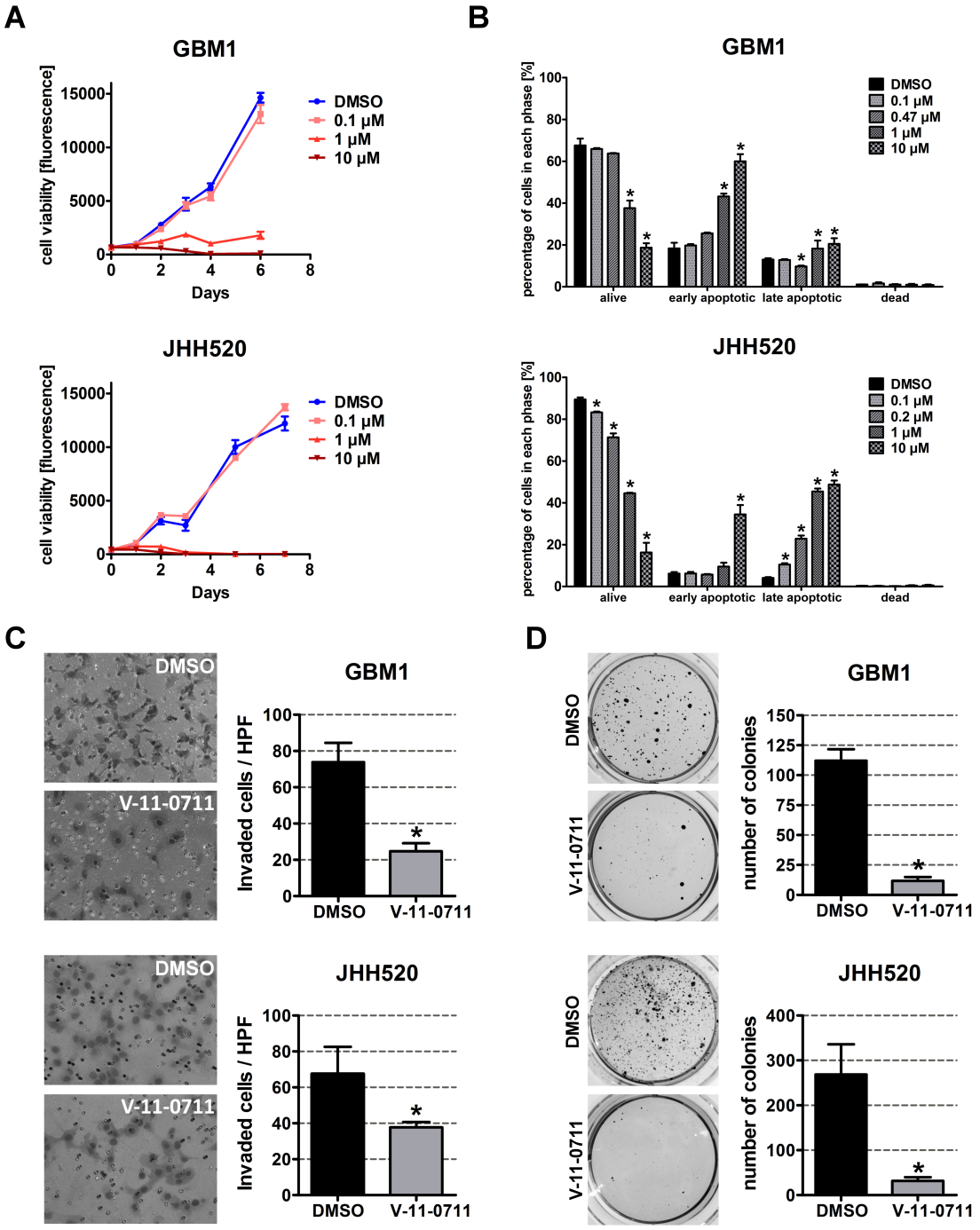


**Figure 2.10: V-11-0711 treatment reduces the viability, invasiveness, and clonogenicity of GBM cells.** **A.** Cell viability was impaired by V-11-0711 treatment in a dose dependent manner. Exponential growth curves were calculated for each condition and displayed in the graphs. **B.** V-11-0711 induces apoptosis as assessed with the Muse® Annexin V and Dead Cell Kit. Pharmacological inhibition of CHK$\alpha$ with 0.47 µM (GBM1) and 0.2 µM (JHH520) V-11-0711 led to diminished invasive capacity (**C**) of GBM1 and JHH520 cells (*$p < 0.05$) and decreased the *in vitro* clonogenicity (*$p < 0.005$) (**D**). Abbreviations: DMSO, dimethyl sulfoxide; NBT, 4-Nitro blue tetrazolium chloride. The data is represented as mean ± SD (n = 3).

**Combination treatment with Temozolomide and V-11-0711 has synergistic effects in a subset of GBM cell lines**

ZEB1 has been associated with chemo resistance in GBMs [39]. In order to assess if CHK$\alpha$ inhibition induces sensitivity to the standard chemotherapeutic in GBM therapy, temozolomide (TMZ), GBM1 and JHH520 cells were treated with either single drugs or drug combinations of V-11-0711 and TMZ. Interestingly, treatment of GBM1 cells with V-11-0711 and TMZ together had synergistic anti-growth effects in all tested drug combinations (correlation index < 1) (Fig. 2.11), whereas for JHH520 we could not detect constant synergy.

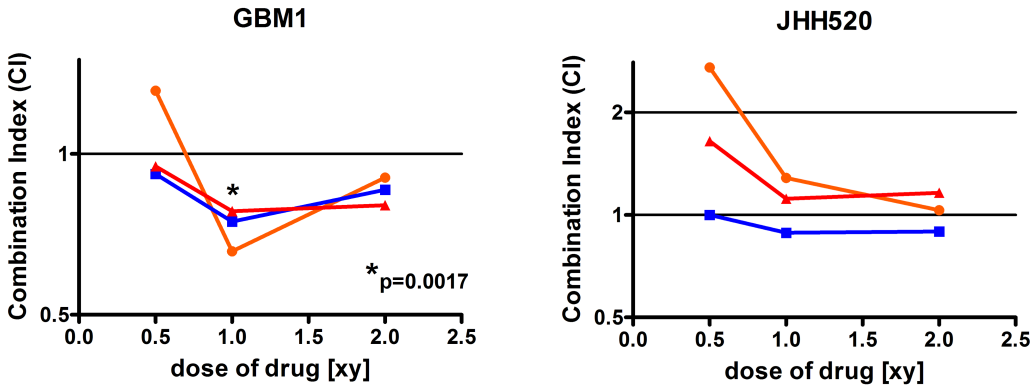


**Figure 2.11: Combinatory treatment with Temozolomide and V-11-0711 has synergistic effects in GBM1 cells.** V-11-0711 in combination with TMZ led constantly to synergistic cytotoxic effects in GBM1 but not in JHH520 cells (*p < 0.05). Abbreviations: DMSO, dimethyl sulfoxide; CI, Combination Index (CI < 1, synergistic; CI = 1, additive; CI >1, antagonistic); [xy], multiple of the single TMZ (x) and V-11-0711 (y) dose; Single TMZ dose (x): 17.5 µM for GBM1 and JHH520; Single V-11-0711 doses (y): 0.47 µM for GBM1 and 0.2 µM for JHH520.

### 2.2.5 Discussion

In this study we could show for the first time that EMT can be reduced by targeting choline metabolism in GBM. Both genetic reduction through RNA interference and pharmacological inhibition of CHK$\alpha$ with the small molecule inhibitor V-11-0711 in GBM cells significantly reduced the expression of EMT activators and EMT target genes. Furthermore, we observed impaired cellular invasiveness, clonogenicity, viability as well as reduced expression of neural stem cell markers, all hallmarks of EMT [42], upon interfering with choline metabolism.

Our approach was to study whether EMT is associated with metabolic processes in GBM cells. We therefore used a previously described EMT inhibition model based on knockdown of ZEB1 [42]. In our model we observed decreased cell viability and changes

in various intracellular metabolite concentrations in cells with reduced ZEB1. The role of ZEB1 in cell proliferation and tumor growth is not fully understood. A hallmark paper investigating the role of ZEB1 in gliomagenesis reported doubling of proliferation upon ZEB1 impairment [39], although changes in ZEB1 caused by activation of WNT signaling had no effect on proliferation [40]. Similarly, contrary results are published in other systems showing that ZEB1 promotes [188, 189], impairs [44, 190], or has no effect [191] on proliferation and cellular growth. On the metabolite level we observed a significant decrease of PC and tCho in LN229 and GBM1 cells (Fig. 2.4). High concentrations of PC and tCho, also referred to as the cholinic phenotype, could be correlated with malignant transformation in various types of cancers [105, 139], thus our results hint at reduced malignancy after EMT inhibition. We found that the molecular cause for the reduced cholinic phenotype is impaired CHK$\alpha$ expression in cells with EMT suppression, both confirmed on mRNA and protein level. Also in breast cancer, CHK$\alpha$ activity has been described as the main regulator of the cholinic phenotype [109]. CHK$\alpha$ catalyzes the phosphorylation of free choline to PC during the synthesis of the membrane lipid phosphatidylcholine, thus CHK$\alpha$ is of highest importance for the integrity of the cell membrane and a variety of signaling pathways involving membrane lipids and membrane anchored proteins [192, 193]. As expected, direct suppression of CHK$\alpha$ through RNA-interference reduced the cholinic phenotype to levels similar or even lower than observed after ZEB1 suppression (Fig. 2.5). Taken together, these results suggest that the activity of CHK$\alpha$ is associated with EMT in GBM cells. CHK$\alpha$ is broadly expressed in our tested cell line models (Fig. 2.6). This is not surprising as CHK$\alpha$ catalyzes important steps during membrane lipid synthesis and thus appears to be indispensable for the cell survival and proper function. Our co-labeling experiments revealed that cells with high levels of CHK$\alpha$ express high levels of the EMT target gene VIMENTIN [180, 181, 182]. Furthermore, we detected strong expression of the neural and glioma stem cell marker SOX2 [194, 195] in all our tested models. We could not detect any differences in SOX2 expression in cells with high or low levels of CHK$\alpha$.

Interestingly, CHK$\alpha$ knockdown reduced the protein expression of the EMT activator ZEB1 in LN229 and GBM1 cells and TWIST1 in JHH520 cells (Fig. 2.7).These results indicate that there is a bidirectional link between EMT and choline metabolism in GBM and that CHK$\alpha$ regulates EMT in a global way affecting the expression of several EMT activators. This hypothesis was further corroborated by the reduced *ZEB1*, *ZEB2*, *SNAI1*, *SNAI2* and *TWIST1* mRNA levels as well as lowered expression of EMT targets N-cadherin and VIMENTIN after CHK$\alpha$ knockdown [180, 181, 182]. Probably as a result of the reduced expression of EMT associated genes, cells with CHK$\alpha$ suppression exhibit fewer phenotypic properties of mesenchymal cells, since we detected significantly reduced invasiveness and clonogenicity in shCHK$\alpha$ cells (Fig. 2.8). Concisely, ZEB1, ZEB2, and TWIST1 have all been described to promote invasion, and clonogenicity in GBM and other tumors [41, 42, 43, 45, 50, 51, 196]. Additionally we found increased CHK$\alpha$ expression on the infiltrative leading edge of GBMs as compared to tumor parenchyma, indicating CHK$\alpha$ expression is associated with invasive properties of the tumor cells in

GBM patients (Suppl. Fig. 2.14). Taken together, this led us hypothesize that CHK$\alpha$ suppression is able to suppress the EMT phenotype in GBM. Of note, previous studies with breast cancer and ovarian cancer cells correlated CHK$\alpha$ expression with increased cellular invasiveness, migration, and proliferation [112, 197], indicating the importance of CHK$\alpha$ as a regulator of the mesenchymal phenotype in other tumors than GBM.

EMT has been associated with cancer stemness in a variety of tumors [35, 36]. Along with the impaired *in vitro* clonogenicity after CHK$\alpha$ blockade, we observed decreased expression of the stem cell genes Nestin and SOX2 after CHK$\alpha$ suppression. Both genes are established BTSC markers with prognostic value and clinical relevance [194, 198].

Mesenchymal transformation is crucial for the generation of chemo- and radioresistant BTSCs in malignant brain tumors [26, 199], thus identifying achievable approaches to inhibit EMT is of highest clinical interest. Given our evidences from the genetic studies that CHK$\alpha$ controls mesenchymal differentiation, we tested the effect of compound based CHK$\alpha$ inhibition using the CHK$\alpha$ inhibitor V-11-0711 which recently has been shown to selectively inhibit CHK$\alpha$ activity [115, 187]. Analysis of metabolic extracts with $^{1}$H-NMR spectroscopy proved the enzyme inhibiting capability of V-11-0711 in GBM cells as we did not detect any CHK$\alpha$ product - PC at 3.22 ppm – after drug exposure (Fig. 2.9). Strikingly, V-11-0711 treatment reduced the expression of the EMT activator ZEB1 in GBM1 and both ZEB1 and TWIST1 in JHH520 cells in a dose-dependent fashion. Furthermore, we detected a significant reduction in cellular viability, survival, invasiveness, and clonogenicity after drug treatment, confirming our data with genetic CHK$\alpha$ inhibition. Since V-11-0711 dose dependently induces apoptosis in GBM cells we used drug concentrations for the invasion and colony forming assays inducing no (GBM1) or very mild (JHH520) apoptosis. We further detected a dose dependent increase of the CHK$\alpha$ protein level in GBM1 cells, indicating a rescue mechanism probably triggered by the dramatically decreased PC concentrations. This also suggests that not the protein level but rather the enzymatic activity of CHK$\alpha$ is crucial for EMT regulation in GBM. Therefore, CHK$\alpha$ suppression could be a novel approach to precisely target highly invasive cancer stem cells. Of note, comprehensive CHK$\alpha$ inhibition through systemic administration of V-11-0711 or other inhibitors will impair the cell membrane synthesis in all cells and phenotypic effects will not be limited to the cancerous lesions. Therefore we envision that this potential form of therapy could be applicable as local therapy in the open resection cavity or continuous through convection enhanced delivery through intratumoraly implanted catheters to target the disseminated single cells in the next vicinity. Another possibility could be highly selective intra-arterial transfer of siRNAs or shRNAs through cerebral circulation over the blood brain barrier (BBB) to the side of the tumor to suppress CHK$\alpha$ by means of RNA interference. It has been described recently that viruses can be transported over the BBB after osmotic disruption using mannitol. This superselective intra-arterial cerebral infusion technique is already in use for the treatment of patients with recurrent malignant glioma in a phase I study and would present an alternative way to suppress CHK$\alpha$ independent from pharmacological compounds [200, 201]. We were able to successfully monitor CHK$\alpha$ and EMT inhibition through reduced intracellular PC and tCho, both after genetic

modification of the cells as well as after drug application using non-invasive $^{1}$H-NMR spectroscopy. This *ex vivo* metabolic imaging technology raises the interesting option to potentially monitor the EMT-status in cells by quantifying their intracellular choline concentrations. *In vivo* proof of principle experiments are necessary to assess whether this concept might be applied for GBM diagnostics and therapeutic treatment surveillance.

The exact mechanism of CHK$\alpha$-dependent suppression of EMT activators and reduction of GBM cell growth, invasiveness, and clonogenicity remains to be investigated. However, choline metabolism and especially CHK$\alpha$ activity has been correlated with malignant progression in various cancers [113, 171, 187, 202]. In the past, the RAS signaling pathway was found to regulate CHK$\alpha$ expression during tumor progression via phosphoinositide 3-kinase (PI3K) [202, 203, 204], thus directly linking CHK$\alpha$ activity to known oncogenes and signaling pathways driving tumor progression. Also EMT is regulated by Ras and PI3K signaling [205, 206, 207], making an indirect connection between choline metabolism and EMT regulation possible. Furthermore, a most recent study of Hu et al. [114] described CHK$\alpha$ itself to be an important player in EGFR/PI3K/AKT signaling in colorectal cancer. Therefore, CHK$\alpha$-mediated EMT induction via activation of EGFR/PI3K/AKT signaling could be a possible explanation for our observations but of course needs further investigations [208, 209]. As previous studies showed that CHK$\alpha$ overexpression increases cellular invasiveness, drug resistance and metastasis formation [114, 197], establishing a CHK$\alpha$ overexpression model in GBM would be a desirable way to further analyze the reciprocal regulation between choline metabolism and EMT in the future.

EMT activation in cancer cells is associated with increased chemotherapeutic resistance [48, 49, 210]. We found that combinatory treatment with the standard of care chemotherapeutic temozolomide (TMZ) and V-11-0711 causes synergistic cytotoxic effects in GBM1 cells (Fig. 2.11). Our results in JHH520 cells were inconsistent, indicating that not the CHK$\alpha$ expression level itself regulates drug resistance and subsequent downstream analyses are needed to address the exact mechanism.

Besides the cholinic phenotype, we detected alterations of intracellular metabolites associated with other metabolic networks after EMT/CHK$\alpha$ inhibition such as increased creatine. Cre has been described as a putative anti-cancer agent and could be correlated with inhibition of tumor cell growth [211, 212]. The observed increase of Cre could result from reduced creatine kinase B (CKB) activity. CKB catalyzes the phosphorylation of creatine to phosphocreatine, which has been shown to promote tumorigenesis [213, 214]. Indeed, depletion of CHK$\alpha$ resulted in reduced mRNA expression of CKB and an increase of the Cre/PCre ratio (Suppl. Fig. 2.13). These results further emphasize the oncogenic role of CHK$\alpha$ in cancer cells and indicate that the effect on cellular metabolism caused by CHK$\alpha$-mediated EMT reduction is not only limited to choline homeostasis.

In conclusion we could identify CHK$\alpha$ as a powerful regulator of EMT in GBM cells. This opens the possibility to target chemotherapy resistant BTSCs through impairing their mesenchymal differentiation. Furthermore, we confirmed V-11-0711 as a potent CHK$\alpha$ and EMT inhibitor and suggest that our identified EMT-oncometabolic network may

also be helpful to develop more tailored diagnostics monitoring the invasive properties of GBMs as well as surveilling the success of anti-EMT therapy. Given the importance of EMT for tumor progression and tumor stem cells in a variety of other tissue types, our discoveries could impact also other fields of oncology.

### 2.2.6 Methods

#### Cell culture and V-11-0711 treatment

LN229 was purchased from American Tissue Culture Collection (Manassas, VA). JHH520 neurospheres were generously provided by G. Riggins (Johns Hopkins Hospital Baltimore, United States of America) and GBM1 neurospheres were generously provided by Dr Angelo Vescovi (Milan, Italy). HEK293T cells were also purchased from American Tissue Culture Collection (Manassas, VA). All cell lines were cultivated under standard cell culture conditions of temperature (37°) and carbon dioxide (5 %). GBM1 and JHH520 cell lines were both cultured as neurospheres in DMEM w/o pyruvate (Gibco) supplemented with 30 % Ham's F12 Nutrient Mix (Gibco), 2 % serum free B27 supplement (Gibco), 20 ng/ml human recombinant bFGF (Peprotech), 20 ng/ml human recombinant EGF (Peprotech), 5 µg/ml Heparin (Sigma Aldrich), and 1x Anti-Anti Penicillin Steptomycin Fungizone® mixture (Gibco). LN229 and HEK293T cells were propagated to monolayer growth in DMEM with pyruvate (Gibco) plus 10 % Fetal Calf Serum (FCS; Biochrome) and 1x Anti-Anti Penicillin Steptomycin Fungizone® mixture (Gibco). Cells were passaged regularly to avoid acidification of media. All cell lines were routinely tested for the absence of mycoplasma contamination using the PCR-based Mycoplasma Test Kit I/C from Promokine and tested for their identity using short tandem repeat testing [215].

A stock solution of the CHK$\alpha$ inhibitor V-11-0711 was prepared in DMSO and stored at 37°. For immunoblotting, cells were cultured for 48 h under general cell culture conditions in the presence of various concentrations of V-11-0711 diluted in neurosphere medium. For all experiments with V-11-0711 we decided to use JHH520 and GBM1 cells as they both can be cultured without 10 % serum which we found to interfere with the activity of small molecules.

For the combinatory treatment with TMZ and V-11-0711, the cells were cultured with different concentrations of the single drugs or both in combination (Single doses of V-11-0711: 0.47 µM for GBM1 and 0.2 µM for JHH520; Single doses of TMZ: 17.5 µM). Therefore, triplicates of 2000 cells in 100 µl were seeded in 96 –wells and cultured in medium supplemented with the desired drug concentration. After six days the cell viability was determined with the CellTiter-Blue® Cell Viability Assay (Promega) due to the manufacturer's instructions. The combination index (CI) was calculated as described before using the program CompuSyn (ComboSyn Inc., Paramus, NJ. 07652 USA) [216]. Due to the algorithm of the software, a CI < 1 accounts for synergistic, a CI = 1 for additive, and a CI > 1 for antagonistic effects. The significance of the synergistic effect (*p < 0.05) was

calculated compared to additive effect (CI = 1).

### Generation of lentiviral particles

The third generation lentiviral packaging system was used for the generation of lentiviral particles as previously described [40]. In brief, HEK293T cells were transfected with the lentiviral vector of choice and three different packaging plasmids (pMDLgpRRE, pRSVREV and pMD2VSVG) using GeneJuice® Transfection Reagent (Merck Millipore). Virus supernatant was collected at time points 48 h, 72 h and 96 h post transfection. Interference RNA sequences against CHK$\alpha$ were designed with the software Primer3 [217] and cloned into the pLKO.1 TRC vector (Addgene plasmid #10878, [218]). Plasmids containing shRNAs against ZEB1 were derived as described previously [42].

### Quantitative Real time PCR

Total RNA was extracted using the RNeasy Mini Kit (Qiagen) due to the manufacturer's instructions. The RNA concentration was photometrically assessed using the Nanodrop2000 spectrometer (Thermo Scientific). Two micrograms of RNA were utilized to synthesize complementary cDNA single strands using M-MLV reverse transcriptase (Promega) and random hexameric primers. Quantitative real time PCR was carried out using the Sso Advanced SYBR Green Supermix (BioRad) in a CFX Connect Thermocycler (BioRad). A total of 10 ng cDNA and 10 pmol per primer were used in each qPCR reaction. The relative quantifications were normalized to the endogenous housekeeping genes $\beta$-actin and $\beta$-2-microglobulin. Calculation of normalized relative gene expression was performed by supplied software of the CFX Connect Real-Time PCR Detection System (Bio-Rad). The figures show data from three independent experiments represented as mean ± SD. An unpaired student t test was performed to calculate statistical significance. The Primer sequences can be found in table 2.2.

### Western Blotting

Cells were lysed in ice-cold RIPA buffer and protein concentrations were determined using the DC Protein Assay Kit (BioRad). Incubation with primary antibodies against ZEB1 (1:2000, Sigma #HPA027524), CHK$\alpha$ (1:500, Abcam #ab88053), TWIST1 (1:100, Santa Cruz #sc-81417), $\beta$-actin (1:1000, Santa Cruz #sc-130657) and $\alpha$-tubulin (1:10000, Sigma #T9026) was performed overnight at 4° on a 3D-shaker in 5 % milk powder (Carl Roth) in TBST. As secondary antibodies we used goat-anti-rabbit IRDye800CW (1:10000, LI-COR #926-32211), goat-anti-mouse IRDye680RD (1:10000, LI-COR #926-68070) and goat anti-rabbit-HRP (1:10000, Jackson Immuno Research #111-035-144) diluted in blocking solution and incubated for 1 h at room temperature. Signal detection was performed either on a film based system by applying Super Signal West Pico Chemiluminescent Substrate (Thermo Scientific) or on a luminescence based

system in a LI-COR Odyssey CLx Imager (LI-COR). Densitometry was done using supplied software from LI-COR or ImageJ software [219]. Densitometry values for ZEB1 and CHK$\alpha$ were normalized to the corresponding $\alpha$-tubulin values, TWIST1 was normalized to $\beta$-actin.

**Dual-phase metabolite extraction of cell cultures**

At least 5x10$^6$ cells were harvested, counted in triplicates and subjected to methanol-chloroform-water (1:1:1, v:v:v) dual-phase extraction as previously described [109, 220]. In brief, cells were washed twice with 10 ml ice-cold saline, resuspended in 850 µl ice-cold dd$H_2O$ and transferred into a pre-chilled glass centrifuge tube. A total of 4 ml of ice-cold methanol were added and the cells were vortexed vigorously and incubated on ice for 15 min. Then 4 ml of ice-cold chloroform were added, vortexed and incubated for 10 min on ice. Finally, 3.15 ml of chilled dd$H_2O$ were added, vortexed and incubated at 4 ° overnight to enable phase separation. Next day, the samples were centrifuged for 30 min at 4500 rpm at 4 °, and the upper phase containing the water soluble metabolites was carefully separated, supplemented with 10 mg of Chelex® 100 resin (Sigma Aldrich) and incubated on ice for 10 min to remove divalent cations. After filtration through a 70 µM mesh the samples were centrifuged for 1 h in a vacuum concentrator at 30 ° to evaporate the methanol. Subsequently, the samples were frozen at –80 °, lyophilized and stored at –80 ° until measurement.

**$^1$H-NMR data acquisition and processing**

The lyophilisates were resuspended in 20 mM phosphate buffer (pH 7.0) containing 10 % $D_2O$ and 4,4-dimethyl-4-silapentane-1-sulfonic acid (DSS, euriso-top) or 3-(Trimethylsilyl) propanoic acid (TSP; Lancaster Synthesis) as an internal standard. $^1$H-NMR spectra of extracts were acquired on a Bruker AVANCE III HD 700 spectrometer equipped with a 5 mm HCN TCI cryo-probe operating at 700 MHz (16.4 T). The $^1$H-NMR data were obtained using excitation sculpting for water suppressing and the following acquisition parameters: 25 ° sample temperature, 9800 Hz sweep width, 3.2 sec repetition time and time-domain data points of 32 K and 256 transients. Spectra were processed and analyzed using Mestrenova version 8.0.1-10878 (Mestrelab Research S.L.). Metabolite intensities of different samples were normalized to a standard of the same concentration in each measurement. The figures show data from three independent experiments represented as mean ± SD. Furthermore, an unpaired student t test was performed to calculate statistical significance.

**Double immunofluorescence stainings**

LN229, GBM1, and JHH529 cells were plated onto coverslips in 24-well plates. For GBM1 and JHH520 cells, the coverslips were pre-coated with 50 µg/ml laminin (Sigma)

for 1 h at 37°. After three hours incubation at 37° and 5 % $CO_2$, the cells were washed with PBS and fixed with 4 % Paraformaldehyde in PBS for 20 min at RT. The cells were washed again with PBS and incubated with blocking buffer (PBS pH 7.4, 10 % Normal Goat Serum (Gibco), 0.5 % TX-100, 0.05 % Tween20) for 2 h at RT. Cells were stained with rabbit-anti-CHK$\alpha$ (1:250, Abcam #ab88053) and either mouse-anti-VIMENTIN (1:1000, #) or mouse-anti-SOX2 (1:100, Cell Signaling #4900S) primary antibodies diluted in blocking buffer overnight at 4°. Secondary antibodies (goat anti-mouse Alexafluor488 (1:1000, Thermo Fisher #A-11029) and goat anti-rabbit Alexafluor594 (1:1000, Thermo Fisher #A-11037) were incubated for 2 h at RT. Preparations were mounted in ProLong Gold + DAPI (Thermo Fisher) and fluorescent images were obtained by a LSM 700 microscope, Carl Zeiss, and analyzed in ZEN software (Carl Zeiss). Controls were performed with omission of one or both primary antibodies.

**Cell viability and Apoptosis assays**

For the assessment of cell viability, cell numbers were adjusted to defined concentrations (20.000 cells/ml for GBM1 and JHH520; 15.000 cells/ml for LN229). For the analysis of ZEB1 and CHK$\alpha$ knockdown cells we used cells from passages 3 to 10 post transduction to exclude a transient effect from viral transduction. Triplicates of 100 µl were plated into each well of a 96-well plate. On five consecutive days the relative viable cell mass was determined using the CellTiter-Blue® Cell Viability Assay (Promega) due to the manufacturer's instructions. Fluorescence was measured after two h substrate incubation on cells using the Tecan Safire 2 Multiplate reader (Tecan) at 560ex/590em. Exponential growth curves were calculated for each condition and displayed in the graphs with GraphPad Prism 5 (GraphPad Software, Inc., USA).

In order to test if V-11-0711 treatment induces apoptosis in GBM cells, GBM1 and JHH520 cells were treated with different concentrations of V-11-0711 for 48 h. Afterwards, the percentages of living, early apoptotic, late apoptotic, and dead cells were assessed using the "Muse® Annexin V and Dead Cell Assay Kit" for the Muse® cell analyzer (Merck Millipore) due to the manufacturer's instructions.

**Invasion and clonogenicity assays**

Invasion of GBM cells was assessed with a modified Boyden chamber assay as described previously [42]. In brief, a total of $1*10^5$ cells were plated per Matrigel (BD) coated insert in DMEM w/o FCS, DMEM with 10 % FCS was added in the lower chamber. After an incubation of 24 h the experiment was terminated and the remaining non-invaded cells on the upper surface of the membrane were removed carefully by swabbing. The filter was fixed with methanol (–20°) for 10 min, washed with PBS and subsequently stained with hematoxylin for 5 min. After destaining with warm water, five pictures were taken per well and the stained invaded cells were counted. For the drug treatment experiments, cells

were pretreated for 24 h with 1 µM (GBM1) or 0.5 µM (JHH520) V-11-0711 in standard culture conditions before assessing their invasiveness in a time window of 24 h.

For the assessment of the clonogenic capacity of GBM cells we performed Soft agar assays as described previously [215]. In brief, six-well plates were coated with 1.5 ml of a base layer of 1 % agarose (Gibco) in neurosphere medium and placed in 4° for 1 h. A top layer containing 0.6 % agarose and a single-cell suspension (3500 cells/well for GBM1 and 5000 cells/well for JHH520) in 2 ml neurosphere medium was plated on top of the base layer and incubated at RT for 1 h. Once the cell layer was solidified 2 ml of neurosphere medium (for V-11-0711 treatment studies either supplemented with drug or vehicle) were added to each well. Every three days 500 µl fresh medium (for V-11-0711 treatment studies either supplemented with drug or vehicle) were added to each well. On day 21, 1 ml of a 1 mg/ml 4-Nitro blue tetrazolium chloride (NBT) solution (Sigma Aldrich) was added and incubated overnight at 37° to stain the colonies. The experiments were quantified using the Clono Counter software [221].

**RNA sequencing data from IVY Glioblastoma Project**

RNA sequencing data was generated from anatomic structures isolated by laser microdissection. Five tumor structures (Leading Edge, Infiltrating Tumor, Cellular Tumor, Microvascular Proliferation, and Pseudopalisading Cells around Necrosis) were identified by H&E staining and compared to hyperplastic blood vessels and the microvascular proliferative region. A total of 122 RNA samples were generated from 10 tumors and used for sequencing. Website: © 2015 Allen Institute for Brain Science. Ivy Glioblastoma Atlas Project [Internet]. Available from: glioblastoma.alleninstitute.org.

**Acknowledgements**

The authors thank Guido Reifenberger and his research team (Department of Neuropathology, University Medical Center Düsseldorf), Kristine Glunde (Department of Radiology, Johns Hopkins University) and Hans-Jakob Steiger (Department of Neurosurgery, University Medical Center Düsseldorf) for their support. The authors would like to thank Vertex Pharmaceuticals Incorporated for providing V-11-0711. The authors acknowledge access to the Jülich-Düsseldorf Biomolecular NMR Center that is jointly run by Forschungszentrum Jülich and Heinrich-Heine-Universitaet Düsseldorf.

**Grant Support**

KK is a scholar of the Düsseldorf School of Oncology (DSO) of HHU University. AKS is supported by the Friedrich-Ebert Stiftung. The work has been co-financed by the SFF Grants of the HHU University, Düsseldorf, Germany, awarded to JM and UDK.

### Disclosure

The authors report no conflict of interest.

## 2.2.7 Supplement

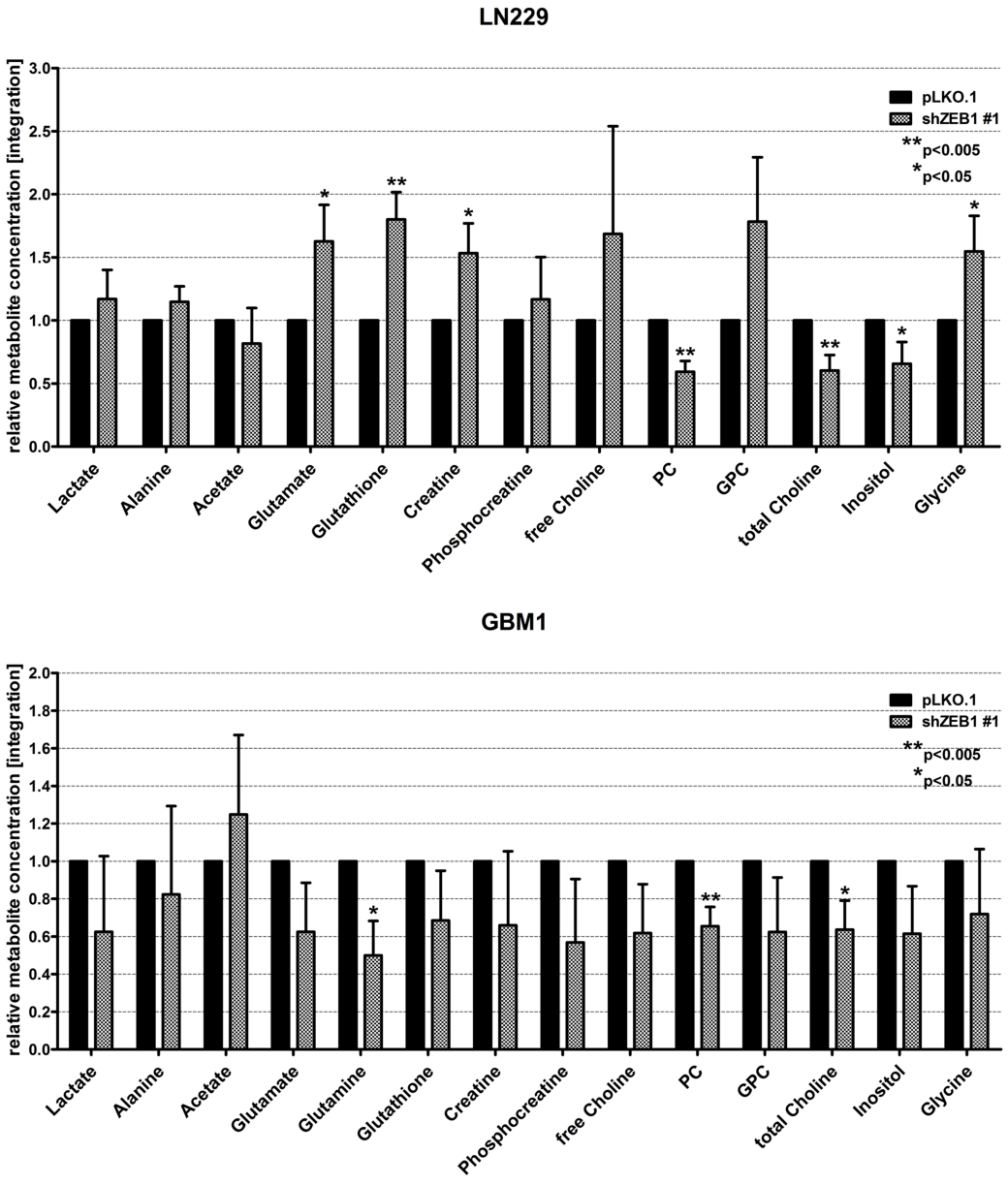


**Figure 2.12: ZEB1 alters the metabolism of LN229 and GBM1 cells.** Water soluble metabolites of shZEB1#1 and pLKO.1 control cells were analyzed with $^{1}$H-NMR spectroscopy. The relative metabolite concentrations of three independent experiments are displayed as mean ± SD.

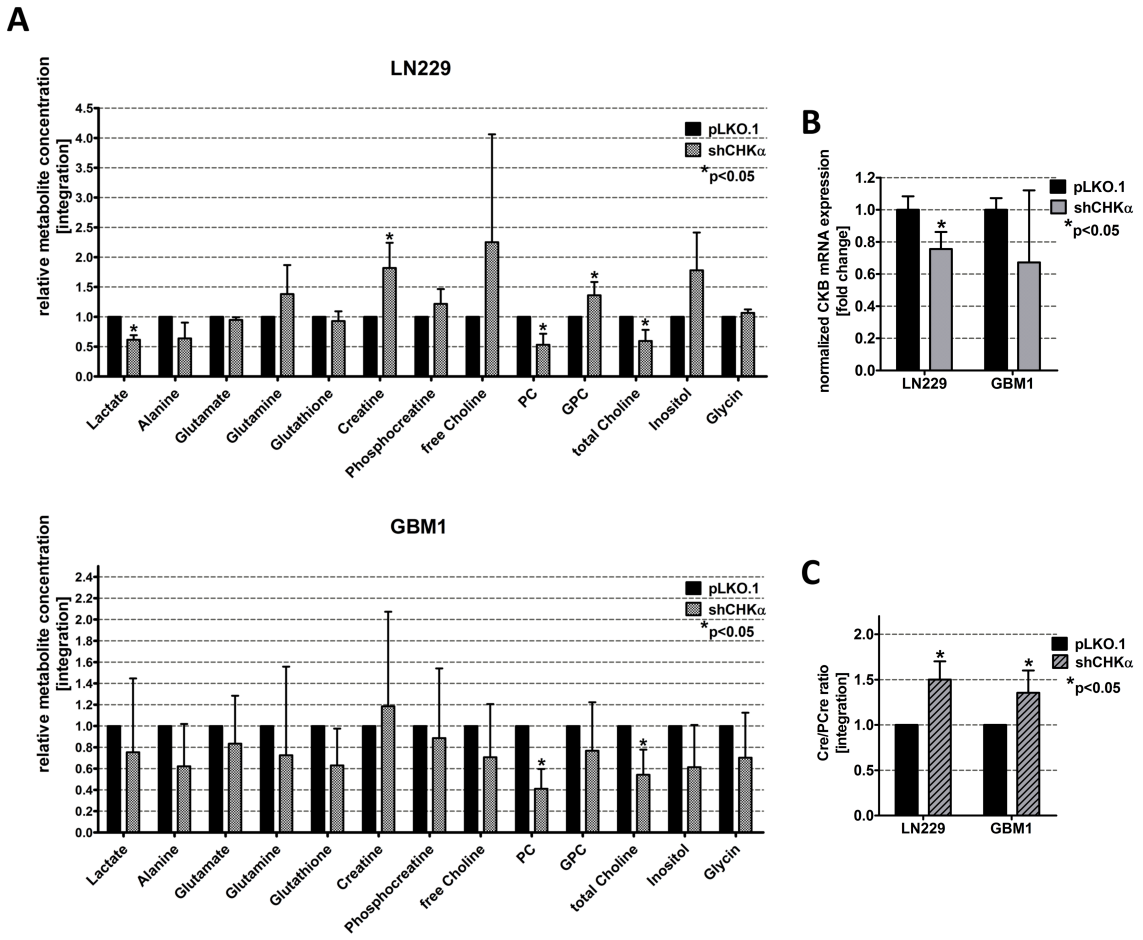


**Figure 2.13: CHK$\alpha$ knockdown alters the metabolism of LN229 and GBM1 cells. A.** Water soluble metabolites of shCHK$\alpha$ and pLKO.1 control cells were analyzed with $^{1}$H-NMR spectroscopy. **B.** The ratio of the relative creatine and phosphocreatine concentrations were calculated from $^{1}$H-NMR spectra of shCHK$\alpha$ and pLKO.1 control cells. **C.** CHK$\alpha$ knockdown decreases the expression of creatine kinase brain-type, the enzyme phosphorylating creatine. The data is represented as mean ± SD (n = 3).

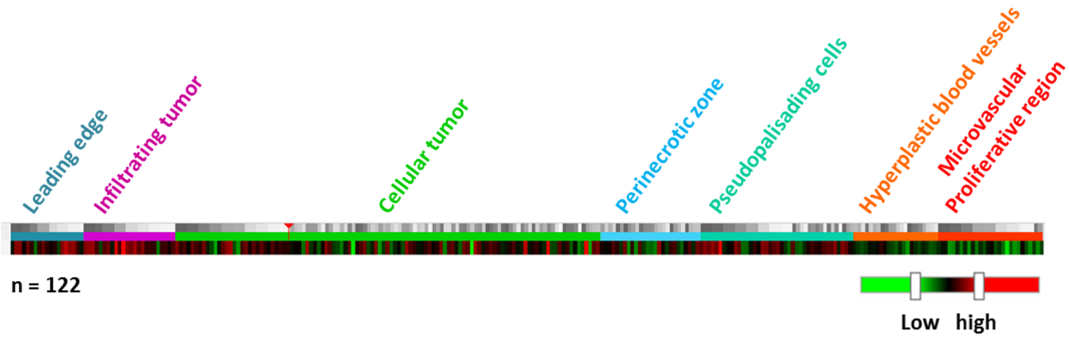


**Figure 2.14: CHK$\alpha$ is expressed in higher levels in the infiltrating zone and the leading edge of GBM.** RNA sequencing data generated from anatomic structures isolated by laser microdissection. A total of 122 RNA samples were generated from 10 tumors and used for sequencing. Data from the IVY Glioblastoma project (Website: © 2015 Allen Institute for Brain Science. Ivy Glioblastoma Atlas Project [Internet]. Available from: glioblastoma.alleninstitute.org). Image credit: Allen Institute.

**Table 2.2:** Primer sequences used in qPCR

| Gene | Gene ID | Forward primer | Reverse primer |
|---|---|---|---|
| ACTB | 60 | CCCAGCACAATGAAGATCAA | CGATCCACACGGAGTACTTG |
| B2M | 567 | GTTGCTCCACAGGTAGCTCTAG | ACAAGCTTTGAGTGCAAGAGATTG |
| CDH2 | 1000 | TATGCCCAAGACAAAGAGACC | CAACTTCTGCTGACTCCTTCA |
| CHKA | 1119 | GAAAGTGCTCCTGCGGCTGTATG | CGGCTCGGGATGAACTGCTC |
| CKB | 1152 | GGCAACATGAAGGAGGTGTT | ATGGGCAGGTGAGGATGTAG |
| NES | 10763 | GGCGCACCTCAAGATGTCC | CTTGGGGTCCTGAAAGCTG |
| SNAI1 | 6615 | GCTGCAGGACTCTAATCC | ATCTCCGGAGGTGGGATC |
| SNAI2 | 6591 | TGGTTGCTTCAAGGACACAT | GTTGCAGTGAGGGCAAGAA |
| SOX2 | 6657 | TGGACAGTTACGCGCACA | CGAGTAGGACATGCTGTA |
| TWIST1 | 7291 | TCCGCGTCCCACTAGCA | TTCTCTGGAAACAATGACATCTAGGT |
| VIM | 7431 | CCCTCACCTGTGAAGTGGAT | TCCAGCAGCTTCCTGTAGGT |
| ZEB1 | 6935 | AAGAATTCACAGTGGAGAGAAGCCA | CGTTTCTTGCAGTTTGGGCATT |
| ZEB2 | 9839 | GCCGCGGCATATGGTGACA | GCCACACTCTGTGCATTTGAA |

## 2.3 Glutaminase inhibition targets c-Myc positive, starvation-resistant glioblastoma stem-like cells

### 2.3.1 General Information

**Title: Glutaminase inhibition targets c-Myc positive, starvation-resistant glioblastoma stem-like cells**

Katharina Koch[1], Rudolf Hartmann[2], Abigail K. Suwala[1], Dayana Herrera Rios[1,3], Hans-Jakob Steiger[1], Dieter Willbold[2,4], Ulf D. Kahlert[1,5], and Jaroslaw Maciaczyk[1,*]

[1] Department of Neurosurgery, University Hospital Düsseldorf, Düsseldorf, Germany

[2] Institute of Complex Systems ICS-6, Research Center Jülich, Jülich, Germany

[3] present address: Skin Cancer Unit of the Dermatology Department, West German Cancer Center, University Duisburg-Essen, Essen, Germany

[4] Institute fuer Physikalische Biology, Heinrich-Heine-University Düsseldorf, Düsseldorf, Germany

[5] German Cancer Consortium (DKTK), Germany

[*] corresponding author, Jaroslaw.Maciaczyk@med.uni-duesseldorf.de

Submitted to: **Cancer Letters**, 05.12.2017.
Journal Impact Factor (2016): 6.37
Contribution: 75 %. Katharina Koch performed the experiments, evaluated the data and wrote the manuscript. For further details see the Declaration of Author's Contribution.

### 2.3.2 Abstract

Cancer stem-like cells mediate tumor initiation, progression, and therapy resistance. Therefore, exploiting their metabolic properties is an attractive approach to identify efficient therapeutic strategies in oncology. Here we analyze the metabolism of glioblastoma stem-like cells (GSC) with high resolution proton nuclear magnetic resonance (HR $^{1}$H-NMR) spectroscopy. We identify intracellular accumulation of known oncometabolites such as lactate, phosphocholine, and glycine in GSCs. Furthermore, we stratify our *in vitro* GSC models into two subtypes based on their relative amount of glutamine in relationship to glutamate (Gln/Glu). Gln/Glu$^{High}$ GSCs are resistant to glutamine deprivation whereas Gln/Glu$^{Low}$ GSCs respond with significantly decreased clonogenicity. Cellular growth is sustained in both subtypes even though the cells show a complete lack of intracellular glutamine. Surprisingly, starvation-resistant GSCs express high levels of the oncogene c-Myc. In contrast, pharmacological glutaminase (GLS) inhibition effectively inhibits growth and clonogenicity of both GSC subtypes. In conclusion, GSCs accumulate known oncometabolites, thereby contributing to a more aggressive metabolic phenotype. Furthermore, monitoring the Gln/Glu ratio of glioblastoma predicts resistance to Gln starvation and we hypothesize that GLS inhibition is an effective pan-GSC therapy efficaciously reducing growth, clonogenicity, and stemness independently of c-Myc.

### 2.3.3 Introduction

Glioblastoma is the most common malignant primary brain tumor with a median overall survival of less than two years [19]. It is believed that glioblastoma stem-like cells (GSCs) do not get targeted by current therapeutics and contribute to therapy resistance and tumor relapse [26, 27, 52, 177]. Exploiting the metabolic properties of cancer cells has emerged as an innovative strategy for therapeutic target and diagnostic biomarker discovery. The identification of the metabolic makeup of GSCs might therefore be of particular interest to effectively target and eradicate this highly malignant cell population [53, 54, 152]. Glycolysis and glutaminolysis, the main anaplerotic pathways in cells, guarantee high levels of energy production, provide substrates for biosynthetic processes, and sustain growth of highly proliferative cells [68]. Both pathways are dysregulated in cancer due to mutational and epigenetic changes [59, 60, 222, 223]. Furthermore, by supporting the synthesis of glutathione (GSH), glutaminolysis is crucial for the clearance of reactive oxygen species (ROS). Targeting aerobic glycolysis was long considered to potently exploit cancers' Achilles heel for therapeutic purposes; however the clinical application of glycolysis inhibitors remains challenging [224, 225]. Therefore, interfering with glutamine homeostasis is a forceful alternative to combat cancer, since tumor cells – compared to normal tissue - show glutamine addiction [57, 226]. However, glutamine dependency does not apply to all tumors and the microenvironment can significantly modulate the tumor cells' response to glutamine deprivation [227]. The relevance of glutamine metabolism for gliomagenesis remains questionable. Glioblastoma compensate mTOR inhibition by induction of glutaminolysis [228]. Contrarily, studies on pharmacological inhibition of glutaminolysis report either reduction [229] or no influence [81] on glioblastoma growth. Only little is known about the importance of glutamine metabolism for GSCs. Therefore, the purpose of this work is to elucidate the metabolic preferences of GSCs by comparing intracellular metabolite compositions of GSC cultures with those subjected to spontaneous or targeted differentiation.

### 2.3.4 Results

#### GSC cultures can be re-differentiated by bone morphogenic protein 4

To enriched the population of highly therapy-resistant GSCs, we transferred glioblastoma cultures from medium containing 10 % into neurosphere medium without FBS, resulting in clustering of the cells into spherical structures. This led to a significant reduction of glial fibrillary acidic protein (GFAP) mRNA expression in all tested cell lines (Suppl. Fig. 2.20A). Furthermore, mRNA levels of the putative GSC marker CD133, which represents a valid marker for GSC enrichment [27, 39, 146], were significantly increased. Immunoblotting of GSC culture lysates revealed differences in the abundance of CD133 protein (Fig. 2.15A). Interestingly, expression of c-Myc, a regulator of glucose and glutamine metabolism, did not correlate with stemness. Nevertheless, CD133 protein directly correlated with expression of stemness markers SOX2, and nestin (NES) (Fig. 2.15B). To exclude that metabolic differences result from differences in media supplements, we re-

differentiated our GSC cultures with bone morphogenic protein 4 (BMP4) in neurosphere medium. BMP4 effectively decreases the GSC pool by inducing glial differentiation [145]. Treatment of GSCs with 50 ng/ml recombinant BMP4 for 48 h significantly increased the expression of GFAP and reduced the expression of CD133, SOX2 (JHH520 and GBM1), and NES (GBM1) (Fig. 2.15C). To assess whether BMP4 treatment reduces stemness in GSC cultures, we performed clonogenicity assays in semi-solid agarose. Strikingly, BMP4-treament almost completely abolished the clonogenic capacity of all GSC cultures (Fig. 2.15D) without inducing significant amounts of apoptosis (Suppl. Fig. 2.20B). That indicates that BMP4 specifically reduces stemness instead of inducing cell death, with culture conditions remaining largely unchanged.

**GSCs reprogram lactate, glutamine, creatine, choline, and glycine metabolism**

Using one-dimensional HR $^{1}$H-NMR spectroscopy we analyzed the abundance of the most prominent water-soluble metabolites in adherent cells, GSC cultures, and GSC cultures re-differentiated with BMP4. JHH520 and 407p GSC cultures exhibited higher levels of the oncometabolites lactate (Lac), phosphocholine (PC), total choline (tCho), and glycine (Gly) than the respective adherent and BMP4-treated cultures (Fig. 2.16). However, BMP4-treatment had only minor effects on the metabolism of GBM1 cells. Thus we observed increased Lac and Gly levels in GSCs compared to adherent cultures only, and PC was reduced both in adherent and BMP4 treated cells. Furthermore, all GSC cultures exhibited lower levels of the putative anti-cancer agent creatine (Cre) than adherent cells [211, 212]. Surprisingly, BMP4-treatment did not reverse this effect but further decreased Cre levels in JHH520 and 407p cultures. Metabolites connected to glutamine (Gln) metabolism were differentially regulated in our GSC models. Both Gln and GSH levels were significantly increased in JHH520 and 407p GSC cultures whereas they were significantly reduced in GBM1 GSC cultures. Since several publications correlated aberrant Gln metabolism with tumor progression, we further analyzed Gln metabolism of GSCs in order to reveal possible anti-GSC therapy targets.

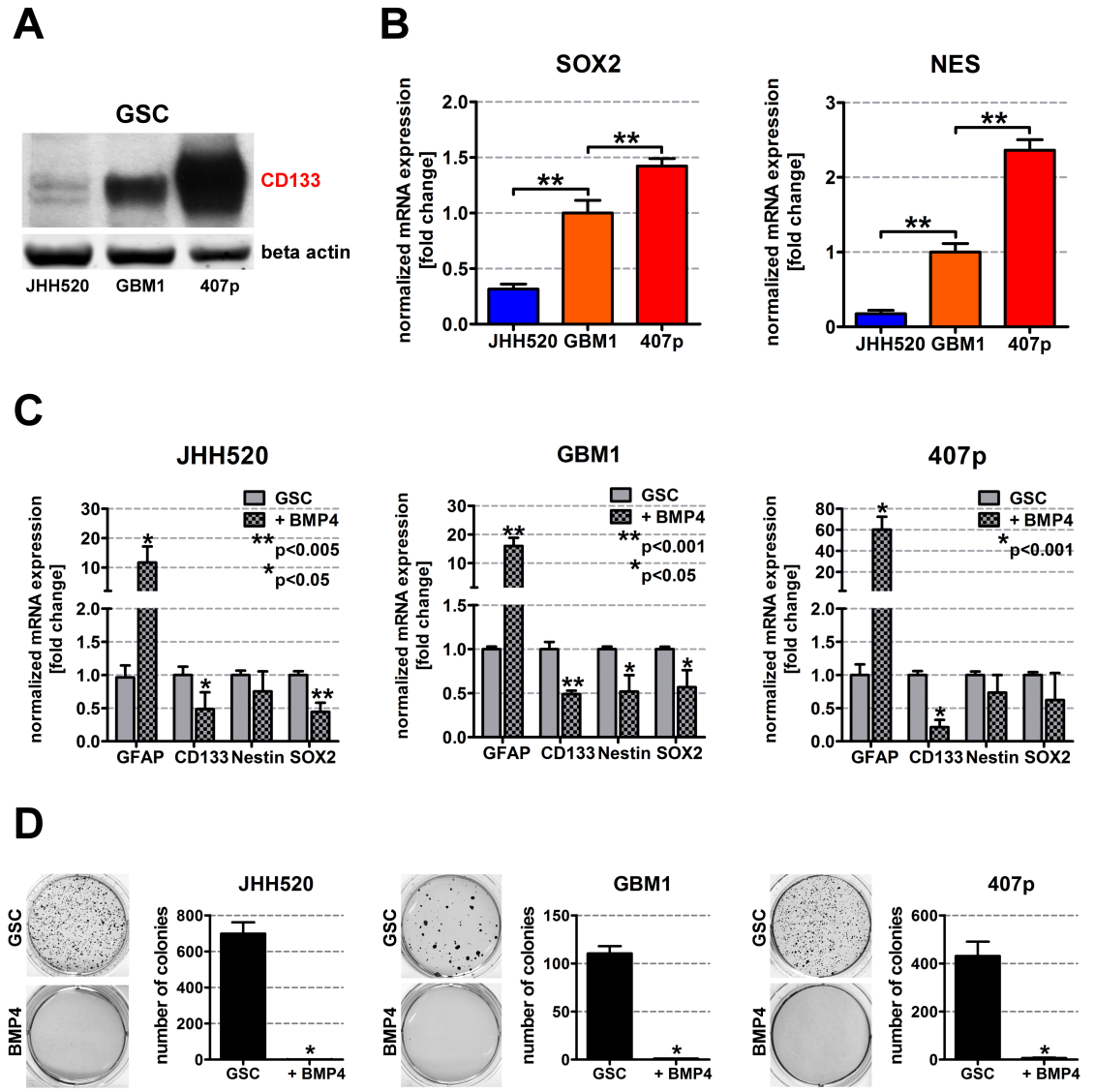


**Figure 2.15: Treatment with BMP4 induces glial differentiation in glioblastoma stem-like cells. A.** Immunoblotting of GSC lysates confirmed expression of the putative glioblastoma stem cell marker CD133 in all three GSC cell lines. **B.** Analysis of SOX2 and NES mRNA expression revealed highest expression of both genes in 407p GSCs and lowest in JHH520 GSCs (**p < 0.005). **C.** GSC cultures (JHH520, GBM1, and 407p) were treated for 48 h with 50 ng/ml BMP4. RT qPCR analysis revealed increased expression of GFAP and decreased expression of CD133, NES, and SOX2 in cells treated with BMP4, compared to control cells. D. Glial differentiation of GSCs with BMP4 reduced the clonogenicity of JHH520, GBM1, and 407p cells as assessed by soft agar assays. Representative pictures of NBT stained colonies and quantifications of three colony forming assays are shown (*p < 0.05). Abbreviations: NBT, 4-nitro blue tetrazolium chloride. The data is represented as mean ± SD (n = 3).

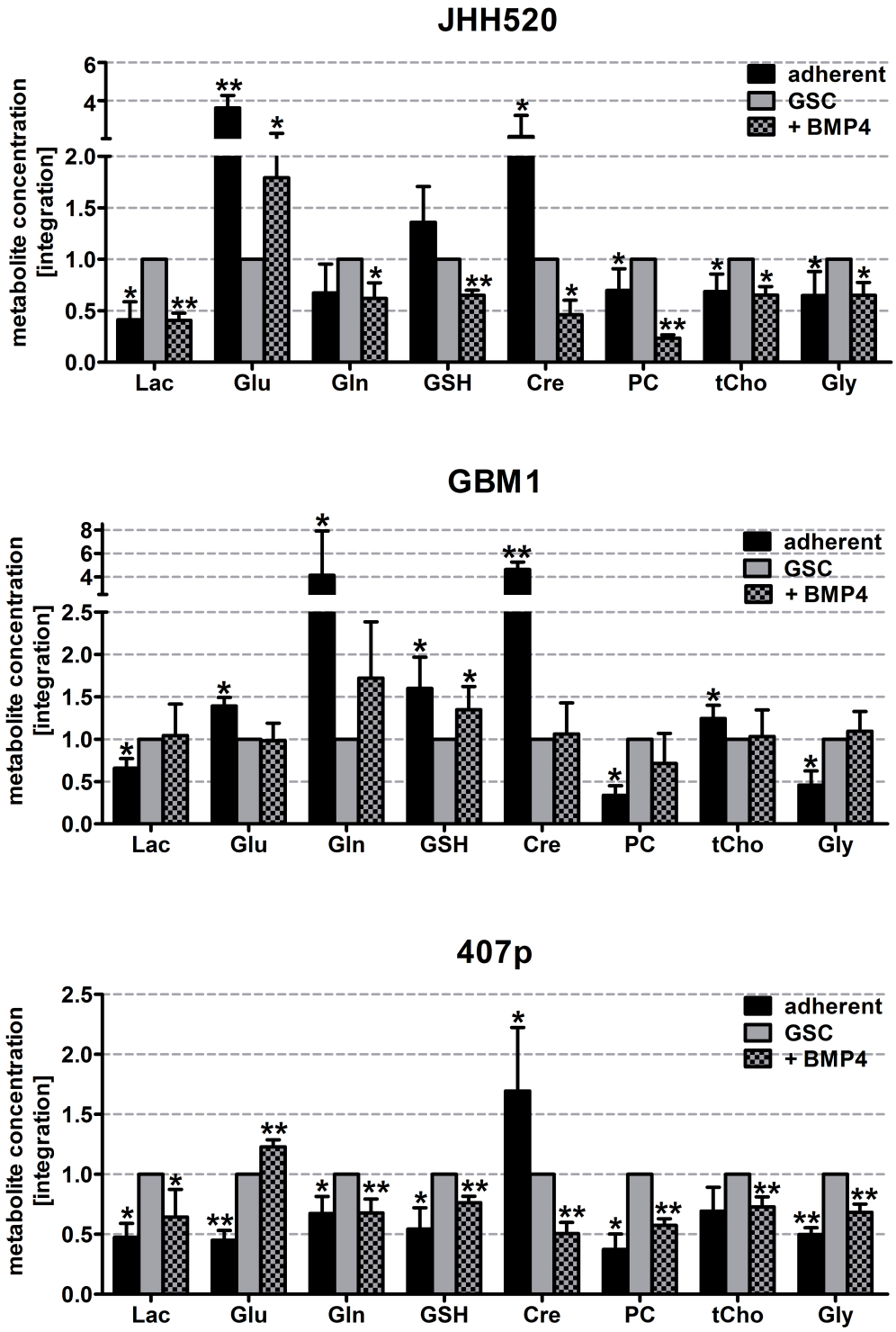


**Figure 2.16: GSCs reprogram lactate, glutamine, phosphocholine, and glycine metabolism.** Relative concentrations of water soluble metabolites extracted from glioblastoma (JHH520, GBM1, and 407p) adherent cells, GSC cultures, and GSC cultured re-differentiated for 48 h with 50 ng/ml BMP4 were assessed with $^{1}$H-NMR spectroscopy (*$p < 0.05$, **$p < 0.001$). Abbreviations: Lac, lactate; Glu, glutamate; Gln, glutamine; GSH, glutathione; Cre, creatine; PC, phosphocholine; tCho, total choline (tCho; comprising free choline, PC, and glycerophosphocholine); Gly, glycine. The relative metabolite concentrations of three independent experiments are displayed as mean ± SD.

### Gln/Glu$^{High}$ GSCs express c-Myc and high levels of the glutamate/cystine antiporter cXT/SLC7A11

Since maturation with BMP4 differentially affected Gln metabolism in our GSC models, we analyzed metabolite ratios and expression of enzymes involved in glutaminolysis. Representative Gln and glutamate (Glu) metabolite peaks of $^{1}$H-NMR spectra and corresponding Gln/Glu ratios are shown in figures 2.17A and 2.17B, respectively. Interestingly, GBM1 GSCs exhibit a much lower Gln/Glu ratio than JHH520 and 407p GSCs. Strikingly, the Gln/Glu ratios neither correlated with stemness (Fig. 2.15A+B), nor could they be explained by baseline expression of glutaminase (GLS) or glutamine synthetase (GS), the enzymes metabolizing Gln into Glu and Glu into Gln, respectively (Suppl. Fig. 2.21A). In accordance with studies correlating high Gln/Glu ratios with low GS expression in glioblastoma xenografts [140], we observed highest GS expression in Gln/Glu$^{Low}$ GBM1 cells. Interestingly, we could correlate high Gln/Glu ratios with c-Myc expression (Fig. 2.15A). Notably, Gln/Glu$^{High}$ cells exhibited significantly higher expression of the glutamate exporter cXT/SLC7A11 than Gln/Glu$^{Low}$ cells (Fig. 2.17C). Concisely, xCT could be correlated with high intracellular Gln in breast cancer [230]. Upon BMP4-treatment, the Gln/Glu ratio significantly decreased in JHH520 and 407p GSCs and increased in GBM1 GSCs (Fig. 2.17D). Furthermore, the xCT expression significantly decreased in all GSC cultures undergoing differentiation (Fig. 2.17E). Impaired xCT activity could explain the decreased Gln/Glu ratios and GSH levels observed in differentiated JHH520 and 407p cells. A reason for the increased Gln/Glu ratio in BMP4-treated GBM1 GSCs could be a simultaneous decrease of Glu synthesis resulting from impaired GLS expression (Suppl. Fig. 2.21B). In conclusion, we identified two GSC subgroups, c-Myc$^{pos}$ Gln/Glu$^{High}$ (JHH520 and 407p) and c-Myc$^{neg}$ Gln/Glu$^{Low}$ (GBM1) cells. The former characterized by high xCT expression and decreased Gln and GSH levels upon differentiation, the later characterized by low xCT expression and increased Gln and GSH levels upon BMP4-treatment.

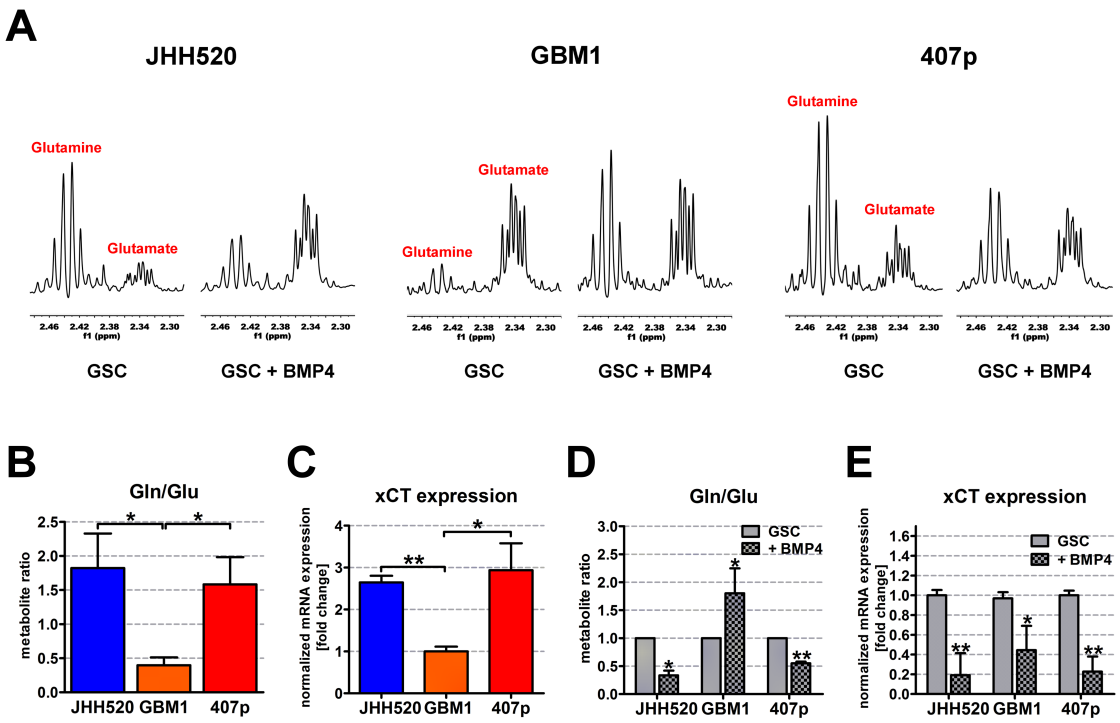


**Figure 2.17: The Gln/Glu ratio of GSCs correlates with expression of the glutamate/cystine antiporter cXT/SLC7A11. A.** Expanded regions of $^{1}$H-NMR spectra showing Gln and Glu multiplets from metabolic extracts of GSCs (JHH520, GBM1, and 407p) either treated with 50 ng/ml BMP4 or vehicle. **B.** GBM1 GSCs have a significant lower Gln/Glu ratio than JHH520 and 407p GSCs (*$p < 0.05$). **C.** Treatment with 50 ng/ml BMP4 decreased the Gln/Glu ratio in JHH520 and 407p GSCs and increases the Gln/Glu ratio in GBM1 GSCs (*$p < 0.05$, **$p < 0.0001$). **D.** Analysis of mRNA expression of the glutamate/cysteine antiporter xCT/SLC7A11 revealed significantly decreased expression in GBM1 GSCs (*$p < 0.01$, **$p < 0.0001$). **E.** In all tested cell lines the xCT mRNA expression was significantly reduced upon treatment with 50 ng/ml BMP4 as assessed with RT qPCR (*$p < 0.05$, **$p < 0.001$). The data is represented as mean ± SD (n = 3).

### Gln/Glu$^{High}$ GSCs are self-sufficient for glutamine and can be sensitized for Gln deprivation by glial differentiation

To assess the susceptibility of Gln/Glu$^{Low}$ and Gln/Glu$^{High}$ GSCs to Gln deprivation, we cultured GSCs in medium with or without L-Gln for six days. Representative $^{1}$H-NMR spectra (Fig. 2.18A) and relative quantifications (Fig. 2.18B) of metabolic extracts from Gln starved GSCs and control cells showed severely reduced Gln levels in starved GSCs, with no detectable Gln in GBM1 GSCs. Furthermore, Glu levels were reduced by 42 % in JHH520, 40 % in 407p, and even 53 % in GBM1 GSCs. Furthermore, Gln starvation increased oncometabolites PC, tCho, and Gly, indicating that GSCs switch to a more aggressive metabolic phenotype to cope with nutrient deprivation. Levels of the antioxidant GSH were markedly more decreased in GBM1 (34 %) GSCs as compared to JHH520 (14 %) and 407p (7 %) GSCs (Fig. 2.18C). Surprisingly, cell viability was not affected (Fig. 2.18D). To assess whether Gln starvation influences stemness in GSCs, we performed clonogenicity assays with Gln-starved and control GSCs. Clonogenicity was significantly reduced by 70 % in Gln/Glu$^{Low}$ ($p<0.05$) but not affected in Gln/Glu$^{High}$ GSCs (Fig. 2.18E). Recent publications stated that GS activation protects glioblastoma cells from Gln starva-

tion [81]. Surprisingly, we observed highest GS protein expression in starvation sensitive GBM1 GSCs (Suppl. Fig. 2.21A). Furthermore, Gln starvation increased GS expression in all three cell lines (Fig. 2.18F). Therefore, GS activation may protect from starvation-dependent proliferation arrest but not from impaired clonogenic capacity. We further analyzed whether the initial high GSH levels and Gln/Glu ratios protect JHH520 and 407p cells from Gln deprivation. Since BMP4-treatment significantly reduced Gln/Glu ratios, GSH levels and xCT expression in Gln/Glu$^{High}$ GSCs (Fig. 2.16, Fig. 2.17D+E), we differentiated JHH520 and 407p GSCs with BMP4 either in the presence or absence of L-Gln. We observed significantly reduced clonogenicity in differentiated JHH520 and 407p cultures starved for Gln (Fig. 2.18G). Furthermore, Gln starvation of differentiated GSCs reduced expression of CD133 in all cell lines, SOX2 expression in GBM1 and increased GFAP expression in JHH520 cells (Suppl. Fig. 2.22B). Besides a reduction of CD133 in JHH520 and increase of GFAP in GBM1, Gln starvation of untreated GSCs did not affect the expression of stemness or differentiation markers (Suppl. Fig. 2.22A). In conclusion, Gln deprivation targets stemness in c-Myc$^{neg}$ Gln/Glu$^{Low}$ GSCs, however, c-Myc$^{pos}$ Gln/Glu$^{High}$ GSCs are protected probably by high levels of Gln and GSH and increased xCT expression. Glial differentiation of Gln/Glu$^{High}$ GSCs restores the sensitivity to Gln starvation.

### Inhibition of glutaminase reduces stemness in both Gln/Glu$^{Low}$ and Gln/Glu$^{High}$ GSCs

Since Gln deprivation failed to target Gln/Glu$^{High}$ GSCs, we decided to interfere with glutaminolysis by inhibition of GLS, the enzyme metabolizing Gln to Glu. GSC cultures were treated for six days with various concentrations of the GLS inhibitor C968 and cell viability was dose-dependently reduced (Fig. 2.19A). Treatment with 10 µM C968 significantly diminished the clonogenic capacity of all tested GSC cultures compared to DMSO-treated cells (Fig. 2.19B). We observed highly reduced total colony numbers and almost no large colonies in C968-treated GSCs. Furthermore, immunoblotting of GSC lysates treated with C968 or vehicle for two and four days showed substantially reduced CD133 protein levels in GBM1 and 407p GSCs and marginally in JHH520 GSCs (Fig. 2.19C). Additionally, we detected reduced SOX2 expression in JHH520 GSCs treated with C968 for two and four days. Therefore, we conclude that GLS inhibition is an effective way to target c-Myc$^{neg}$ Gln/Glu$^{Low}$ and c-Myc$^{pos}$ Gln/Glu$^{High}$ GSCs significantly reducing their stemness.

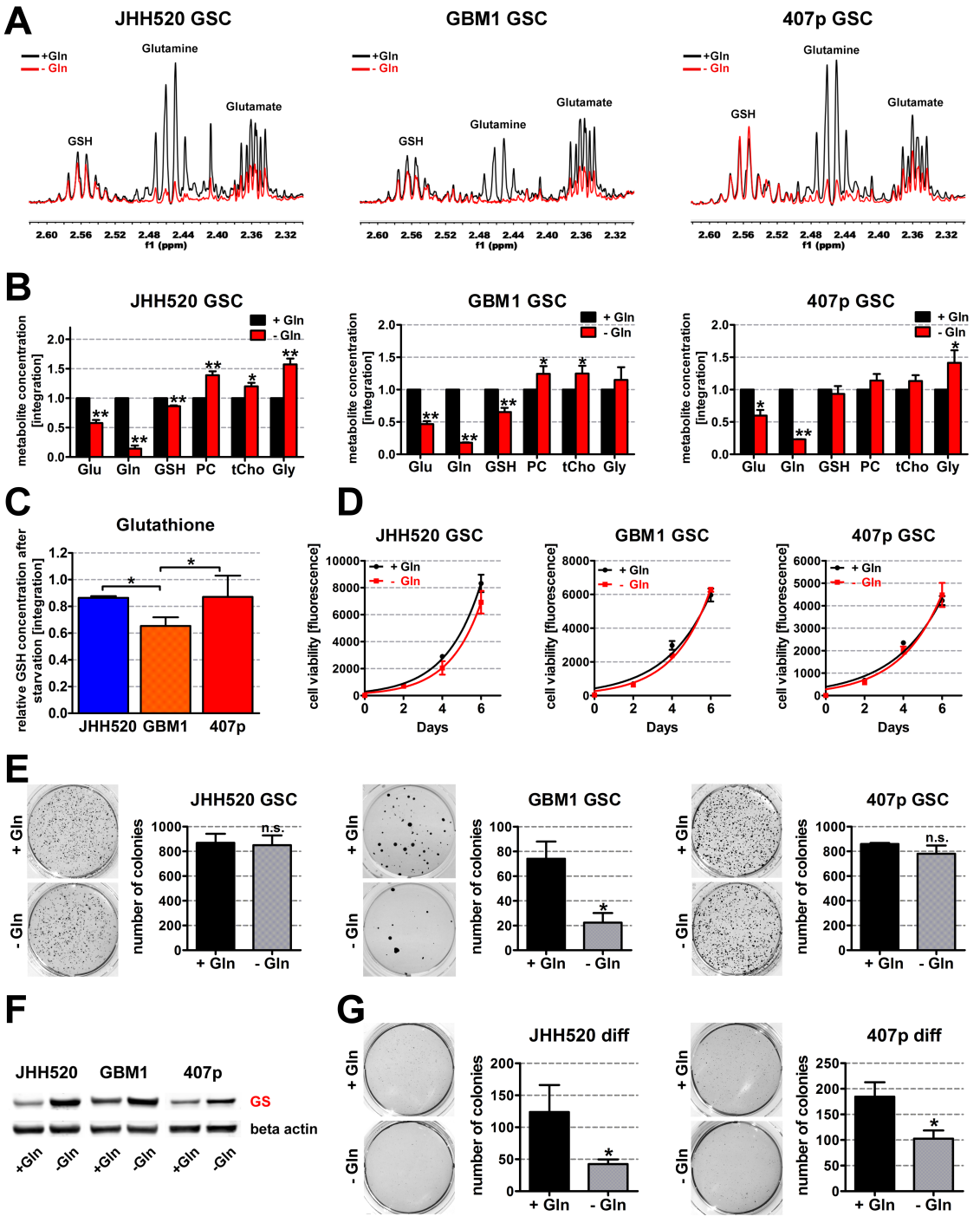


**Figure 2.18: BMP4-dependent reduction of Gln, GSH, and xCT expression restores sensitivity of starvation-resistant Gln/Glu$^{High}$ GSCs.** Expanded regions of $^{1}$H-NMR spectra showing GSH, Gln, and Glu multiplets (**A**) and relative concentrations of selected water-soluble metabolites (**B**) from metabolic extracts of GSCs either cultured in medium with or without L-Gln (*p < 0.05, **p < 0.001). **C.** Relative glutathione concentration in GSCs after Gln starvation compared to control cells (*p < 0.05). **D.** Gln starvation did not affect the viability of GSCs. Exponential growth curves were calculated for each condition and displayed in the graphs. **E.** Gln starvation reduced the clonogenic capacity of Gln/Glu$^{Low}$ (GBM1) but not Gln/Glu$^{High}$ (JHH520, 407p) GSCs (*p < 0.05). **F.** Immunoblotting revealed increased glutamine synthetase protein expression in GSCs upon Gln starvation. β-actin immunoblotting was used as loading controls. **G.** Glial differentiation with 25 ng/ml restored the sensitivity of Gln/Glu$^{High}$ GSCs (JHH520 and 407p) for Gln starvation. Colonies remain small due to the general anti-clonogenic effect of BMP4. Clonogenicity was assessed with soft-agar assays. Representative pictures of NBT stained colonies and quantifications of three colony forming assays are shown (*p < 0.05). Abbreviations: NBT, 4-nitro blue tetrazolium chloride. The data is represented as mean ± SD (n = 3).

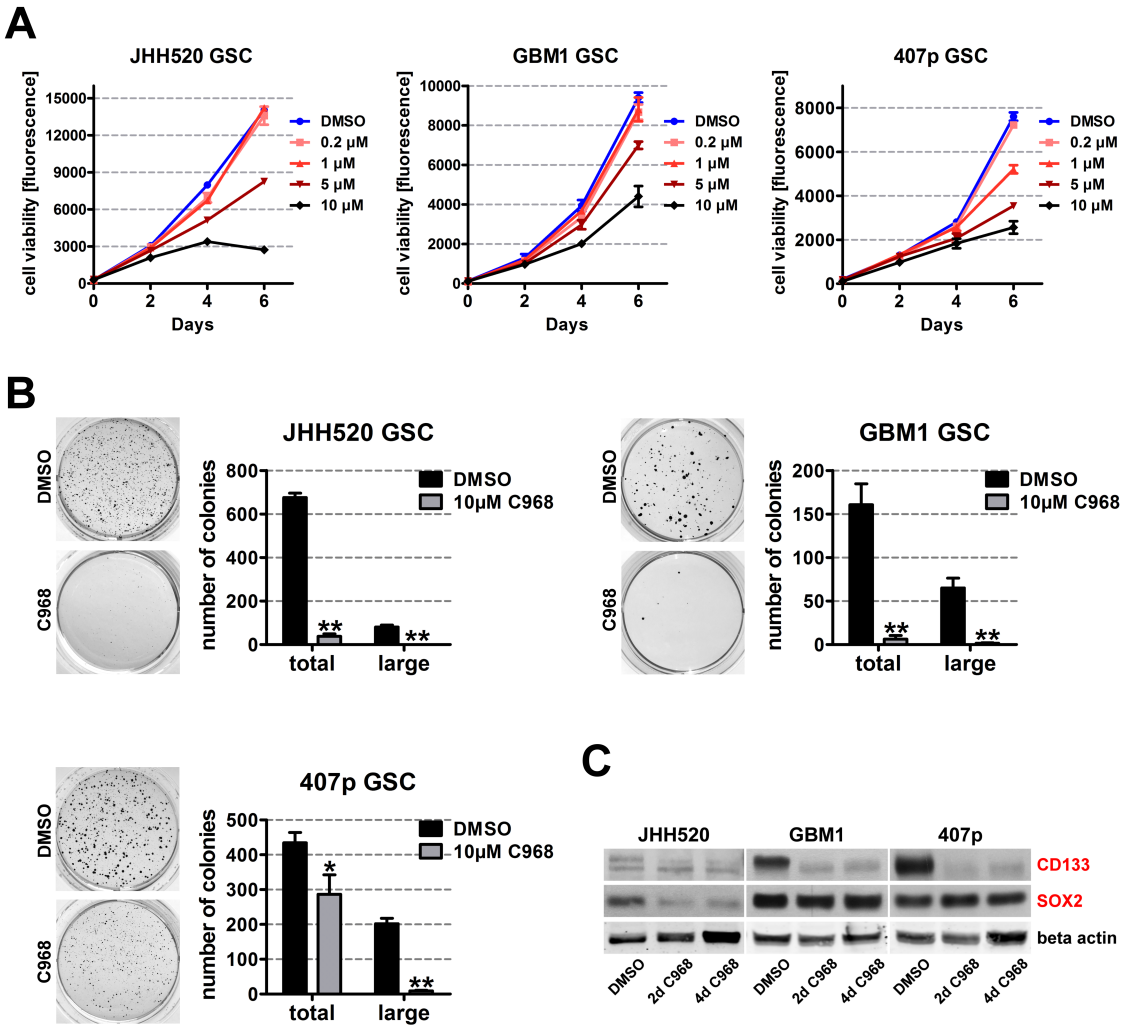


**Figure 2.19: Glutaminase inhibition effectively targets Gln/Glu$^{Low}$ and Gln/Glu$^{High}$ GSC cultures. A.** The cell viability of JHH520, GBM1, and 407p GSC cultures was dose-dependently impaired by treatment with the GLS inhibitor C968. Exponential growth curves were calculated for each condition and displayed in the graphs. **B.** Treatment with 10 µM C968 significantly reduced the clonogenicity of JHH520, GBM1, and 407 GSC cultures. Representative pictures of NBT stained colonies and quantifications of three colony forming assays are shown (*p < 0.05, **p < 0.001). **C.** Immunoblotting experiments showed that GLS inhibition with 10 µM C968 over two and four days reduced the protein expression of CD133 (JHH520, GBM1, and 407) and SOX2 (JHH520) as compared to DMSO treated control cultures. β-actin immunoblotting was used as loading controls. Abbreviations: DMSO, dimethyl sulfoxide; GLS, glutaminase. The data is represented as mean ± SD (n = 3).

### 2.3.5 Discussion

GSCs cause chemoresistance and tumor recurrence in glioblastoma and despite significant research efforts their unequivocal identification remains elusive [27]. Recent technical advantages in cancer research significantly increased our understanding on how oncoproteins influence cellular metabolism. However, the metabolic and bioenergetic needs of GSCs are not fully understood [55]. We compared the intracellular metabolome of GSC neurosphere cultures with their differentiated counterparts and could correlate elevated Lac, PC, tCho, and Gly levels with GSC enrichment. Aerobic glycolysis causes lactate accumulation in cancer [61, 62] and lactate dehydrogenase-A (LDH), the enzyme converting pyruvate into lactate, promotes survival of GSCs *in vivo* [231]. Moreover, epithelial-mesenchymal-like transition (EMT), the developmental program enriching stemness in glioblastoma [37], enhances glycolysis in GSCs [232] and increases Lac production [233]. Our results are in concordance with previous reports describing lactate accumulation in glioblastoma neurospheres [234].

The stemness dependent shifts in choline derivatives correspond with previous reports from our lab. The observed cholinic phenotype [105, 109], characterized by high PC and tCho levels, is associated with expression of the EMT activator ZEB1 and high clonogenic capacity [172].

Tumor tissues exhibit elevated glycine levels [235] and *ex vivo* assessment of tumor biopsies correlated Gly accumulation with higher tumor grade [168]. Furthermore, glycine receptor $\alpha 1$ promotes self-renewal and tumorigenicity in glioblastoma xenografts [236]. Importantly, in hypoxic microenvironment such as pseudopalisades, tight regulations prevent Gly accumulation in order to maintain GSC survival [153]. We hypothesize that in normoxic glioblastoma, elevated intracellular Gly - alongside with Lac accumulation and the cholinic phenotype - indicates the existence of a higher fraction of GSCs.

Glutaminolysis is the second main anaplerotic pathway and enhanced in lactate producing cancer cells [57, 237]. Concisely, we observed increased levels of Gln and GSH in JHH520 and 407p GSCs compared to differentiated cells, whereas stemness enriched GBM1 cultures significantly decreased Gln and GSH. Furthermore, through stratification of our GSC models according to their Gln/Glu ratio we were able to efficiently predict their resistance to Gln starvation. Glu deprivation significantly reduced clonogenicity in Gln/Glu$^{Low}$ but had no consequence in Gln/Glu$^{High}$ GSC cultures. Interestingly, differentiation of Gln/Glu$^{High}$ GSCs reduced Gln, GSH, and the Gln/Glu ratio and restored their sensitivity to Gln starvation, indicating that the initial high Gln and GSH levels and high Gln/Glu ratios protect Gln/Glu$^{High}$ GSCs from nutrient starvation. This is supported by recent studies showing that Gln maintains stemness by promoting GSH synthesis [238]. Induction of GS has been described to mediate resistance to nutrient stress [81]. Indeed, Gln starvation increased GS expression in GSCs, however, also in starvation sensitive GBM1 GSCs. Since starvation did not affect cell viability we conclude that GS may protect GSCs from starvation-dependent death, but not from the loss of self-renewing capacity. Of note, despite significant GS upregulation we could not detect any intracellular Gln in starved GBM1 and just very little in JHH520 and 407p cells, indicating that the Gln/Glu

ratio is not substantially regulated by GS activity. This assumption is further supported by studies identifying high Gln/Glu ratios correlating with low GS expression in tumor tissue compared to normal brain tissue [140]. Concisely, we detected significantly lower GS expression in Gln/Glu$^{High}$ JHH520 and 407p compared to Gln/Glu$^{Low}$ GBM1 GSCs.

The glutamate/cystine antiporter xCT/SLC7A11 exports intracellular glutamate in exchange for cystine, a crucial step in the synthesis of the antioxidant GSH. Furthermore, xCT expression correlates with increased glutamine uptake and tumor progression [76, 230, 239]. Concisely, Gln/Glu$^{High}$ GSCs exhibited significantly higher xCT expression than Gln/Glu$^{Low}$ GSCs. Elevated Glu export and increased Gln uptake could explain the high Gln/Glu ratios in JHH520 and 407p GSCs. Furthermore, Gln starvation reduced GSH levels significantly stronger in Gln/Glu$^{Low}$ than Gln/Glu$^{High}$ cells, indicating that the low xCT expression in Gln/Glu$^{Low}$ cells does not provide sufficient protection from reactive oxygen species and that GSH promotes stemness in glioblastoma as well [238]. This is supported by the observation that differentiation of Gln/Glu$^{High}$ cells reduced xCT expression and GSH levels and thereby restored sensitivity to Gln starvation. However, further experiments are needed to proof this hypothesis.

Glutaminase inhibition is another promising strategy in cancer therapy and GLS inhibitors are currently being evaluated in clinical trials [94, 229, 240, 241]. Indeed, pharmacological inhibition of GLS caused significant suppression of cell viability, clonogenicity, and stem cell marker expression in all our GSC models. Interestingly, sensitivity to GLS inhibitor C968 neither correlated with baseline GLS expression nor with the Gln/Glu ratio. Consistent with recent literature we correlated high xCT expression with increased sensitivity to glutaminase inhibition [242], since GBM1 ($IC_{50}$ day 6 = 10 µM) GSCs were less sensitive to C968 than JHH520 and 407p ($IC_{50}$ day 6 = 5 µM) GSCs. Therefore, the xCT expression could function as a marker for the susceptibility to GLS inhibition but more cell models and *in vivo* studies are needed to validate this suggestion. Only little is known about the importance of glutaminolysis for GSCs. Our group previously showed that γ-secretase inhibitors (GSI) target GSCs and reduce intracellular glutamate as a consequence of glutaminase inhibition. We hypothesized that the observed therapeutic benefits of GSIs in glioblastomas are at least in part attributable to glutaminolysis inhibition [243]. The here presented data further supports the concept that GSCs are maintained through GLS activation and that GLS inhibition is a potent anti-GSC therapy that overcomes resistance to glutamine starvation.

The activation of oncogene c-Myc has been extensively investigated in its role to control Gln addiction in cancer cells [244, 245]. Surprisingly, neither the sensitivity to GLS inhibition nor the resistance to Gln starvation correlated with baseline expression of c-Myc in our GSC cell models. In fact, Gln/Glu$^{Low}$, Gln starvation sensitive GBM1 GSCs showed lowest expression of c-Myc protein. Our data is thereby in strong conflict with previous reports where c-Myc predicts sensitivity to Gln starvation including in glioblastoma cells [60]. Further studies are needed to elucidate possible mechanistic causalities explaining our observations.

In conclusion, the presented work suggests that therapy-resistant GSCs accumulate Lac, PC, and Gly, thereby contributing to a more aggressive metabolic phenotype than classical glioblastoma cultures. Moreover, our work postulates that monitoring the Gln/Glu ratio and xCT expression in glioblastoma samples may indicate the existence of GSCs and predict for the tumor's resistance to Gln starvation and GLS inhibition, respectively. *In vivo* validation of these results is needed to verify their relevance for diagnostic purposes. Furthermore, we want to emphasize GLS inhibitor C968 as a potent anti-GSC drug and highlight its effectiveness in reducing growth, clonogenicity, and stemness in glioblastoma independently of c-Myc activation status.

### 2.3.6 Methods

#### Cell culture

JHH520 cells were generously provided by G. Riggins (Baltimore, USA), GBM1 by A. Vescovi (Milan, Italy), and 407p by M.S. Carro (Freiburg, Germany). Adherent cells were cultured in DMEM (Gibco), 10 % FCS, and 1x Anti-Anti (Gibco) and GSC neurospheres in DMEM w/o pyruvate (Gibco), 30 % Ham's F12 Nutrient Mix (Gibco), 2 % B27 supplement (Gibco), 20 ng/ml human bFGF (Peprotech), 20 ng/ml human EGF (Peprotech), 5 µg/ml Heparin (Sigma), and 1x Anti-Anti (Gibco). All cells were cultured at 37 ° and 5 % $CO_2$. GSCs were re-differentiated for 48 h with 50 ng/ml recombinant BMP4 (Gibco, #PHC9534) in neurosphere medium. BMP4 was stored as a stock of 1 mg/ml in 10 mM citric acid (pH 3.0). For glutaminase inhibition GSCs were cultured for 48 h or 96 h in neurosphere medium containing 10 µM C968 (Merck, #352010). GSCs were starved for glutamine by cultivation in neurosphere medium containing DMEM w/o L-glutamine (Gibco, #11960044) and medium supplemented with 2.6 mM L-glutamine as control.

#### Quantitative Real time PCR

Total RNA was extracted using the NucleoSpin® RNA Kit (Macherey-Nagel) due to the manufacturer's instructions. cDNA single strands were synthesized from 2 µg total RNA using M-MLV reverse transcriptase (Promega). Quantitative real time PCR was performed using 10 ng cDNA, 10 pmol/primer, and 1x SYBR Green (BioRad, #1725272) in a CFX Connect Thermocycler (BioRad). The relative quantifications were normalized to the endogenous housekeeping genes β-actin and β-2-microglobulin using supplied software of the CFX Connect Real-Time PCR Detection System (Bio-Rad). Primer sequences are depicted in table 2.3.

#### Western Blotting

Cell lysates were electrophoretically separated by SDS PAGE and transferred onto nitrocellulose membranes as described previously [172]. Primary antibodies against CD133 (1:100, Milteny, #W6B3C1), c-Myc (1:1000, Thermo, #9E10), SOX2 (1:1000, Cell

Signaling, #L1D6A2), GLS (1:1000, abcam, #ab93434), GS (1:2500, BD, #610518), and β-actin (1:500, Santa Cruz, #sc-130657) were incubated overnight at 4° in 5 % milk powder in TBST. The secondary antibodies goat-anti-rabbit IRDye800CW (1:10000, LI-COR #926-32211), goat-anti-mouse IRDye680RD (1:10000, LI-COR #926-68070), and goat anti-mouse-HRP (1:10000, Jackson, #111-035-144) were diluted in 5 % milk powder in TBST and incubated for 1 h at room temperature. Chemiluminescent signals were detected on a film based system using chemiluminescent substrates (Thermo Scientific, #34096). Fluorescence-labelled antibodies were detected with a LI-COR Odyssey CLx Imager (LI-COR). Densitometry was performed with supplied software from LI-COR or ImageJ software [219].

**Dual-phase metabolite extraction**

Water soluble metabolites were extracted as previously described [109, 172, 220]. In brief, a minimum of $5x10^6$ cells were harvested, washed with PBS, and extracted with the dual-phase methanol/chloroform/water (1:1:1, v/v/v) method. Therefore, the cells were washed twice with 5 ml ice-cold 0.9 mM NaCl, re-suspended in 850 µl ice-cold $ddH_2O$ and transferred into pre-chilled glass tubes. After addition of 4 ml of ice-cold methanol the tubes were vortexed vigorously and incubated on ice for 15 min. Then 4 ml of ice-cold chloroform were added, vortexed, and incubated for 10 min on ice. Finally, 3.15 ml of ice-cold $ddH_2O$ were added, vortexed, and incubated overnight at 4°. The samples were centrifuged for 30 min at 4° and 4500 rpm. The upper water-methanol phase was separated and incubated for 10 min with 10 mg Chelex® 100 resin (Sigma) on ice. The samples were filtered through a 70 µm mesh and the methanol was evaporated for 1 h at 30° in a vacuum concentrator. Finally, the samples were frozen at –80°, lyophilized, and stored at –20° until spectroscopy measurement.

**NMR Data Acquisition and Processing**

Prior to measurement, the lyophilisates were re-suspended in 20 mM phosphate buffer (pH 7.0) containing 10 % $D_2O$ and 3-(Trimethylsilyl) propionic acid (TSP; Lancaster Synthesis) as an internal standard as described previously [172]. One-dimensional $^1$H-NMR spectra were acquired using a Bruker AVANCE III HD 700 spectrometer equipped with a 5 mm HCN TCI cryo-probe operating at 700 MHz (16.4 T). The $^1$H-NMR data were obtained using excitation sculpting for water suppressing and the following acquisition parameters: 25° sample temperature, 9800 Hz sweep width, 256 transients with 32 K time-domain data points were accumulated with a repetition time of 3.2 sec as previously described [172]. Mestrenova version 8.0.1-10878 (Mestrelab Research S.L.) software was used to process and analyze the $^1$H-NMR spectra. Equal concentrations of TSP in each sample were used as an internal standard for normalization. The figures show $^1$H-NMR data from three independent experiments presented as mean ± SD and statistical

significance was calculated with unpaired student t tests.

### Cell viability and Apoptosis assays

Cell viability was assessed as described previously [172]. The cell number was adjusted to 10 000 cells/ml and triplicates of 100 µl were plated per 96-well. To assess the effect of glutamine starvation, we plated the cells either in neurosphere medium with or without L-glutamine. For the C968 treatment, we plated the cells in neurosphere medium containing various drug concentrations (0.2 µM, 1 µM, 5 µM, 10 µM). Every other day the viable cell mass was assessed using the CellTiter-Blue® Cell Viability Assay (Promega) according to the manufacturer's instructions. The fluorescence was measured at 560ex/590em using a Safire 2 multiplate reader (Tecan). Exponential growth curves were calculated with GraphPad Prism 5 software (GraphPad Software, Inc., USA) and displayed in the graphs.

Apoptosis induction was measured with the Muse® Annexin V and Dead Cell Assay Kit. Therefore, GSCs were cultured in medium containing 50 ng/ml BMP4 for 48 h and flow cytometry measurements were performed on a Muse® cell analyzer (Merck Millipore) due to the manufacturer's instructions.

### Clonogenicity assays

The clonogenicity of GSCs was assessed with colony forming assays in semi-solid agarose medium as described previously [172]. Therefore, six-well plates were coated with 1.5 ml of 1 % agarose (Gibco, #18300012) in pre-warmed neurosphere medium. After 1 h incubation at 4 °, we added 2 ml of a single-cell suspension (3500 cells/well) in 0.6 % agarose in neurosphere medium. After 1 h incubation at room temperature, 2 ml neurosphere medium were added. To test GSC clonogenicity after glutamine starvation, all layers were prepared either with neurosphere medium with or without L-glutamine. To test the effect of BMP4 and C968 on GSC clonogenicity, we either added drugs (50 ng/ml BMP4 or 10 µM C968) or vehicles (citric acid or DMSO) to the upper medium layer. Twice a week 500 µl medium (with drug or vehicle) were added. After three weeks the top medium layer was removed, replaced by 1 ml of 1 mg/ml 4-Nitro blue tetrazolium chloride (NBT) (Sigma) in PBS and incubated overnight at 37 °. The stained colonies were counted using the Clono Counter software [221].

### Acknowledgements

The authors thank Guido Reifenberger and his research team (Department of Neuropathology, University Medical Center Düsseldorf) for their support. The authors acknowledge access to the Jülich-Düsseldorf Biomolecular NMR Center that is jointly run by Forschungszentrum Jülich and Heinrich-Heine-Universität Düsseldorf. The authors thank Kevin Bochinsky for technical assistance with spectra acquisition. The authors

thank Marc Remke (Department of Pediatric Oncology, Hematology and Immunology, University Medical Center Düsseldorf) for supplying the c-Myc antibody and Dieter Häussinger (Department of Clinic for Gastroenterology, Hepatology and Infectious Diseases, University Medical Center Düsseldorf) for supplying the GLS and GS antibodies.

**Grant Support**

KK is a scholar of the Düsseldorf School of Oncology (DSO) of HHU University. AKS is supported by the Friedrich-Ebert Stiftung. The work has been co-financed by the SFF Grants of the HHU University, Düsseldorf, Germany, awarded to JM and UDK. The work of UDK is supported by the Federal Ministry of Research and Education (03VP03791).

**Conflict of interest**

None.

### 2.3.7 Supplement

**Table 2.3:** Primer sequences used in qPCR

| Gene | Gene ID (NCBI) | Forward primer | Reverse primer |
|---|---|---|---|
| *ACTB* | 60 | CCCAGCACAATGAAGATCAA | CGATCCACACGGAGTACTTG |
| *B2M* | 567 | GTTGCTCCACAGGTAGCTCTAG | ACAAGCTTTGAGTGCAAGAGATTG |
| *GFAP* | 2670 | GGCAAAAGCACCAAAGACGG | GGCGGCGTTCCATTTACAAT |
| *GLS* | 2744 | CAGAAGGCACAGACATGGTTGG | GGCAGAAACCACCATTAGCCAG |
| *NES* | 10763 | GGCGCACCTCAAGATGTCC | CTTGGGGTCCTGAAAGCTG |
| *PROM1* | 8842 | CATCCACAGATGCTCCTA | GCTTTATGGGAGTCTTGG |
| *SLC7A11* | 23657 | CCTGGCATTTGGACGCTACAT | TCAGAATTGCTGTGAGCTTGCA |
| *SOX2* | 6657 | TGGACAGTTACGCGCACA | CGAGTAGGACATGCTGTA |

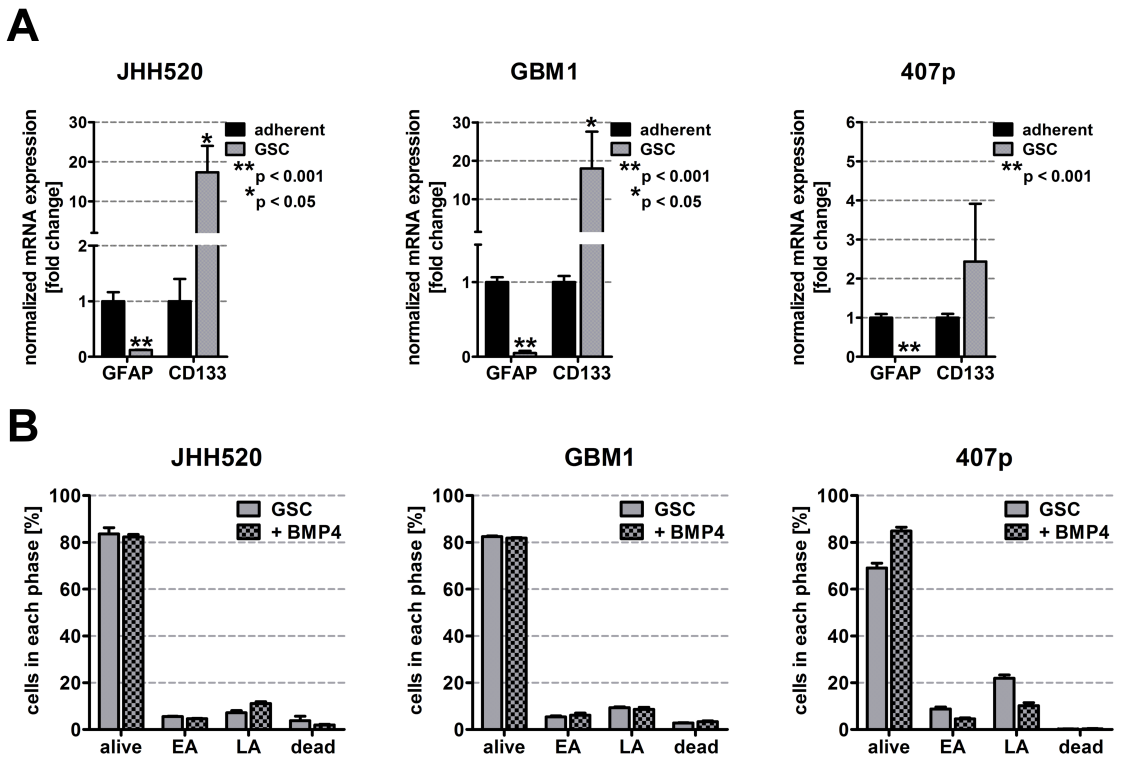


**Figure 2.20: Neurosphere culture induces stemness and BMP4 treatment only induces mild apoptosis. A.** Transfer from adherent to neurosphere culture (GSC) decreases GFAP and increases CD133 mRNA expression in all tested glioblastoma cell lines, as assessed with RT qPCR. **B.** BMP4 treatment induces very mild apoptosis in JHH520 GSCs and no apoptosis in GBM1 or 407p GSCs as assessed with the Muse® Annexin V and Dead Cell Kit. Abbreviations: EA, early apoptotic; LA, late apoptotic. The data is represented as mean ± SD (n = 3).

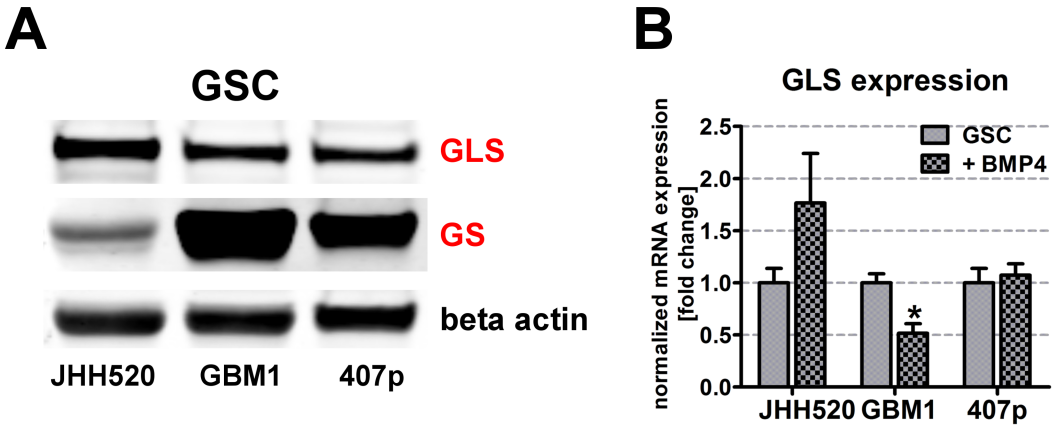


**Figure 2.21: GS and GLS expression do not correlate with Gln/Glu ratios and GLS expression is affected by BMP4 treatment. A.** GS and GLS baseline protein expression in GSC cultures was assessed by immunoblotting. β-actin immunoblotting was used as loading controls. **B.** Treatment with 50 ng/ml BMP4 over 48 h increases GLS1 mRNA expression in JHH520, decreases GLS1 expression in GBM1 and has no effect on GLS1 expression in 407p GSC cultures (*p < 0.05). The data is represented as mean ± SD (n = 3).

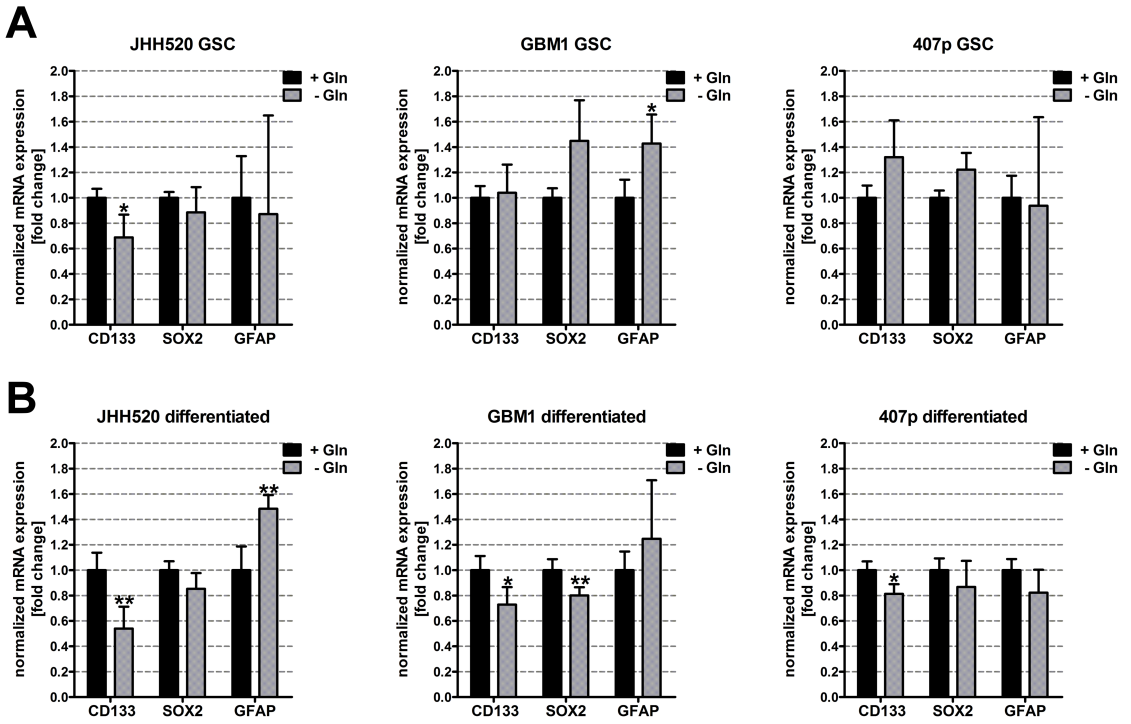


**Figure 2.22: Glutamine starvation reduces stemness and increases differentiation marker expression in differentiated GSC cultures.** The mRNA expression of CD133, SOX2, and GFAP was analyzed by RT qPCR in GSCs differentiated for 48 h with 50 ng/ml BMP4 either in the presence (**A**) or absence (**B**) of L-Gln (*p < 0.05, **p < 001). The data is represented as mean ± SD (n = 3).

# 3 General Discussion

This PhD thesis describes metabolic changes accompanying the formation of highly aggressive glioblastoma stem-like cells which substantially contributes to therapy resistance and tumor recurrence. The high malignancy and poor prognosis of glioblastoma is attributable to the existence of GSCs which are enriched by a developmental program called epithelial-mesenchymal transition [26, 35]. The failure of standard glioblastoma therapy to eradicate GSCs elucidates the need of innovative therapies specifically targeting GSCs in glioblastoma. Reprogrammed metabolism is well described for cancer cells [54, 105, 246] and contributes to proliferation and maintenance of redox balance, however, whether the formation of GSCs is accompanied or even driven by metabolic changes remain elusive. Here we show that GSCs reprogram known metabolic pathways involved in tumor progression and therapy resistance, thereby providing diagnostic markers for monitoring of GSC therapy as well as new targets for GSC-specific therapies.

Using HR $^{1}$H-NMR spectroscopy we were able to perform metabolic analysis on *ex vivo* cellular extracts generating high-resolution spectra of the water-soluble metabolome. To analyze whether stemness affects cellular metabolism, we generated glioblastoma cultures with different degrees of stemness. We effectively reduced the GSC population by ZEB1-dependent inhibition of EMT (Sec. 2.2), by spontaneous differentiation by propagation to adherent cell growth (Sec. 2.1 and 2.3), and by BMP4-induced targeted glial differentiation (Sec. 2.3) [145]. Several studies confirmed that ZEB1 regulates invasiveness in glioblastoma [39, 40, 42, 51] and is highly expressed in the invasive front of human xenografts and patient tumors [39, 52]. Furthermore, the GSC marker CD133 is a direct target of ZEB1, indicating that ZEB1 is a direct regulator of GSC enrichment [39]. Concisely, ZEB1 expression levels correlate with higher tumor grade in malignant gliomas [42], emphasizing that ZEB1 suppression is a valid tool to decrease the GSC fraction in glioblastoma cultures. Less clear is the effect of ZEB1 expression on cell viability. Contrary results have been published in recent years, showing ZEB1 promoting [188, 189], impairing [44, 190], or having no effect [191] on cell viability. We postulate that ZEB1 expression is crucial for the viability of GSCs since we observed significantly reduced cell viability upon ZEB1 inhibition in all tested glioblastoma neurosphere lines (Sec. 2.2).

ZEB1-dependent reduction of EMT significantly impaired choline metabolism in glioblastoma neurospheres (Sec. 2.2), since we observed highly reduced metabolite levels of phosphatidylcholine and total choline in all tested cell lines. This effect seems to be attributable to the reduced fraction of GSCs in cells with impaired mesenchymal transformation since spontaneous and targeted differentiation of GSC cultures showed similar results (Sec. 2.3). Furthermore, we observed significantly elevated tCho/tCre ratios in neurospheres expressing high levels of CD133 compared to adherent cells with low CD133 expression (Sec. 2.1). Therefore, we conclude that ZEB1 enhances choline metabolism by enrichment of GSCs in culture. Phosphocholine is the main precursor of phosphatidylcholine synthesis and therefore crucial for plasma membrane integrity and synthesis of second messengers. The cholinic phenotype (high PC and tCho) we

observed in GSCs could be correlated with malignant progression in several tumor entities [105, 139]. Furthermore, we speculate that the cholinic phenotype in GSCs is attributable to increased choline kinase alpha expression, since CHK$\alpha$ mRNA levels were significantly reduced in cells with impaired EMT due to ZEB1 inhibition (Fig. 2.4). CHK$\alpha$ activity has been described to regulate tumorigenicity, cell cycle progression, and correlates with poor prognosis in various cancers including breast, ovarian, bladder and prostate tumors [109, 112, 113, 114]. Our findings illustrate that GSCs upregulate CHK$\alpha$ expression, thereby increasing the cholinic phenotype and contributing to tumor malignancy. Furthermore, we hypothesize that the CHK$\alpha$ expression level directly correlates with the stem cell character of glioblastomas. The positive correlation between the expression levels of CHK$\alpha$ and the mesenchymal marker VIMENTIN [180, 181, 182] we observed in immunocytochemistry stainings further supports this assumption (Fig. 2.6).

We were further able to confirm that CHK$\alpha$ activation is responsible for the increased cholinic phenotype observed in GSCs since knockdown of CHK$\alpha$ in glioblastoma neurospheres dramatically reduced PC and tCho to levels even lower than after ZEB1 inhibition (Fig. 2.5). Considering that CHK$\alpha$ expression is directly linked to invasiveness and tumor aggressiveness in various tumors, we analyzed whether suppression of CHK$\alpha$ is able to reverse EMT and target the GSC fraction in glioblastoma cells. Indeed, both genetic knockdown using RNA interference technology and pharmacological CHK$\alpha$ inhibition with the small molecule inhibitor V11-0711 significantly reduced the expression of several EMT activators including ZEB1 and TWIST1. Both ZEB1 and TWIST1 promote invasion in human glioblastomas [45, 178]. Concisely, we observed impaired invasiveness and clonogenicity in glioblastoma neurospheres with impaired CHK$\alpha$ activity (Fig. 2.8 and 2.10). Clonogenicity is a key feature of GSCs, since they are able to serve as a seed for tumor formation in mice and induce tumor recurrence in patients [175]. Therefore, the reduced clonogenic capacity we observed after CHK$\alpha$ inhibition indicates a shrinkage of the GSC population. This is further supported by the reduced expression of the GSC markers SOX2 and NES we detected in CHK$\alpha$ knockdown cells (Fig. 2.7). Our results elucidate that CHK$\alpha$ is a potent regulator of GSCs in glioblastoma and therefore represents an interesting target for novel anti-GSC therapies.

This is further supported by the observed synergistic effects of combined treatment with CHK$\alpha$ inhibitor V11-0711 and the standard of care chemotherapeutic for glioblastoma, Temozolomide (Fig. 2.11). However, synergistic effects were only significant in GBM1 cells. ZEB1 has been described as a regulator of MGMT expression, a methyltransferase that antagonizes the genotoxic effects of alkylating agents such as TMZ [18, 39]. Considering that CHK$\alpha$ regulates ZEB1 expression, the observed synergistic effects could result from impaired MGMT expression and thus better performance of the alkylating agent TMZ in cells with suppressed CHK$\alpha$. However, further studies on MGMT in cells with impaired CHK$\alpha$ expression are needed to prove this point. Also in breast cancer cells, the combination treatment with CHK$\alpha$ inhibitors and the standard of care treatment 5-fluorouracil has synergistic effects [105, 132]. In general, pharmacological inhibition of CHK$\alpha$ has been shown to irreversibly reduce proliferation in oncogene transformed

but not non-malignant cells [131], further supporting the relevance of CHK$\alpha$ inhibition in cancer therapy. Since CHK$\alpha$ correlates with malignancy in several tumor types, we hypothesize that CHK$\alpha$ regulates EMT and GSC enrichment in other tumors as well.

Although we highlighted the reciprocal regulation between CHK$\alpha$ and EMT, the underlying mechanisms remain unknown. One possible explanation could be regulation of the phosphoinositide 3-kinase pathway. Previous studies have shown that CHK$\alpha$ expression is regulated by PI3K signaling in oncogene transformed cells inducing increased uptake of choline and accumulation of intracellular PC and tCho metabolites [105, 120]. Reciprocally, CHK$\alpha$ has been described to mediate PI3K signaling thereby increasing cell proliferation in transformed cells [121]. Strikingly, also EMT is regulated by Ras and PI3K signaling [205, 206, 207], enabling regulation of EMT by CHK$\alpha$ via the PI3K signaling pathway. A second possibility is the mutual regulation of CHK$\alpha$ and EMT via HIF1$\alpha$ signaling. Previous reports state that GSCs are enriched in regions with severe hypoxia and that they express high levels of HIF proteins contributing to neurosphere formation and expression of stem cell markers [32]. Moreover, suppression of HIF signaling impaired self-renewing potential, proliferation, and survival of GSCs *in vitro* and *in vivo* [32]. Furthermore, both ZEB1 expression and EMT have been directly linked to HIF1$\alpha$ expression in colorectal cancer and malignant gliomas [42, 247, 248]. Interestingly, also CHK$\alpha$ is upregulated by HIF1$\alpha$ signaling and putative hypoxia response elements (HRE), binding sites for HIF proteins, have been identified within the CHK$\alpha$ promoter region [111]. In conclusion, both PI3K and HIF1$\alpha$ signaling represent possible explanations for the mutual regulation of choline metabolism and EMT in GSC cultures, however further investigations are needed to prove our assumptions.

Besides the increased cholinic phenotype, we observed accumulation of intracellular lactate in GSCs compared to their differentiated counterparts (Sec. 2.3). Concisely, suppression of both ZEB1 and CHK$\alpha$ reduced Lac levels in glioblastoma neurospheres (Sec. 2.2), however only significant in LN229 CHK$\alpha$ knockdown cells. Of note, JHH520 and 407p cells were not used in this study. These results indicate that targeted differentiation with BMP4 is more potent in reducing stemness than ZEB1- or CHK$\alpha$-mediated inhibition of EMT. The observed Lac accumulation in GSCs indicates elevated levels of aerobic glycolysis, a phenomenon extensively observed in highly proliferative cells such as cancer cells [61, 62]. Interestingly, expression of lactate dehydrogenase A, the enzyme metabolizing pyruvate to lactate, promotes stemness in glioblastoma [231]. Reciprocally, EMT increases the glycolytic activity of GSCs [232] and causes intracellular Lac accumulation [233]. Therefore, our results support previous reports identifying elevated levels of aerobic glycolysis as a feature of GSCs [234].

In highly proliferative cells, aerobic glycolysis coincides with upregulation of glutaminolysis [57, 237]. Concisely, we observed deregulated glutamine metabolism in lactate-accumulating GSCs compared to their differentiated counterparts (Sec. 2.3). Based on the relative metabolite concentrations assessed with HR $^{1}$H-NMR spectroscopy of *ex vivo* cellular extracts, we were able to stratify our different GSC cell lines into two groups: Cells with relatively high Gln compared to Glu levels (Gln/Glu$^{High}$) and cells with rela-

tively low Gln comparted to Glu levels (Gln/Glu$^{Low}$) (Fig. 2.17). Strikingly, the Gln/Glu ratio did not correlate with expression of glutaminase or glutamine synthetase, the enzymes metabolizing Gln to Glu and Glu to Gln, respectively. Starvation of GSC cultures for extracellular glutamine dramatically reduced the amount of Gln in Gln/Glu$^{High}$ and Gln/Glu$^{Low}$ cells, completely diminishing the intracellular Gln pool without affecting cell viability. However, glutamine starvation significantly reduced the clonogenicity of Gln/Glu$^{Low}$ but not of Gln/Glu$^{High}$ GSCs (Fig. 2.18). Recent studies identified upregulation of GS to be involved in resistance to glutamine starvation in glioblastoma [81]. Since we observed GS upregulation both in starvation-resistant and starvation-sensitive GSCs (Fig. 2.18), we conclude that GS upregulation protects GSCs from death but not from the loss of self-renewing capability. Furthermore, we assessed highest GS baseline expression in starvation-sensitive Gln/Glu$^{Low}$ GBM1 cells. This is in concordance with studies correlating high Gln/Glu ratios with low GS expression in tumors compared to the surrounding tissue [140]. We further observed stronger starvation-dependent reduction of GSH in Gln/Glu$^{Low}$ compared to Gln/Glu$^{High}$ GSCs (Fig. 2.18), giving rise to the question whether Gln/Glu$^{High}$ GSCs are protected from Gln starvation by initially high levels of Gln and GSH. This assumption is supported by recent studies identifying glutamine as a regulator of stemness by promoting glutathione synthesis [238]. Concisely, glial differentiation of Gln/Glu$^{High}$ GSCs reduced Gln and GSH levels (Fig. 2.16) and restored the sensitivity for glutamine deprivation, since we observed significantly impaired clonogenicity and reduced expression of CD133 in differentiated Gln/Glu$^{High}$ GSCs starved for Gln (Fig. 2.18). Therefore we conclude that high Gln/Glu ratios and GSH levels protect GSCs from glutamine starvation and that the Gln/Glu ratio is a prognostic marker for starvation sensitivity and aggressiveness of glioblastoma.

We could further identify expression of the glutamate/cystine antiporter xCT/SLC7A11 as a possible cause for the different Gln/Glu ratios we observed in GSCs, since we could correlate high Gln/Glu ratios with increased cXT expression (Fig. 2.17). Considering that xCT imports cystine, a substrate of GSH synthesis, reduced xCT activity causes the accumulation of reactive oxygen species and reduces cell proliferation [65, 75]. Reciprocally, elevated xCT expression promotes stemness and tumorigenicity [76, 77, 78]. Elevated xCT levels in Gln/Glu$^{High}$ GSCs cause increased export of Glu and therefore lead to higher Gln/Glu ratios. Since glutamine starvation reduced GSH levels, sensitivity of Gln/Glu$^{Low}$ GSCs to glutamine starvation could be due to reduced anti-oxidative capacity. Concisely, targeted differentiation of Gln/Glu$^{High}$ GSCs reduced xCT expression, GSH levels, and restored sensitivity to starvation. In conclusion, our results highlight xCT as a possible target in novel anti-GSC therapies. However, further studies are needed to prove its contribution in starvation resistance of GSCs.

Targeting glutaminolysis by inhibition of glutaminase reduces proliferation, tumorigenicity and oncogenic transformation in several tumor types [94, 95, 240, 241]. Concisely, we identified GLS as a powerful target in anti-GSC therapies, since treatment of GSC cultures with the GLS inhibitor C968 reduced cell viability, clonogenicity, and expression of the GSC markers CD133 and SOX2 (Fig. 2.19). Strikingly, GLS treatment targeted both

Gln/Glu$^{Low}$ and starvation-resistant Gln/Glu$^{High}$ GSCs. Furthermore, sensitivity to glutaminase inhibition did not correlate with expression of GLS but with expression of xCT, since we observed lower IC50s in Gln/Glu$^{High}$ than Gln/Glu$^{Low}$ cells. This is in accordance with recent literature showing that xCT expression increases sensitivity for glutaminase treatment [242]. The xCT expression status could therefore function as a prognostic biomarker for the efficacy of GLS inhibition in glioblastoma.

Interestingly, we could correlate the Gln/Glu ratio with c-Myc expression, since Gln/Glu$^{Low}$ GSC exhibited highly decreased c-Myc protein (Fig. 2.15). This is in strong conflict with recent literature, where c-Myc was described to cause glutamine addiction and promote glutaminolysis [58, 59, 60, 249]. We showed that starvation resistant GSCs expressed high c-Myc levels. This could be a phenomenon limited to GSCs but further studies are needed to understand underlying mechanism.

We further observed that GSCs downregulate creatine metabolism since cultivation as neurospheres highly reduced the amount of creatine (Cre) inside the cell (Sec. 2.3). Concisely, impairment of EMT and knockdown of CHK$\alpha$ increased intracellular Cre (Sec. 2.2). Furthermore, we observed increased tCho/tCre ratio in neurospheres compared to adherent cells (Sec. 2.1). However, this effect is at least in part attributable to the increase of tCho in neurospheres. Surprisingly, targeted differentiation by BMP4-treatment did not increase but decreased the amount of intracellular Cre (Fig. 2.16), suggesting that BMP4 signaling influences Cre metabolism independent of GSC regulation. Cre has been described as a putative anti-cancer agent and could be correlated with inhibition of tumor growth [211, 212]. Creatine kinase B (CKB), the enzyme catalyzing the phosphorylation of creatine to phosphocreatine, has been shown to promote tumorigenesis [213, 214]. Concisely, CHK$\alpha$ inhibition in GSCs not only increased intracellular Cre it further decreased mRNA expression of CKB causing an increase of the Cre/PCre ratio (Suppl. Fig. 2.13). Our results therefore suggest that creatine metabolites and CKB expression suppress tumorigenicity by contributing to a reduced fraction of GSCs in glioblastoma.

Finally, we observed accumulation of glycine in GSC cultures compared to their differentiated counterparts (Sec. 2.3). Furthermore, the ratio between Gly and myo-inositol (myo) was increased in glioblastoma neurospheres compared to adherent cultures (Sec. 2.1). Elevated Gly/myo ratios have been described as a marker for high-grade gliomas [168] since myo is reduced in high-grade brain tumors [151]. Therefore, an increase in the Gly/myo ratio could either be due to a decrease of myo, an increase of Gly, or both. Since Gly can be synthetized from Cho [170], we assessed the Gly/tCho ratios and observed them significantly diminished (75 %) in neurospheres compared to adherent cells (Sec. 2.1). A possible explanation could be that the increase in intracellular tCho we observed in cultures with high stemness (Sec. 2.2 and 2.3) is more pronounced than the increase in Gly, or the use of different substrates for Gly synthesis in GSCs (e.g. serine or threonine) [170]. Studies on glioblastoma patients revealed elevated Gly in the tumor compared to the surrounding tissue [235]. Furthermore, *ex vivo* assessment of tumor biopsies revealed that Gly levels correlate with the malignancy grade of tumors [168]. In accordance with our data in GSC cultures, Gly directly correlates with stemness, since the glycine recep-

tor $\alpha$1 (GLRA1) promotes self-renewal and tumorigenicity in glioblastoma xenografts and correlates with high tumor grade [236]. Reciprocally, knockdown of GLRA1 impairs the formation of neurospheres [236]. Furthermore, glycine is a component of the antioxidant GSH and therefore crucial for the maintenance of redox homeostasis. In GSCs exposed to targeted differentiation (Fig. 2.16) we observed positive correlation between Gly and GSH levels, possibly resulting from impaired GSH synthesis due to reduced Gly levels. Elevated Gly in tumors is in conflict with studies reporting the necessity of glycine clearance for GSC survival in hypoxic microenvironment such as pseudopalisades [153]. However, in normoxic glioblastoma, we hypothesize that elevated intracellular Gly indicates the existence of a higher GSC fraction.

In conclusion, this work highlights that GSCs reprogram several metabolic pathways, thereby most likely contributing to increased chemo resistance and tumor aggressiveness. In order to cope with high energy demands of highly proliferative cells [61] and promote stemness [231], GSCs upregulate aerobic glycolysis leading to lactate accumulation. This demands the upregulation of other pathways fueling the TCA cycle, such as glutaminolysis. We observed deregulated glutamine metabolism in GSCs and could stratify our cultures into starvation-resistant Gln/Glu$^{High}$ and starvation-sensitive Gln/Glu$^{Low}$ GSCs. Moreover, GSCs increase the cholinic phenotype due to upregulation of CHK$\alpha$, thereby promoting invasiveness, stemness and therapy resistance. We postulate that oncometabolite levels of Lac, PC, tCho, and Gly should be used in glioblastoma diagnostics and therapy monitoring in order to assess the GSC content. Furthermore, our results indicate that the Gln/Glu ratio can predict efficacy of glutamine starvation. Finally, we identified two promising targets for novel anti-GSC therapies, CHK$\alpha$ and GLS, whose inhibition robustly reduces stemness in glioblastoma cultures.

# 4 Bibliography


[1] M. Weller, W. Wick, K. Aldape, M. Brada, M. Berger, S. M. Pfister, R. Nishikawa, M. Rosenthal, P. Y. Wen, R. Stupp, and G. Reifenberger. Glioma. *Nat Rev Dis Primers*, 1:15017, 2015.

[2] I. T. Gavrilovic and J. B. Posner. Brain metastases: epidemiology and pathophysiology. *J Neurooncol*, 75(1):5–14, 2005.

[3] Q. T. Ostrom, H. Gittleman, P. Liao, T. Vecchione-Koval, Y. Wolinsky, C. Kruchko, and J. S. Barnholtz-Sloan. Cbtrus statistical report: Primary brain and other central nervous system tumors diagnosed in the united states in 2010-2014. *Neuro Oncol*, 19(5):1–88, 2017.

[4] M. Z. Braganza, C. M. Kitahara, A. Berrington de Gonzalez, P. D. Inskip, K. J. Johnson, and P. Rajaraman. Ionizing radiation and the risk of brain and central nervous system tumors: a systematic review. *Neuro Oncol*, 14(11):1316–24, 2012.

[5] M. C. Turner. Epidemiology: allergy history, ige, and cancer. *Cancer Immunol Immunother*, 61(9):1493–510, 2012.

[6] D. Ricard, A. Idbaih, F. Ducray, M. Lahutte, K. Hoang-Xuan, and J. Y. Delattre. Primary brain tumours in adults. *Lancet*, 379(9830):1984–96, 2012.

[7] D. N. Louis, A. Perry, G. Reifenberger, A. von Deimling, D. Figarella-Branger, W. K. Cavenee, H. Ohgaki, O. D. Wiestler, P. Kleihues, and D. W. Ellison. The 2016 world health organization classification of tumors of the central nervous system: a summary. *Acta Neuropathol*, 131(6):803–20, 2016.

[8] M. J. van den Bent. Interobserver variation of the histopathological diagnosis in clinical trials on glioma: a clinician's perspective. *Acta Neuropathol*, 120(3):297–304, 2010.

[9] H. Yan, D. W. Parsons, G. Jin, R. McLendon, B. A. Rasheed, W. Yuan, I. Kos, I. Batinic-Haberle, S. Jones, G. J. Riggins, H. Friedman, A. Friedman, D. Reardon, J. Herndon, K. W. Kinzler, V. E. Velculescu, B. Vogelstein, and D. D. Bigner. Idh1 and idh2 mutations in gliomas. *N Engl J Med*, 360(8):765–73, 2009.

[10] P. J. Killela, C. J. Pirozzi, P. Healy, Z. J. Reitman, E. Lipp, B. A. Rasheed, R. Yang, B. H. Diplas, Z. Wang, P. K. Greer, H. Zhu, C. Y. Wang, A. B. Carpenter, H. Friedman, A. H. Friedman, S. T. Keir, J. He, Y. He, R. E. McLendon, 2nd Herndon, J. E., H. Yan, and D. D. Bigner. Mutations in idh1, idh2, and in the tert promoter define clinically distinct subgroups of adult malignant gliomas. *Oncotarget*, 5(6):1515–25, 2014.

[11] Z. J. Reitman and H. Yan. Isocitrate dehydrogenase 1 and 2 mutations in cancer: alterations at a crossroads of cellular metabolism. *J Natl Cancer Inst*, 102(13):932–41, 2010.

[12] D. W. Parsons, S. Jones, X. Zhang, J. C. Lin, R. J. Leary, P. Angenendt, P. Mankoo, H. Carter, I. M. Siu, G. L. Gallia, A. Olivi, R. McLendon, B. A. Rasheed, S. Keir, T. Nikolskaya, Y. Nikolsky, D. A. Busam, H. Tekleab, Jr. Diaz, L. A., J. Hartigan, D. R. Smith, R. L. Strausberg, S. K. Marie, S. M. Shinjo, H. Yan, G. J. Riggins, D. D. Bigner, R. Karchin, N. Papadopoulos, G. Parmigiani, B. Vogelstein, V. E. Velculescu, and K. W. Kinzler. An integrated genomic analysis of human glioblastoma multiforme. *Science*, 321(5897):1807–12, 2008.

[13] W. Xu, H. Yang, Y. Liu, Y. Yang, P. Wang, S. H. Kim, S. Ito, C. Yang, P. Wang, M. T. Xiao, L. X. Liu, W. Q. Jiang, J. Liu, J. Y. Zhang, B. Wang, S. Frye, Y. Zhang, Y. H. Xu, Q. Y. Lei, K. L. Guan, S. M. Zhao, and Y. Xiong. Oncometabolite 2-hydroxyglutarate is a competitive inhibitor of alpha-ketoglutarate-dependent dioxygenases. *Cancer Cell*, 19(1):17–30, 2011.

[14] H. Noushmehr, D. J. Weisenberger, K. Diefes, H. S. Phillips, K. Pujara, B. P. Berman, F. Pan, C. E. Pelloski, E. P. Sulman, K. P. Bhat, R. G. Verhaak, K. A. Hoadley, D. N. Hayes, C. M. Perou, H. K. Schmidt, L. Ding, R. K. Wilson, D. Van Den Berg, H. Shen, H. Bengtsson, P. Neuvial, L. M. Cope, J. Buckley, J. G. Herman, S. B. Baylin, P. W. Laird, K. Aldape, and Network Cancer Genome Atlas Research. Identification of a cpg island methylator phenotype that defines a distinct subgroup of glioma. *Cancer Cell*, 17(5):510–22, 2010.

[15] S. Turcan, D. Rohle, A. Goenka, L. A. Walsh, F. Fang, E. Yilmaz, C. Campos, A. W. Fabius, C. Lu, P. S. Ward, C. B. Thompson, A. Kaufman, O. Guryanova, R. Levine, A. Heguy, A. Viale, L. G. Morris, J. T. Huse, I. K. Mellinghoff, and T. A. Chan. Idh1 mutation is sufficient to establish the glioma hypermethylator phenotype. *Nature*, 483(7390):479–83, 2012.

[16] M. Sanson, Y. Marie, S. Paris, A. Idbaih, J. Laffaire, F. Ducray, S. El Hallani, B. Boisselier, K. Mokhtari, K. Hoang-Xuan, and J. Y. Delattre. Isocitrate dehydrogenase 1 codon 132 mutation is an important prognostic biomarker in gliomas. *J Clin Oncol*, 27(25):4150–4, 2009.

[17] J. G. Cairncross, K. Ueki, M. C. Zlatescu, D. K. Lisle, D. M. Finkelstein, R. R. Hammond, J. S. Silver, P. C. Stark, D. R. Macdonald, Y. Ino, D. A. Ramsay, and D. N. Louis. Specific genetic predictors of chemotherapeutic response and survival in patients with anaplastic oligodendrogliomas. *J Natl Cancer Inst*, 90(19):1473–9, 1998.

[18] M. E. Hegi, A. C. Diserens, T. Gorlia, M. F. Hamou, N. de Tribolet, M. Weller, J. M. Kros, J. A. Hainfellner, W. Mason, L. Mariani, J. E. Bromberg, P. Hau, R. O. Mirimanoff, J. G. Cairncross, R. C. Janzer, and R. Stupp. Mgmt gene silencing and benefit from temozolomide in glioblastoma. *N Engl J Med*, 352(10):997–1003, 2005.

[19] R. Stupp, W. P. Mason, M. J. van den Bent, M. Weller, B. Fisher, M. J. Taphoorn, K. Belanger, A. A. Brandes, C. Marosi, U. Bogdahn, J. Curschmann, R. C. Janzer, S. K. Ludwin, T. Gorlia, A. Allgeier, D. Lacombe, J. G. Cairncross, E. Eisenhauer, R. O. Mirimanoff, Research European Organisation for, Tumor Treatment of Cancer Brain, Groups Radiotherapy, and Group National Cancer Institute of Canada Clinical Trials. Radiotherapy plus concomitant and adjuvant temozolomide for glioblastoma. *N Engl J Med*, 352(10):987–96, 2005.

[20] R. L. Siegel, K. D. Miller, and A. Jemal. Cancer statistics, 2017. *CA Cancer J Clin*, 67(1):7–30, 2017.

[21] G. Tabatabai, R. Stupp, M. J. van den Bent, M. E. Hegi, J. C. Tonn, W. Wick, and M. Weller. Molecular diagnostics of gliomas: the clinical perspective. *Acta Neuropathol*, 120(5):585–92, 2010.

[22] R. J. Diaz, S. Ali, M. G. Qadir, M. I. De La Fuente, M. E. Ivan, and R. J. Komotar. The role of bevacizumab in the treatment of glioblastoma. *J Neurooncol*, 133(3):455–467, 2017.

[23] D. Sturm, H. Witt, V. Hovestadt, D. A. Khuong-Quang, D. T. Jones, C. Konermann, E. Pfaff, M. Tonjes, M. Sill, S. Bender, M. Kool, M. Zapatka, N. Becker, M. Zucknick, T. Hielscher, X. Y. Liu, A. M. Fontebasso, M. Ryzhova, S. Albrecht, K. Jacob, M. Wolter, M. Ebinger, M. U. Schuhmann, T. van Meter, M. C. Fruhwald, H. Hauch, A. Pekrun, B. Radlwimmer, T. Niehues, G. von Komorowski, M. Durken, A. E. Kulozik, J. Madden, A. Donson, N. K. Foreman, R. Drissi, M. Fouladi, W. Scheurlen, A. von Deimling, C. Monoranu, W. Roggendorf, C. Herold-Mende, A. Unterberg, C. M. Kramm, J. Felsberg, C. Hartmann, B. Wiestler, W. Wick, T. Milde, O. Witt, A. M. Lindroth, J. Schwartzentruber, D. Faury, A. Fleming, M. Zakrzewska, P. P. Liberski, K. Zakrzewski, P. Hauser, M. Garami, A. Klekner, L. Bognar, S. Morrissy, F. Cavalli, M. D. Taylor, P. van Sluis, J. Koster, R. Versteeg, R. Volckmann, T. Mikkelsen, K. Aldape, G. Reifenberger, V. P. Collins, J. Majewski, A. Korshunov, P. Lichter, C. Plass, N. Jabado, and S. M. Pfister. Hotspot mutations in h3f3a and idh1 define distinct epigenetic and biological subgroups of glioblastoma. *Cancer Cell*, 22(4):425–37, 2012.

[24] B. S. Paugh, C. Qu, C. Jones, Z. Liu, M. Adamowicz-Brice, J. Zhang, D. A. Bax, B. Coyle, J. Barrow, D. Hargrave, J. Lowe, A. Gajjar, W. Zhao, A. Broniscer, D. W. Ellison, R. G. Grundy, and S. J. Baker.

Integrated molecular genetic profiling of pediatric high-grade gliomas reveals key differences with the adult disease. *J Clin Oncol*, 28(18):3061–8, 2010.

[25] R. G. Verhaak, K. A. Hoadley, E. Purdom, V. Wang, Y. Qi, M. D. Wilkerson, C. R. Miller, L. Ding, T. Golub, J. P. Mesirov, G. Alexe, M. Lawrence, M. O'Kelly, P. Tamayo, B. A. Weir, S. Gabriel, W. Winckler, S. Gupta, L. Jakkula, H. S. Feiler, J. G. Hodgson, C. D. James, J. N. Sarkaria, C. Brennan, A. Kahn, P. T. Spellman, R. K. Wilson, T. P. Speed, J. W. Gray, M. Meyerson, G. Getz, C. M. Perou, D. N. Hayes, and Network Cancer Genome Atlas Research. Integrated genomic analysis identifies clinically relevant subtypes of glioblastoma characterized by abnormalities in pdgfra, idh1, egfr, and nf1. *Cancer Cell*, 17(1):98–110, 2010.

[26] S. K. Singh, I. D. Clarke, M. Terasaki, V. E. Bonn, C. Hawkins, J. Squire, and P. B. Dirks. Identification of a cancer stem cell in human brain tumors. *Cancer Res*, 63(18):5821–8, 2003.

[27] G. Liu, X. Yuan, Z. Zeng, P. Tunici, H. Ng, I. R. Abdulkadir, L. Lu, D. Irvin, K. L. Black, and J. S. Yu. Analysis of gene expression and chemoresistance of cd133+ cancer stem cells in glioblastoma. *Mol Cancer*, 5:67, 2006.

[28] D. L. Schonberg, D. Lubelski, T. E. Miller, and J. N. Rich. Brain tumor stem cells: Molecular characteristics and their impact on therapy. *Mol Aspects Med*, 39:82–101, 2014.

[29] C. Hirschmann-Jax, A. E. Foster, G. G. Wulf, J. G. Nuchtern, T. W. Jax, U. Gobel, M. A. Goodell, and M. K. Brenner. A distinct "side population" of cells with high drug efflux capacity in human tumor cells. *Proc Natl Acad Sci U S A*, 101(39):14228–33, 2004.

[30] L. Campos, J. P. Rouault, O. Sabido, P. Oriol, N. Roubi, C. Vasselon, E. Archimbaud, J. P. Magaud, and D. Guyotat. High expression of bcl-2 protein in acute myeloid leukemia cells is associated with poor response to chemotherapy. *Blood*, 81(11):3091–6, 1993.

[31] S. Bao, Q. Wu, S. Sathornsumetee, Y. Hao, Z. Li, A. B. Hjelmeland, Q. Shi, R. E. McLendon, D. D. Bigner, and J. N. Rich. Stem cell-like glioma cells promote tumor angiogenesis through vascular endothelial growth factor. *Cancer Res*, 66(16):7843–8, 2006.

[32] Z. Li, S. Bao, Q. Wu, H. Wang, C. Eyler, S. Sathornsumetee, Q. Shi, Y. Cao, J. Lathia, R. E. McLendon, A. B. Hjelmeland, and J. N. Rich. Hypoxia-inducible factors regulate tumorigenic capacity of glioma stem cells. *Cancer Cell*, 15(6):501–13, 2009.

[33] T. W. Owens and M. J. Naylor. Breast cancer stem cells. *Front Physiol*, 4(225), 2013.

[34] E. D. Hay. An overview of epithelio-mesenchymal transformation. *Acta Anat (Basel)*, 154(1):8–20, 1995.

[35] S. A. Mani, W. Guo, M. J. Liao, E. N. Eaton, A. Ayyanan, A. Y. Zhou, M. Brooks, F. Reinhard, C. C. Zhang, M. Shipitsin, L. L. Campbell, K. Polyak, C. Brisken, J. Yang, and R. A. Weinberg. The epithelial-mesenchymal transition generates cells with properties of stem cells. *Cell*, 133(4):704–15, 2008.

[36] C. Scheel and R. A. Weinberg. Cancer stem cells and epithelial-mesenchymal transition: concepts and molecular links. *Semin Cancer Biol*, 22(5-6):396–403, 2012.

[37] U. D. Kahlert, J. V. Joseph, and F. A. E. Kruyt. Emt- and met-related processes in nonepithelial tumors: importance for disease progression, prognosis, and therapeutic opportunities. *Mol Oncol*, 11(7):860–877, 2017.

[38] U. D. Kahlert, G. Nikkhah, and J. Maciaczyk. Epithelial-to-mesenchymal(-like) transition as a relevant molecular event in malignant gliomas. *Cancer Lett*, 331(2):131–8, 2013.

[39] F. A. Siebzehnrubl, D. J. Silver, B. Tugertimur, L. P. Deleyrolle, D. Siebzehnrubl, M. R. Sarkisian, K. G. Devers, A. T. Yachnis, M. D. Kupper, D. Neal, N. H. Nabilsi, M. P. Kladde, O. Suslov, S. Brabletz, T. Brabletz, B. A. Reynolds, and D. A. Steindler. The zeb1 pathway links glioblastoma initiation, invasion and chemoresistance. *EMBO Mol Med*, 5(8):1196–212, 2013.

[40] U. D. Kahlert, D. Maciaczyk, S. Doostkam, B. A. Orr, B. Simons, T. Bogiel, T. Reithmeier, M. Prinz, J. Schubert, G. Niedermann, T. Brabletz, C. G. Eberhart, G. Nikkhah, and J. Maciaczyk. Activation of canonical wnt/beta-catenin signaling enhances in vitro motility of glioblastoma cells by activation of zeb1 and other activators of epithelial-to-mesenchymal transition. *Cancer Lett*, 325(1):42–53, 2012.

[41] J. Dou, X. He, Y. Liu, Y. Wang, F. Zhao, X. Wang, D. Chen, F. Shi, and J. Wang. Effect of downregulation of zeb1 on vimentin expression, tumour migration and tumourigenicity of melanoma b16f10 cells and cscs. *Cell Biol Int*, 38(4):452–61, 2014.

[42] U. D. Kahlert, A. K. Suwala, E. H. Raabe, F. A. Siebzehnrubl, M. J. Suarez, B. A. Orr, E. E. Bar, J. Maciaczyk, and C. G. Eberhart. Zeb1 promotes invasion in human fetal neural stem cells and hypoxic glioma neurospheres. *Brain Pathol*, 25(6):724–32, 2015.

[43] H. Liu, H. Wang, X. Liu, and T. Yu. mir-1271 inhibits migration, invasion and epithelial-mesenchymal transition by targeting zeb1 and twist1 in pancreatic cancer cells. *Biochem Biophys Res Commun*, 472(2):346–52, 2016.

[44] Y. Liu, S. El-Naggar, D. S. Darling, Y. Higashi, and D. C. Dean. Zeb1 links epithelial-mesenchymal transition and cellular senescence. *Development*, 135(3):579–88, 2008.

[45] S. A. Mikheeva, A. M. Mikheev, A. Petit, R. Beyer, R. G. Oxford, L. Khorasani, J. P. Maxwell, C. A. Glackin, H. Wakimoto, I. Gonzalez-Herrero, I. Sanchez-Garcia, J. R. Silber, P. J. Horner, and R. C. Rostomily. Twist1 promotes invasion through mesenchymal change in human glioblastoma. *Mol Cancer*, 9:194, 2010.

[46] E. Sanchez-Tillo, L. Fanlo, L. Siles, S. Montes-Moreno, A. Moros, G. Chiva-Blanch, R. Estruch, A. Martinez, D. Colomer, B. Gyorffy, G. Roue, and A. Postigo. The emt activator zeb1 promotes tumor growth and determines differential response to chemotherapy in mantle cell lymphoma. *Cell Death Differ*, 21(2):247–57, 2014.

[47] U. Weyemi, C. E. Redon, T. K. Sethi, A. S. Burrell, P. Jailwala, M. Kasoji, N. Abrams, A. Merchant, and W. M. Bonner. Twist1 and slug mediate h2ax-regulated epithelial-mesenchymal transition in breast cells. *Cell Cycle*, page 0, 2016.

[48] A. Singh and J. Settleman. Emt, cancer stem cells and drug resistance: an emerging axis of evil in the war on cancer. *Oncogene*, 29(34):4741–51, 2010.

[49] H. Sui, L. Zhu, W. Deng, and Q. Li. Epithelial-mesenchymal transition and drug resistance: role, molecular mechanisms, and therapeutic strategies. *Oncol Res Treat*, 37(10):584–9, 2014.

[50] N. Wang, D. Guo, Y. Y. Zhao, C. Y. Dong, X. Y. Liu, B. X. Yang, S. W. Wang, L. Wang, Q. G. Liu, Q. Ren, Y. M. Lin, and X. T. Ma. Twist-1 promotes cell growth, drug resistance and progenitor clonogenic capacities in myeloid leukemia and is a novel poor prognostic factor in acute myeloid leukemia. *Oncotarget*, 6(25):20977–92, 2015.

[51] H. Pang, Y. Zheng, Y. Zhao, X. Xiu, and J. Wang. mir-590-3p suppresses cancer cell migration, invasion and epithelial-mesenchymal transition in glioblastoma multiforme by targeting zeb1 and zeb2. *Biochem Biophys Res Commun*, 468(4):739–45, 2015.

[52] L. Cheng, Q. Wu, O. A. Guryanova, Z. Huang, Q. Huang, J. N. Rich, and S. Bao. Elevated invasive potential of glioblastoma stem cells. *Biochem Biophys Res Commun*, 406(4):643–8, 2011.

[53] L. K. Boroughs and R. J. DeBerardinis. Metabolic pathways promoting cancer cell survival and growth. *Nat Cell Biol*, 17(4):351–9, 2015.

[54] R. J. DeBerardinis and N. S. Chandel. Fundamentals of cancer metabolism. *Sci Adv*, 2(5):e1600200, 2016.

[55] U. D. Kahlert, S. M. Mooney, M. Natsumeda, H. J. Steiger, and J. Maciaczyk. Targeting cancer stem-like cells in glioblastoma and colorectal cancer through metabolic pathways. *Int J Cancer*, 140(1):10–22, 2017.

[56] D. Hanahan and R. A. Weinberg. Hallmarks of cancer: the next generation. *Cell*, 144(5):646–74, 2011.

[57] B. J. Altman, Z. E. Stine, and C. V. Dang. From krebs to clinic: glutamine metabolism to cancer therapy. *Nat Rev Cancer*, 16(10):619–34, 2016.

[58] A. J. Bott, I. C. Peng, Y. Fan, B. Faubert, L. Zhao, J. Li, S. Neidler, Y. Sun, N. Jaber, D. Krokowski, W. Lu, J. A. Pan, S. Powers, J. Rabinowitz, M. Hatzoglou, D. J. Murphy, R. Jones, S. Wu, G. Girnun, and W. X. Zong. Oncogenic myc induces expression of glutamine synthetase through promoter demethylation. *Cell Metab*, 22(6):1068–77, 2015.

[59] P. Gao, I. Tchernyshyov, T. C. Chang, Y. S. Lee, K. Kita, T. Ochi, K. I. Zeller, A. M. De Marzo, J. E. Van Eyk, J. T. Mendell, and C. V. Dang. c-myc suppression of mir-23a/b enhances mitochondrial glutaminase expression and glutamine metabolism. *Nature*, 458(7239):762–5, 2009.

[60] D. R. Wise, R. J. DeBerardinis, A. Mancuso, N. Sayed, X. Y. Zhang, H. K. Pfeiffer, I. Nissim, E. Daikhin, M. Yudkoff, S. B. McMahon, and C. B. Thompson. Myc regulates a transcriptional program that stimulates mitochondrial glutaminolysis and leads to glutamine addiction. *Proc Natl Acad Sci U S A*, 105(48):18782–7, 2008.

[61] S. Y. Lunt and M. G. Vander Heiden. Aerobic glycolysis: meeting the metabolic requirements of cell proliferation. *Annu Rev Cell Dev Biol*, 27:441–64, 2011.

[62] O. Warburg. On the origin of cancer cells. *Science*, 123(3191):309–14, 1956.

[63] R. J. DeBerardinis, A. Mancuso, E. Daikhin, I. Nissim, M. Yudkoff, S. Wehrli, and C. B. Thompson. Beyond aerobic glycolysis: transformed cells can engage in glutamine metabolism that exceeds the requirement for protein and nucleotide synthesis. *Proc Natl Acad Sci U S A*, 104(49):19345–50, 2007.

[64] H. Shime, M. Yabu, T. Akazawa, K. Kodama, M. Matsumoto, T. Seya, and N. Inoue. Tumor-secreted lactic acid promotes il-23/il-17 proinflammatory pathway. *J Immunol*, 180(11):7175–83, 2008.

[65] J. Zhang, N. N. Pavlova, and C. B. Thompson. Cancer cell metabolism: the essential role of the nonessential amino acid, glutamine. *EMBO J*, 36(10):1302–1315, 2017.

[66] C. T. Hensley, A. T. Wasti, and R. J. DeBerardinis. Glutamine and cancer: cell biology, physiology, and clinical opportunities. *J Clin Invest*, 123(9):3678–84, 2013.

[67] J. Fan, J. J. Kamphorst, R. Mathew, M. K. Chung, E. White, T. Shlomi, and J. D. Rabinowitz. Glutamine-driven oxidative phosphorylation is a major atp source in transformed mammalian cells in both normoxia and hypoxia. *Mol Syst Biol*, 9:712, 2013.

[68] R. J. DeBerardinis and T. Cheng. Q's next: the diverse functions of glutamine in metabolism, cell biology and cancer. *Oncogene*, 29(3):313–24, 2010.

[69] K. Birsoy, T. Wang, W. W. Chen, E. Freinkman, M. Abu-Remaileh, and D. M. Sabatini. An essential role of the mitochondrial electron transport chain in cell proliferation is to enable aspartate synthesis. *Cell*, 162(3):540–51, 2015.

[70] L. B. Sullivan, D. Y. Gui, A. M. Hosios, L. N. Bush, E. Freinkman, and M. G. Vander Heiden. Supporting aspartate biosynthesis is an essential function of respiration in proliferating cells. *Cell*, 162(3):552–63, 2015.

[71] P. Xu, M. H. Oosterveer, S. Stein, H. Demagny, D. Ryu, N. Moullan, X. Wang, E. Can, N. Zamboni, A. Comment, J. Auwerx, and K. Schoonjans. Lrh-1-dependent programming of mitochondrial glutamine processing drives liver cancer. *Genes Dev*, 30(11):1255–60, 2016.

[72] Y. Hao, Y. Samuels, Q. Li, D. Krokowski, B. J. Guan, C. Wang, Z. Jin, B. Dong, B. Cao, X. Feng, M. Xiang, C. Xu, S. Fink, N. J. Meropol, Y. Xu, R. A. Conlon, S. Markowitz, K. W. Kinzler, V. E. Velculescu, H. Brunengraber, J. E. Willis, T. LaFramboise, M. Hatzoglou, G. F. Zhang, B. Vogelstein, and Z. Wang. Oncogenic pik3ca mutations reprogram glutamine metabolism in colorectal cancer. *Nat Commun*, 7:11971, 2016.

[73] N. Vie, V. Copois, C. Bascoul-Mollevi, V. Denis, N. Bec, B. Robert, C. Fraslon, E. Conseiller, F. Molina, C. Larroque, P. Martineau, M. Del Rio, and C. Gongora. Overexpression of phosphoserine aminotransferase psat1 stimulates cell growth and increases chemoresistance of colon cancer cells. *Mol Cancer*, 7:14, 2008.

[74] C. Gorrini, I. S. Harris, and T. W. Mak. Modulation of oxidative stress as an anticancer strategy. *Nat Rev Drug Discov*, 12(12):931–47, 2013.

[75] L. A. Timmerman, T. Holton, M. Yuneva, R. J. Louie, M. Padro, A. Daemen, M. Hu, D. A. Chan, S. P. Ethier, L. J. van 't Veer, K. Polyak, F. McCormick, and J. W. Gray. Glutamine sensitivity analysis identifies the xct antiporter as a common triple-negative breast tumor therapeutic target. *Cancer Cell*, 24(4):450–65, 2013.

[76] S. Lanzardo, L. Conti, R. Rooke, R. Ruiu, N. Accart, E. Bolli, M. Arigoni, M. Macagno, G. Barrera, S. Pizzimenti, L. Aurisicchio, R. A. Calogero, and F. Cavallo. Immunotargeting of antigen xct attenuates stem-like cell behavior and metastatic progression in breast cancer. *Cancer Res*, 76(1):62–72, 2016.

[77] K. Tsuchihashi, S. Okazaki, M. Ohmura, M. Ishikawa, O. Sampetrean, N. Onishi, H. Wakimoto, M. Yoshikawa, R. Seishima, Y. Iwasaki, T. Morikawa, S. Abe, A. Takao, M. Shimizu, T. Masuko, M. Nagane, F. B. Furnari, T. Akiyama, M. Suematsu, E. Baba, K. Akashi, H. Saya, and O. Nagano. The egf receptor promotes the malignant potential of glioma by regulating amino acid transport system xc(-). *Cancer Res*, 76(10):2954–63, 2016.

[78] S. M. Robert, S. C. Buckingham, S. L. Campbell, S. Robel, K. T. Holt, T. Ogunrinu-Babarinde, P. P. Warren, D. M. White, M. A. Reid, J. M. Eschbacher, M. E. Berens, A. C. Lahti, L. B. Nabors, and H. Sontheimer. Slc7a11 expression is associated with seizures and predicts poor survival in patients with malignant glioma. *Sci Transl Med*, 7(289):289ra86, 2015.

[79] E. A. Maher, I. Marin-Valencia, R. M. Bachoo, T. Mashimo, J. Raisanen, K. J. Hatanpaa, A. Jindal, F. M. Jeffrey, C. Choi, C. Madden, D. Mathews, J. M. Pascual, B. E. Mickey, C. R. Malloy, and R. J. DeBerardinis. Metabolism of [u-13 c]glucose in human brain tumors in vivo. *NMR Biomed*, 25(11):1234–44, 2012.

[80] T. Cheng, J. Sudderth, C. Yang, A. R. Mullen, E. S. Jin, J. M. Mates, and R. J. DeBerardinis. Pyruvate carboxylase is required for glutamine-independent growth of tumor cells. *Proc Natl Acad Sci U S A*, 108(21):8674–9, 2011.

[81] S. Tardito, A. Oudin, S. U. Ahmed, F. Fack, O. Keunen, L. Zheng, H. Miletic, P. O. Sakariassen, A. Weinstock, A. Wagner, S. L. Lindsay, A. K. Hock, S. C. Barnett, E. Ruppin, S. H. Morkve, M. Lund-Johansen, A. J. Chalmers, R. Bjerkvig, S. P. Niclou, and E. Gottlieb. Glutamine synthetase activity fuels nucleotide biosynthesis and supports growth of glutamine-restricted glioblastoma. *Nat Cell Biol*, 17(12):1556–68, 2015.

[82] G. Weber, N. Prajda, M. S. Lui, J. E. Denton, T. Aoki, J. Sebolt, Y. S. Zhen, M. E. Burt, M. A. Faderan, and M. A. Reardon. Multi-enzyme-targeted chemotherapy by acivicin and actinomycin. *Adv Enzyme Regul*, 20:75–96, 1982.

[83] T. Aoki and H. Oya. Acivicin inhibits crithidia fasciculata growth in a serum-free medium and inactivates carbamoyl-phosphate synthetase ii in vivo. *Comp Biochem Physiol C*, 90(2):391–6, 1988.

[84] M. S. Lui, H. Kizaki, and G. Weber. Biochemical pharmacology of acivicin in rat hepatoma cells. *Biochem Pharmacol*, 31(21):3469–73, 1982.

[85] G. S. Ahluwalia, J. L. Grem, Z. Hao, and D. A. Cooney. Metabolism and action of amino acid analog anti-cancer agents. *Pharmacol Ther*, 46(2):243–71, 1990.

[86] B. Levenberg, I. Melnick, and J. M. Buchanan. Biosynthesis of the purines. xv. the effect of aza-l-serine and 6-diazo-5-oxo-l-norleucine on inosinic acid biosynthesis de novo. *J Biol Chem*, 225(1):163–76, 1957.

[87] S. A. Taylor, J. Crowley, T. W. Pollock, H. J. Eyre, C. Jaeckle, H. E. Hynes, and R. L. Stephens. Objective antitumor activity of acivicin in patients with recurrent cns malignancies: a southwest oncology group trial. *J Clin Oncol*, 9(8):1476–9, 1991.

[88] R. Catane, D. D. Von Hoff, D. L. Glaubiger, and F. M. Muggia. Azaserine, don, and azotomycin: three diazo analogs of l-glutamine with clinical antitumor activity. *Cancer Treat Rep*, 63(6):1033–8, 1979.

[89] M. Hassanein, M. D. Hoeksema, M. Shiota, J. Qian, B. K. Harris, H. Chen, J. E. Clark, W. E. Alborn, R. Eisenberg, and P. P. Massion. Slc1a5 mediates glutamine transport required for lung cancer cell growth and survival. *Clin Cancer Res*, 19(3):560–70, 2013.

[90] A. D. Marshall, M. van Geldermalsen, N. J. Otte, T. Lum, M. Vellozzi, A. Thoeng, A. Pang, R. Nagarajah, B. Zhang, Q. Wang, L. Anderson, J. E. J. Rasko, and J. Holst. Asct2 regulates glutamine uptake and cell growth in endometrial carcinoma. *Oncogenesis*, 6(7):e367, 2017.

[91] S. Cardaci, S. Rizza, G. Filomeni, R. Bernardini, F. Bertocchi, M. Mattei, M. Paci, G. Rotilio, and M. R. Ciriolo. Glutamine deprivation enhances antitumor activity of 3-bromopyruvate through the stabilization of monocarboxylate transporter-1. *Cancer Res*, 72(17):4526–36, 2012.

[92] M. M. Robinson, S. J. McBryant, T. Tsukamoto, C. Rojas, D. V. Ferraris, S. K. Hamilton, J. C. Hansen, and N. P. Curthoys. Novel mechanism of inhibition of rat kidney-type glutaminase by bis-2-(5-phenylacetamido-1,2,4-thiadiazol-2-yl)ethyl sulfide (bptes). *Biochem J*, 406(3):407–14, 2007.

[93] A. Le, A. N. Lane, M. Hamaker, S. Bose, A. Gouw, J. Barbi, T. Tsukamoto, C. J. Rojas, B. S. Slusher, H. Zhang, L. J. Zimmerman, D. C. Liebler, R. J. Slebos, P. K. Lorkiewicz, R. M. Higashi, T. W. Fan, and C. V. Dang. Glucose-independent glutamine metabolism via tca cycling for proliferation and survival in b cells. *Cell Metab*, 15(1):110–21, 2012.

[94] J. B. Wang, J. W. Erickson, R. Fuji, S. Ramachandran, P. Gao, R. Dinavahi, K. F. Wilson, A. L. Ambrosio, S. M. Dias, C. V. Dang, and R. A. Cerione. Targeting mitochondrial glutaminase activity inhibits oncogenic transformation. *Cancer Cell*, 18(3):207–19, 2010.

[95] T. Han, M. Guo, T. Zhang, M. Gan, C. Xie, and J. B. Wang. A novel glutaminase inhibitor-968 inhibits the migration and proliferation of non-small cell lung cancer cells by targeting egfr/erk signaling pathway. *Oncotarget*, 8(17):28063–28073, 2017.

[96] K. Kitayama, M. Yashiro, T. Morisaki, Y. Miki, T. Okuno, H. Kinoshita, T. Fukuoka, H. Kasashima, G. Masuda, T. Hasegawa, K. Sakurai, N. Kubo, H. Irakawa K, and M. Ohira. Pyruvate kinase isozymes m2 and glutaminase might be promising molecular targets for the treatment of gastric cancer. *Cancer Sci*, 2017.

[97] J. M. Thornburg, K. K. Nelson, B. F. Clem, A. N. Lane, S. Arumugam, A. Simmons, J. W. Eaton, S. Telang, and J. Chesney. Targeting aspartate aminotransferase in breast cancer. *Breast Cancer Res*, 10(5):R84, 2008.

[98] G. Qing, B. Li, A. Vu, N. Skuli, Z. E. Walton, X. Liu, P. A. Mayes, D. R. Wise, C. B. Thompson, J. M. Maris, M. D. Hogarty, and M. C. Simon. Atf4 regulates myc-mediated neuroblastoma cell death upon glutamine deprivation. *Cancer Cell*, 22(5):631–44, 2012.

[99] Z. Li and D. E. Vance. Phosphatidylcholine and choline homeostasis. *J Lipid Res*, 49(6):1187–94, 2008.

[100] F. Gibellini and T. K. Smith. The kennedy pathway–de novo synthesis of phosphatidylethanolamine and phosphatidylcholine. *IUBMB Life*, 62(6):414–28, 2010.

[101] C. E. Mountford and L. C. Wright. Organization of lipids in the plasma membranes of malignant and stimulated cells: a new model. *Trends Biochem Sci*, 13(5):172–7, 1988.

[102] E. P. Kennedy and S. B. Weiss. The function of cytidine coenzymes in the biosynthesis of phospholipides. *J Biol Chem*, 222(1):193–214, 1956.

[103] A. Cuadrado, A. Carnero, F. Dolfi, B. Jimenez, and J. C. Lacal. Phosphorylcholine: a novel second messenger essential for mitogenic activity of growth factors. *Oncogene*, 8(11):2959–68, 1993.

[104] B. D. Price, J. D. Morris, C. J. Marshall, and A. Hall. Stimulation of phosphatidylcholine hydrolysis, diacylglycerol release, and arachidonic acid production by oncogenic ras is a consequence of protein kinase c activation. *J Biol Chem*, 264(28):16638–43, 1989.

[105] K. Glunde, Z. M. Bhujwalla, and S. M. Ronen. Choline metabolism in malignant transformation. *Nat Rev Cancer*, 11(12):835–48, 2011.

[106] F. Podo, S. Canevari, R. Canese, M. E. Pisanu, A. Ricci, and E. Iorio. Mr evaluation of response to targeted treatment in cancer cells. *NMR Biomed*, 24(6):648–72, 2011.

[107] W. Negendank. Studies of human tumors by mrs: a review. *NMR Biomed*, 5(5):303–24, 1992.

[108] E. O. Aboagye and Z. M. Bhujwalla. Malignant transformation alters membrane choline phospholipid metabolism of human mammary epithelial cells. *Cancer Res*, 59(1):80–4, 1999.

[109] K. Glunde, C. Jie, and Z. M. Bhujwalla. Molecular causes of the aberrant choline phospholipid metabolism in breast cancer. *Cancer Res*, 64(12):4270–6, 2004.

[110] A. Ramirez de Molina, A. Rodriguez-Gonzalez, R. Gutierrez, L. Martinez-Pineiro, J. Sanchez, F. Bonilla, R. Rosell, and J. Lacal. Overexpression of choline kinase is a frequent feature in human tumor-derived cell lines and in lung, prostate, and colorectal human cancers. *Biochem Biophys Res Commun*, 296(3):580–3, 2002.

[111] K. Glunde, T. Shah, Jr. Winnard, P. T., V. Raman, T. Takagi, F. Vesuna, D. Artemov, and Z. M. Bhujwalla. Hypoxia regulates choline kinase expression through hypoxia-inducible factor-1 alpha signaling in a human prostate cancer model. *Cancer Res*, 68(1):172–80, 2008.

[112] A. Granata, R. Nicoletti, V. Tinaglia, L. De Cecco, M. E. Pisanu, A. Ricci, F. Podo, S. Canevari, E. Iorio, M. Bagnoli, and D. Mezzanzanica. Choline kinase-alpha by regulating cell aggressiveness and drug sensitivity is a potential druggable target for ovarian cancer. *Br J Cancer*, 110(2):330–40, 2014.

[113] E. Hernando, J. Sarmentero-Estrada, T. Koppie, C. Belda-Iniesta, V. Ramirez de Molina, P. Cejas, C. Ozu, C. Le, J. J. Sanchez, M. Gonzalez-Baron, J. Koutcher, C. Cordon-Cardo, B. H. Bochner, J. C. Lacal, and A. Ramirez de Molina. A critical role for choline kinase-alpha in the aggressiveness of bladder carcinomas. *Oncogene*, 28(26):2425–35, 2009.

[114] L. Hu, R. Y. Wang, J. Cai, D. Feng, G. Z. Yang, Q. G. Xu, Y. X. Zhai, Y. Zhang, W. P. Zhou, and Q. P. Cai. Overexpression of chka contributes to tumor progression and metastasis and predicts poor prognosis in colorectal carcinoma. *Oncotarget*, 2016.

[115] N. Mori, F. Wildes, S. Kakkad, D. Jacob, M. Solaiyappan, K. Glunde, and Z. M. Bhujwalla. Choline kinase-alpha protein and phosphatidylcholine but not phosphocholine are required for breast cancer cell survival. *NMR Biomed*, 28(12):1697–706, 2015.

[116] A. Ramirez de Molina, R. Gutierrez, M. A. Ramos, J. M. Silva, J. Silva, F. Bonilla, J. J. Sanchez, and J. C. Lacal. Increased choline kinase activity in human breast carcinomas: clinical evidence for a potential novel antitumor strategy. *Oncogene*, 21(27):4317–22, 2002.

[117] Q. Zeng, H. Liu, K. Zhang, C. Li, and G. Zhou. Noninvasive evaluation of cerebral glioma grade by using multivoxel 3d proton mr spectroscopy. *Magn Reson Imaging*, 29(1):25–31, 2011.

[118] K. Glunde and Z. M. Bhujwalla. Choline kinase alpha in cancer prognosis and treatment. *Lancet Oncol*, 8(10):855–7, 2007.

[119] A. Ramirez de Molina, J. Sarmentero-Estrada, C. Belda-Iniesta, M. Taron, V. Ramirez de Molina, P. Cejas, M. Skrzypski, D. Gallego-Ortega, J. de Castro, E. Casado, M. A. Garcia-Cabezas, J. J. Sanchez, M. Nistal, R. Rosell, M. Gonzalez-Baron, and J. C. Lacal. Expression of choline kinase alpha to predict outcome in patients with early-stage non-small-cell lung cancer: a retrospective study. *Lancet Oncol*, 8(10):889–97, 2007.

[120] T. Wang, J. Li, F. Chen, Y. Zhao, X. He, D. Wan, and J. Gu. Choline transporters in human lung adenocarcinoma: expression and functional implications. *Acta Biochim Biophys Sin (Shanghai)*, 39(9):668–74, 2007.

[121] A. Yalcin, B. Clem, S. Makoni, A. Clem, K. Nelson, J. Thornburg, D. Siow, A. N. Lane, S. E. Brock, U. Goswami, J. W. Eaton, S. Telang, and J. Chesney. Selective inhibition of choline kinase simultaneously attenuates mapk and pi3k/akt signaling. *Oncogene*, 29(1):139–49, 2010.

[122] A. Ramirez de Molina, D. Gallego-Ortega, J. Sarmentero-Estrada, D. Lagares, T. Gomez Del Pulgar, E. Bandres, J. Garcia-Foncillas, and J. C. Lacal. Choline kinase as a link connecting phospholipid metabolism and cell cycle regulation: implications in cancer therapy. *Int J Biochem Cell Biol*, 40(9):1753–63, 2008.

[123] I. S. Gribbestad, B. Sitter, S. Lundgren, J. Krane, and D. Axelson. Metabolite composition in breast tumors examined by proton nuclear magnetic resonance spectroscopy. *Anticancer Res*, 19(3A):1737–46, 1999.

[124] M. G. Swanson, K. R. Keshari, Z. L. Tabatabai, J. P. Simko, K. Shinohara, P. R. Carroll, A. S. Zektzer, and J. Kurhanewicz. Quantification of choline- and ethanolamine-containing metabolites in human prostate tissues using 1h hr-mas total correlation spectroscopy. *Magn Reson Med*, 60(1):33–40, 2008.

[125] E. Iorio, A. Ricci, M. Bagnoli, M. E. Pisanu, G. Castellano, M. Di Vito, E. Venturini, K. Glunde, Z. M. Bhujwalla, D. Mezzanzanica, S. Canevari, and F. Podo. Activation of phosphatidylcholine cycle enzymes in human epithelial ovarian cancer cells. *Cancer Res*, 70(5):2126–35, 2010.

[126] T. R. McKnight, K. R. Lamborn, T. D. Love, M. S. Berger, S. Chang, W. P. Dillon, A. Bollen, and S. J. Nelson. Correlation of magnetic resonance spectroscopic and growth characteristics within grades ii and iii gliomas. *J Neurosurg*, 106(4):660–6, 2007.

[127] D. L. Morse, D. Carroll, S. Day, H. Gray, P. Sadarangani, S. Murthi, C. Job, B. Baggett, N. Raghunand, and R. J. Gillies. Characterization of breast cancers and therapy response by mrs and quantitative gene expression profiling in the choline pathway. *NMR Biomed*, 22(1):114–27, 2009.

[128] J. C. Lacal. Choline kinase: a novel target for antitumor drugs. *IDrugs*, 4(4):419–26, 2001.

[129] R. Hernandez-Alcoceba, L. Saniger, J. Campos, M. C. Nunez, F. Khaless, M. A. Gallo, A. Espinosa, and J. C. Lacal. Choline kinase inhibitors as a novel approach for antiproliferative drug design. *Oncogene*, 15(19):2289–301, 1997.

[130] K. Glunde, V. Raman, N. Mori, and Z. M. Bhujwalla. Rna interference-mediated choline kinase suppression in breast cancer cells induces differentiation and reduces proliferation. *Cancer Res*, 65(23):11034–43, 2005.

[131] A. Rodriguez-Gonzalez, A. Ramirez de Molina, F. Fernandez, M. A. Ramos, M. del Carmen Nunez, J. Campos, and J. C. Lacal. Inhibition of choline kinase as a specific cytotoxic strategy in oncogene-transformed cells. *Oncogene*, 22(55):8803–12, 2003.

[132] N. Mori, K. Glunde, T. Takagi, V. Raman, and Z. M. Bhujwalla. Choline kinase down-regulation increases the effect of 5-fluorouracil in breast cancer cells. *Cancer Res*, 67(23):11284–90, 2007.

[133] N. M. Al-Saffar, H. Troy, A. Ramirez de Molina, L. E. Jackson, B. Madhu, J. R. Griffiths, M. O. Leach, P. Workman, J. C. Lacal, I. R. Judson, and Y. L. Chung. Noninvasive magnetic resonance spectroscopic pharmacodynamic markers of the choline kinase inhibitor mn58b in human carcinoma models. *Cancer Res*, 66(1):427–34, 2006.

[134] S. Basu and A. Alavi. Molecular imaging (pet) of brain tumors. *Neuroimaging Clin N Am*, 19(4):625–46, 2009.

[135] R. E. Coleman, J. M. Hoffman, M. W. Hanson, H. D. Sostman, and S. C. Schold. Clinical application of pet for the evaluation of brain tumors. *J Nucl Med*, 32(4):616–22, 1991.

[136] L. Zhu, K. Ploessl, R. Zhou, D. Mankoff, and H. F. Kung. Metabolic imaging of glutamine in cancer. *J Nucl Med*, 58(4):533–537, 2017.

[137] K. N. Rajagopalan and R. J. DeBerardinis. Role of glutamine in cancer: therapeutic and imaging implications. *J Nucl Med*, 52(7):1005–8, 2011.

[138] C. Choi, I. E. Dimitrov, D. Douglas, A. Patel, L. G. Kaiser, C. A. Amezcua, and E. A. Maher. Improvement of resolution for brain coupled metabolites by optimized (1)h mrs at 7t. *NMR Biomed*, 23(9):1044–52, 2010.

[139] E. Ackerstaff, K. Glunde, and Z. M. Bhujwalla. Choline phospholipid metabolism: a target in cancer cells? *J Cell Biochem*, 90(3):525–33, 2003.

[140] I. Marin-Valencia, C. Yang, T. Mashimo, S. Cho, H. Baek, X. L. Yang, K. N. Rajagopalan, M. Maddie, V. Vemireddy, Z. Zhao, L. Cai, L. Good, B. P. Tu, K. J. Hatanpaa, B. E. Mickey, J. M. Mates, J. M. Pascual, E. A. Maher, C. R. Malloy, R. J. Deberardinis, and R. M. Bachoo. Analysis of tumor metabolism reveals mitochondrial glucose oxidation in genetically diverse human glioblastomas in the mouse brain in vivo. *Cell Metab*, 15(6):827–37, 2012.

[141] C. T. Hensley, B. Faubert, Q. Yuan, N. Lev-Cohain, E. Jin, J. Kim, L. Jiang, B. Ko, R. Skelton, L. Loudat, M. Wodzak, C. Klimko, E. McMillan, Y. Butt, M. Ni, D. Oliver, J. Torrealba, C. R. Malloy, K. Kernstine, R. E. Lenkinski, and R. J. DeBerardinis. Metabolic heterogeneity in human lung tumors. *Cell*, 164(4):681–94, 2016.

[142] M. Hassanein, M. R. Hight, J. R. Buck, M. N. Tantawy, M. L. Nickels, M. D. Hoeksema, B. K. Harris, K. Boyd, P. P. Massion, and H. C. Manning. Preclinical evaluation of 4-[18f]fluoroglutamine pet to assess asct2 expression in lung cancer. *Mol Imaging Biol*, 18(1):18–23, 2016.

[143] R. A. Cairns, I. S. Harris, and T. W. Mak. Regulation of cancer cell metabolism. *Nat Rev Cancer*, 11(2):85–95, 2011.

[144] P. Zhang, Y. Sun, and L. Ma. Zeb1: at the crossroads of epithelial-mesenchymal transition, metastasis and therapy resistance. *Cell Cycle*, 14(4):481–7, 2015.

[145] S. G. Piccirillo, B. A. Reynolds, N. Zanetti, G. Lamorte, E. Binda, G. Broggi, H. Brem, A. Olivi, F. Dimeco, and A. L. Vescovi. Bone morphogenetic proteins inhibit the tumorigenic potential of human brain tumour-initiating cells. *Nature*, 444(7120):761–5, 2006.

[146] U. D. Kahlert, K. Koch, A. K. Suwala, R. Hartmann, M. Cheng, D. Maciaczyk, D. Willbold, C. G. Eberhart, K. Glunde, and J. Maciaczyk. The effect of neurosphere culture conditions on the cellular metabolism of glioma cells. *Folia Neuropathol*, 53(3):219–25, 2015.

[147] P. C. De Witt Hamer, A. A. Van Tilborg, P. P. Eijk, P. Sminia, D. Troost, C. J. Van Noorden, B. Ylstra, and S. Leenstra. The genomic profile of human malignant glioma is altered early in primary cell culture and preserved in spheroids. *Oncogene*, 27(14):2091–6, 2008.

[148] M. Ahmad, K. Frei, E. Willscher, A. Stefanski, K. Kaulich, P. Roth, K. Stuhler, G. Reifenberger, H. Binder, and M. Weller. How stemlike are sphere cultures from long-term cancer cell lines? lessons from mouse glioma models. *J Neuropathol Exp Neurol*, 73(11):1062–77, 2014.

[149] M. Witusik-Perkowska, P. Rieske, K. Hulas-Bigoszewska, M. Zakrzewska, R. Stawski, D. Kulczycka-Wojdala, M. Bienkowski, E. Stoczynska-Fidelus, S. M. Gresner, S. Piaskowski, D. J. Jaskolski, W. Papierz, K. Zakrzewski, M. Kolasa, J. W. Ironside, and P. P. Liberski. Glioblastoma-derived spheroid cultures as an experimental model for analysis of egfr anomalies. *J Neurooncol*, 102(3):395–407, 2011.

[150] L. Bianchi, E. De Micheli, A. Bricolo, C. Ballini, M. Fattori, C. Venturi, F. Pedata, K. F. Tipton, and L. Della Corte. Extracellular levels of amino acids and choline in human high grade gliomas: an intraoperative microdialysis study. *Neurochem Res*, 29(1):325–34, 2004.

[151] M. Castillo, J. K. Smith, and L. Kwock. Correlation of myo-inositol levels and grading of cerebral astrocytomas. *AJNR Am J Neuroradiol*, 21(9):1645–9, 2000.

[152] P. Chinnaiyan, E. Kensicki, G. Bloom, A. Prabhu, B. Sarcar, S. Kahali, S. Eschrich, X. Qu, P. Forsyth, and R. Gillies. The metabolomic signature of malignant glioma reflects accelerated anabolic metabolism. *Cancer Res*, 72(22):5878–88, 2012.

[153] D. Kim, B. P. Fiske, K. Birsoy, E. Freinkman, K. Kami, R. L. Possemato, Y. Chudnovsky, M. E. Pacold, W. W. Chen, J. R. Cantor, L. M. Shelton, D. Y. Gui, M. Kwon, S. H. Ramkissoon, K. L. Ligon, S. W. Kang, M. Snuderl, M. G. Vander Heiden, and D. M. Sabatini. Shmt2 drives glioma cell survival in ischaemia but imposes a dependence on glycine clearance. *Nature*, 520(7547):363–7, 2015.

[154] C. L. Liao, M. M. Herman, and K. G. Bensch. Prolongation of g1 and s phase in c-6 glioma cells treated with maple syrup urine disease metabolits. morphologic and cell cycle studies. *Lab Invest*, 38(2):122–33, 1978.

[155] L. I. A. Metwally, S.E. El-din, O. Abdelaziz, I. M. Hamdy, A. K. Elsamman, and A. M. Abdelalim. Predicting grade of cerebral gliomas using myo-inositol/creatine ratio. *Egypt J Radiol Nucl Med*, 45(1):211–217, 2014.

[156] W. Shao, J. Gu, C. Huang, D. Liu, H. Huang, Z. Huang, Z. Lin, W. Yang, K. Liu, D. Lin, and T. Ji. Malignancy-associated metabolic profiling of human glioma cell lines using 1h nmr spectroscopy. *Mol Cancer*, 13:197, 2014.

[157] K. Christensen, C. Aaberg-Jessen, C. Andersen, D. Goplen, R. Bjerkvig, and B. W. Kristensen. Immunohistochemical expression of stem cell, endothelial cell, and chemosensitivity markers in primary glioma spheroids cultured in serum-containing and serum-free medium. *Neurosurgery*, 66(5):933–47, 2010.

[158] N. Platet, S. Y. Liu, M. E. Atifi, L. Oliver, F. M. Vallette, F. Berger, and D. Wion. Influence of oxygen tension on cd133 phenotype in human glioma cell cultures. *Cancer Lett*, 258(2):286–90, 2007.

[159] Z. Li. Cd133: a stem cell biomarker and beyond. *Exp Hematol Oncol*, 2(1):17, 2013.

[160] S. Jackowski. Cell cycle regulation of membrane phospholipid metabolism. *J Biol Chem*, 271(34):20219–22, 1996.

[161] T. R. McKnight, K. J. Smith, P. W. Chu, K. S. Chiu, C. P. Cloyd, S. M. Chang, J. J. Phillips, and M. S. Berger. Choline metabolism, proliferation, and angiogenesis in nonenhancing grades 2 and 3 astrocytoma. *J Magn Reson Imaging*, 33(4):808–16, 2011.

[162] D. Ott, J. Hennig, and T. Ernst. Human brain tumors: assessment with in vivo proton mr spectroscopy. *Radiology*, 186(3):745–52, 1993.

[163] J. Sabatier, V. Gilard, M. Malet-Martino, J. P. Ranjeva, C. Terral, S. Breil, M. B. Delisle, C. Manelfe, M. Tremoulet, and I. Berry. Characterization of choline compounds with in vitro 1h magnetic resonance spectroscopy for the discrimination of primary brain tumors. *Invest Radiol*, 34(3):230–5, 1999.

[164] C. M. Segebarth, D. F. Baleriaux, P. R. Luyten, and J. A. den Hollander. Detection of metabolic heterogeneity of human intracranial tumors in vivo by 1h nmr spectroscopic imaging. *Magn Reson Med*, 13(1):62–76, 1990.

[165] U. D. Kahlert, D. Maciaczyk, F. Dai, R. Claus, E. Firat, S. Doostkam, T. Bogiel, M. S. Carro, M. Dobrossy, C. Herold-Mende, G. Niedermann, M. Prinz, G. Nikkhah, and J. Maciaczyk. Resistance to hypoxia-induced, bnip3-mediated cell death contributes to an increase in a cd133-positive cell population in human glioblastomas in vitro. *J Neuropathol Exp Neurol*, 71(12):1086–99, 2012.

[166] C. Choi, S. K. Ganji, A. Madan, K. M. Hulsey, Z. An, S. Zhang, M. C. Pinho, R. J. DeBerardinis, R. M. Bachoo, and E. A. Maher. In vivo detection of citrate in brain tumors by 1h magnetic resonance spectroscopy at 3t. *Magn Reson Med*, 72(2):316–23, 2014.

[167] A. A. Maudsley, R. K. Gupta, R. Stoyanova, N. A. Parra, B. Roy, S. Sheriff, N. Hussain, and S. Behari. Mapping of glycine distributions in gliomas. *AJNR Am J Neuroradiol*, 35(6 Suppl):S31–6, 2014.

[168] V. Righi, O. C. Andronesi, D. Mintzopoulos, P. M. Black, and A. A. Tzika. High-resolution magic angle spinning magnetic resonance spectroscopy detects glycine as a biomarker in brain tumors. *Int J Oncol*, 36(2):301–6, 2010.

[169] Y. Kinoshita, H. Kajiwara, A. Yokota, and Y. Koga. Proton magnetic resonance spectroscopy of astrocytic tumors: an in vitro study. *Neurol Med Chir (Tokyo)*, 33(6):350–9, 1993.

[170] W. Wang, Z. Wu, Z. Dai, Y. Yang, J. Wang, and G. Wu. Glycine metabolism in animals and humans: implications for nutrition and health. *Amino Acids*, 45(3):463–77, 2013.

[171] G. Tedeschi, N. Lundbom, R. Raman, S. Bonavita, J. H. Duyn, J. R. Alger, and G. Di Chiro. Increased choline signal coinciding with malignant degeneration of cerebral gliomas: a serial proton magnetic resonance spectroscopy imaging study. *J Neurosurg*, 87(4):516–24, 1997.

[172] K. Koch, R. Hartmann, F. Schroter, A. K. Suwala, D. Maciaczyk, A. C. Kruger, D. Willbold, U. D. Kahlert, and J. Maciaczyk. Reciprocal regulation of the cholinic phenotype and epithelial-mesenchymal transition in glioblastoma cells. *Oncotarget*, 7(45):73414–73431, 2016.

[173] R. Stupp, M. E. Hegi, W. P. Mason, M. J. van den Bent, M. J. Taphoorn, R. C. Janzer, S. K. Ludwin, A. Allgeier, B. Fisher, K. Belanger, P. Hau, A. A. Brandes, J. Gijtenbeek, C. Marosi, C. J. Vecht, K. Mokhtari, P. Wesseling, S. Villa, E. Eisenhauer, T. Gorlia, M. Weller, D. Lacombe, J. G. Cairncross, R. O. Mirimanoff, Research European Organisation for, Tumour Treatment of Cancer Brain, Groups Radiation Oncology, and Group National Cancer Institute of Canada Clinical Trials. Effects

of radiotherapy with concomitant and adjuvant temozolomide versus radiotherapy alone on survival in glioblastoma in a randomised phase iii study: 5-year analysis of the eortc-ncic trial. *Lancet Oncol*, 10(5):459–66, 2009.

[174] F. B. Furnari, T. Fenton, R. M. Bachoo, A. Mukasa, J. M. Stommel, A. Stegh, W. C. Hahn, K. L. Ligon, D. N. Louis, C. Brennan, L. Chin, R. A. DePinho, and W. K. Cavenee. Malignant astrocytic glioma: genetics, biology, and paths to treatment. *Genes Dev*, 21(21):2683–710, 2007.

[175] S. K. Singh, C. Hawkins, I. D. Clarke, J. A. Squire, J. Bayani, T. Hide, R. M. Henkelman, M. D. Cusimano, and P. B. Dirks. Identification of human brain tumour initiating cells. *Nature*, 432(7015):396–401, 2004.

[176] B. B. Zhou, H. Zhang, M. Damelin, K. G. Geles, J. C. Grindley, and P. B. Dirks. Tumour-initiating cells: challenges and opportunities for anticancer drug discovery. *Nat Rev Drug Discov*, 8(10):806–23, 2009.

[177] S. Bao, Q. Wu, R. E. McLendon, Y. Hao, Q. Shi, A. B. Hjelmeland, M. W. Dewhirst, D. D. Bigner, and J. N. Rich. Glioma stem cells promote radioresistance by preferential activation of the dna damage response. *Nature*, 444(7120):756–60, 2006.

[178] M. C. Elias, K. R. Tozer, J. R. Silber, S. Mikheeva, M. Deng, R. S. Morrison, T. C. Manning, D. L. Silbergeld, C. A. Glackin, T. A. Reh, and R. C. Rostomily. Twist is expressed in human gliomas and promotes invasion. *Neoplasia*, 7(9):824–37, 2005.

[179] S. P. Han, J. H. Kim, M. E. Han, H. E. Sim, K. S. Kim, S. Yoon, S. Y. Baek, B. S. Kim, and S. O. Oh. Snai1 is involved in the proliferation and migration of glioblastoma cells. *Cell Mol Neurobiol*, 31(3):489–96, 2011.

[180] V. R. Praveen Kumar, P. Sehgal, B. Thota, S. Patil, V. Santosh, and P. Kondaiah. Insulin like growth factor binding protein 4 promotes gbm progression and regulates key factors involved in emt and invasion. *J Neurooncol*, 116(3):455–64, 2014.

[181] J. J. Lin, T. Z. Zhao, W. K. Cai, Y. X. Yang, C. Sun, Z. Zhang, Y. Q. Xu, T. Chang, and Z. Y. Li. Inhibition of histamine receptor 3 suppresses glioblastoma tumor growth, invasion, and epithelial-to-mesenchymal transition. *Oncotarget*, 6(19):17107–20, 2015.

[182] J. J. Cai, Z. X. Qi, L. C. Chen, Y. Yao, Y. Gong, and Y. Mao. mir-124 suppresses the migration and invasion of glioma cells in vitro via capn4. *Oncol Rep*, 35(1):284–90, 2016.

[183] R. Sanchez-Martinez, S. Cruz-Gil, M. Gomez de Cedron, M. Alvarez-Fernandez, T. Vargas, S. Molina, B. Garcia, J. Herranz, J. Moreno-Rubio, G. Reglero, M. Perez-Moreno, J. Feliu, M. Malumbres, and A. Ramirez de Molina. A link between lipid metabolism and epithelial-mesenchymal transition provides a target for colon cancer therapy. *Oncotarget*, 6(36):38719–36, 2015.

[184] J. L. Griffin and J. P. Shockcor. Metabolic profiles of cancer cells. *Nat Rev Cancer*, 4(7):551–61, 2004.

[185] S. Herminghaus, U. Pilatus, W. Moller-Hartmann, P. Raab, H. Lanfermann, W. Schlote, and F. E. Zanella. Increased choline levels coincide with enhanced proliferative activity of human neuroepithelial brain tumors. *NMR Biomed*, 15(6):385–92, 2002.

[186] J. Gruber, W. C. See Too, M. T. Wong, A. Lavie, T. McSorley, and M. Konrad. Balance of human choline kinase isoforms is critical for cell cycle regulation: implications for the development of choline kinase-targeted cancer therapy. *FEBS J*, 279(11):1915–28, 2012.

[187] S. C. Falcon, C. S. Hudson, Y. Huang, M. Mortimore, J. M. Golec, P. A. Charlton, P. Weber, and H. Sundaram. A non-catalytic role of choline kinase alpha is important in promoting cancer cell survival. *Oncogenesis*, 2:e38, 2013.

[188] Y. Wang, M. Wen, Y. Kwon, Y. Xu, Y. Liu, P. Zhang, X. He, Q. Wang, Y. Huang, K. Y. Jen, M. A. LaBarge, L. You, S. C. Kogan, J. W. Gray, J. H. Mao, and G. Wei. Cul4a induces epithelial-mesenchymal transition and promotes cancer metastasis by regulating zeb1 expression. *Cancer Res*, 74(2):520–31, 2014.

[189] E. Sintov, G. Nathan, S. Knoller, M. Pasmanik-Chor, H. A. Russ, and S. Efrat. Inhibition of zeb1 expression induces redifferentiation of adult human beta cells expanded in vitro. *Sci Rep*, 5:13024, 2015.

[190] H. J. Hugo, L. Pereira, R. Suryadinata, Y. Drabsch, T. J. Gonda, N. P. Gunasinghe, C. Pinto, E. T. Soo, B. J. van Denderen, P. Hill, R. G. Ramsay, B. Sarcevic, D. F. Newgreen, and E. W. Thompson. Direct repression of myb by zeb1 suppresses proliferation and epithelial gene expression during epithelial-to-mesenchymal transition of breast cancer cells. *Breast Cancer Res*, 15(6):R113, 2013.

[191] U. Wellner, J. Schubert, U. C. Burk, O. Schmalhofer, F. Zhu, A. Sonntag, B. Waldvogel, C. Vannier, D. Darling, A. zur Hausen, V. G. Brunton, J. Morton, O. Sansom, J. Schuler, M. P. Stemmler, C. Herzberger, U. Hopt, T. Keck, S. Brabletz, and T. Brabletz. The emt-activator zeb1 promotes tumorigenicity by repressing stemness-inhibiting microrna. *Nat Cell Biol*, 11(12):1487–95, 2009.

[192] S. Furse and A. I. de Kroon. Phosphatidylcholine's functions beyond that of a membrane brick. *Mol Membr Biol*, 32(4):117–9, 2015.

[193] R. Cazzolli, A. N. Shemon, M. Q. Fang, and W. E. Hughes. Phospholipid signalling through phospholipase d and phosphatidic acid. *IUBMB Life*, 58(8):457–61, 2006.

[194] R. M. Gangemi, F. Griffero, D. Marubbi, M. Perera, M. C. Capra, P. Malatesta, G. L. Ravetti, G. L. Zona, A. Daga, and G. Corte. Sox2 silencing in glioblastoma tumor-initiating cells causes stop of proliferation and loss of tumorigenicity. *Stem Cells*, 27(1):40–8, 2009.

[195] R. Favaro, M. Valotta, A. L. Ferri, E. Latorre, J. Mariani, C. Giachino, C. Lancini, V. Tosetti, S. Ottolenghi, V. Taylor, and S. K. Nicolis. Hippocampal development and neural stem cell maintenance require sox2-dependent regulation of shh. *Nat Neurosci*, 12(10):1248–56, 2009.

[196] G. J. Rahme and M. A. Israel. Id4 suppresses mmp2-mediated invasion of glioblastoma-derived cells by direct inactivation of twist1 function. *Oncogene*, 34(1):53–62, 2015.

[197] T. Shah, F. Wildes, M. F. Penet, Jr. Winnard, P. T., K. Glunde, D. Artemov, E. Ackerstaff, B. Gimi, S. Kakkad, V. Raman, and Z. M. Bhujwalla. Choline kinase overexpression increases invasiveness and drug resistance of human breast cancer cells. *NMR Biomed*, 23(6):633–42, 2010.

[198] R. H. Dahlrot, S. K. Hermansen, S. Hansen, and B. W. Kristensen. What is the clinical value of cancer stem cell markers in gliomas? *Int J Clin Exp Pathol*, 6(3):334–48, 2013.

[199] U. D. Kahlert, N. O. Bender, D. Maciaczyk, T. Bogiel, E. E. Bar, C. G. Eberhart, G. Nikkhah, and J. Maciaczyk. Cd133/cd15 defines distinct cell subpopulations with differential in vitro clonogenic activity and stem cell-related gene expression profile in in vitro propagated glioblastoma multiforme-derived cell line with a pnet-like component. *Folia Neuropathol*, 50(4):357–68, 2012.

[200] C. P. Foley, D. G. Rubin, A. Santillan, D. Sondhi, J. P. Dyke, Y. P. Gobin, R. G. Crystal, and D. J. Ballon. Intra-arterial delivery of aav vectors to the mouse brain after mannitol mediated blood brain barrier disruption. *J Control Release*, 196:71–8, 2014.

[201] M. Janowski, P. Walczak, and M. S. Pearl. Predicting and optimizing the territory of blood-brain barrier opening by superselective intra-arterial cerebral infusion under dynamic susceptibility contrast mri guidance. *J Cereb Blood Flow Metab*, 36(3):569–75, 2016.

[202] S. Janardhan, P. Srivani, and G. N. Sastry. Choline kinase: an important target for cancer. *Curr Med Chem*, 13(10):1169–86, 2006.

[203] A. Ramirez de Molina, V. Penalva, L. Lucas, and J. C. Lacal. Regulation of choline kinase activity by ras proteins involves ral-gds and pi3k. *Oncogene*, 21(6):937–46, 2002.

[204] A. Ramirez de Molina, A. Rodriguez-Gonzalez, V. Penalva, L. Lucas, and J. C. Lacal. Inhibition of chok is an efficient antitumor strategy for harvey-, kirsten-, and n-ras-transformed cells. *Biochem Biophys Res Commun*, 285(4):873–9, 2001.

[205] K. Wu, J. Fan, L. Zhang, Z. Ning, J. Zeng, J. Zhou, L. Li, Y. Chen, T. Zhang, X. Wang, J. T. Hsieh, and D. He. Pi3k/akt to gsk3beta/beta-catenin signaling cascade coordinates cell colonization for bladder cancer bone metastasis through regulating zeb1 transcription. *Cell Signal*, 24(12):2273–82, 2012.

[206] J. C. Tse and R. Kalluri. Mechanisms of metastasis: epithelial-to-mesenchymal transition and contribution of tumor microenvironment. *J Cell Biochem*, 101(4):816–29, 2007.

[207] M. Saitoh, K. Endo, S. Furuya, M. Minami, A. Fukasawa, T. Imamura, and K. Miyazawa. Stat3 integrates cooperative ras and tgf-beta signals that induce snail expression. *Oncogene*, 35(8):1049–57, 2016.

[208] Z. Zhong, Z. Hu, Y. Jiang, R. Sun, X. Chen, H. Chu, M. Zeng, and C. Sun. Interleukin-11 promotes epithelial-mesenchymal transition in anaplastic thyroid carcinoma cells through pi3k/akt/gsk3beta signaling pathway activation. *Oncotarget*, 2016.

[209] J. C. Cheng, N. Auersperg, and P. C. Leung. Egf-induced emt and invasiveness in serous borderline ovarian tumor cells: a possible step in the transition to low-grade serous carcinoma cells? *PLoS One*, 7(3):e34071, 2012.

[210] Y. Shang, X. Cai, and D. Fan. Roles of epithelial-mesenchymal transition in cancer drug resistance. *Curr Cancer Drug Targets*, 13(9):915–29, 2013.

[211] E. E. Miller, A. E. Evans, and M. Cohn. Inhibition of rate of tumor growth by creatine and cyclocreatine. *Proc Natl Acad Sci U S A*, 90(8):3304–8, 1993.

[212] P. L. Campos-Ferraz, B. Gualano, W. das Neves, I. T. Andrade, I. Hangai, R. T. Pereira, R. N. Bezerra, R. Deminice, M. Seelaender, and A. H. Lancha. Exploratory studies of the potential anti-cancer effects of creatine. *Amino Acids*, 2016.

[213] T. Wallimann, M. Tokarska-Schlattner, and U. Schlattner. The creatine kinase system and pleiotropic effects of creatine. *Amino Acids*, 40(5):1271–96, 2011.

[214] J. M. Loo, A. Scherl, A. Nguyen, F. Y. Man, E. Weinberg, Z. Zeng, L. Saltz, P. B. Paty, and S. F. Tavazoie. Extracellular metabolic energetics can promote cancer progression. *Cell*, 160(3):393–406, 2015.

[215] U. D. Kahlert, A. K. Suwala, K. Koch, M. Natsumeda, B. A. Orr, M. Hayashi, J. Maciaczyk, and C. G. Eberhart. Pharmacologic wnt inhibition reduces proliferation, survival, and clonogenicity of glioblastoma cells. *J Neuropathol Exp Neurol*, 74(9):889–900, 2015.

[216] K. J. Martin, S. F. Chen, G. M. Clark, D. Degen, M. Wajima, D. D. Von Hoff, and R. Kaddurah-Daouk. Evaluation of creatine analogues as a new class of anticancer agents using freshly explanted human tumor cells. *J Natl Cancer Inst*, 86(8):608–13, 1994.

[217] A. Untergasser, I. Cutcutache, T. Koressaar, J. Ye, B. C. Faircloth, M. Remm, and S. G. Rozen. Primer3–new capabilities and interfaces. *Nucleic Acids Res*, 40(15):e115, 2012.

[218] J. Moffat, D. A. Grueneberg, X. Yang, S. Y. Kim, A. M. Kloepfer, G. Hinkle, B. Piqani, T. M. Eisenhaure, B. Luo, J. K. Grenier, A. E. Carpenter, S. Y. Foo, S. A. Stewart, B. R. Stockwell, N. Hacohen, W. C. Hahn, E. S. Lander, D. M. Sabatini, and D. E. Root. A lentiviral rnai library for human and mouse genes applied to an arrayed viral high-content screen. *Cell*, 124(6):1283–98, 2006.

[219] C. A. Schneider, W. S. Rasband, and K. W. Eliceiri. Nih image to imagej: 25 years of image analysis. *Nat Methods*, 9(7):671–5, 2012.

[220] R. K. Tyagi, A. Azrad, H. Degani, and Y. Salomon. Simultaneous extraction of cellular lipids and water-soluble metabolites: evaluation by nmr spectroscopy. *Magn Reson Med*, 35(2):194–200, 1996.

[221] M. Niyazi, I. Niyazi, and C. Belka. Counting colonies of clonogenic assays by using densitometric software. *Radiat Oncol*, 2:4, 2007.

[222] D. R. Donohoe and S. J. Bultman. Metaboloepigenetics: interrelationships between energy metabolism and epigenetic control of gene expression. *J Cell Physiol*, 227(9):3169–77, 2012.

[223] J. Yun, J. L. Johnson, C. L. Hanigan, and J. W. Locasale. Interactions between epigenetics and metabolism in cancers. *Front Oncol*, 2:163, 2012.

[224] L. Galluzzi, O. Kepp, M. G. Vander Heiden, and G. Kroemer. Metabolic targets for cancer therapy. *Nat Rev Drug Discov*, 12(11):829–46, 2013.

[225] H. Pelicano, D. S. Martin, R. H. Xu, and P. Huang. Glycolysis inhibition for anticancer treatment. *Oncogene*, 25(34):4633–46, 2006.

[226] D. R. Wise and C. B. Thompson. Glutamine addiction: a new therapeutic target in cancer. *Trends Biochem Sci*, 35(8):427–33, 2010.

[227] Abigail S. Krall and Heather R. Christofk. Rethinking glutamine addiction. *Nat Cell Biol*, 17(12):1515–1517, 2015.

[228] K. Tanaka, T. Sasayama, Y. Irino, K. Takata, H. Nagashima, N. Satoh, K. Kyotani, T. Mizowaki, T. Imahori, Y. Ejima, K. Masui, B. Gini, H. Yang, K. Hosoda, R. Sasaki, P. S. Mischel, and E. Kohmura. Compensatory glutamine metabolism promotes glioblastoma resistance to mtor inhibitor treatment. *J Clin Invest*, 125(4):1591–602, 2015.

[229] M. J. Seltzer, B. D. Bennett, A. D. Joshi, P. Gao, A. G. Thomas, D. V. Ferraris, T. Tsukamoto, C. J. Rojas, B. S. Slusher, J. D. Rabinowitz, C. V. Dang, and G. J. Riggins. Inhibition of glutaminase preferentially slows growth of glioma cells with mutant idh1. *Cancer Res*, 70(22):8981–7, 2010.

[230] A. Muir, L. V. Danai, D. Y. Gui, C. Y. Waingarten, C. A. Lewis, and M. G. Vander Heiden. Environmental cystine drives glutamine anaplerosis and sensitizes cancer cells to glutaminase inhibition. *Elife*, 6, 2017.

[231] S. Daniele, C. Giacomelli, E. Zappelli, C. Granchi, M. L. Trincavelli, F. Minutolo, and C. Martini. Lactate dehydrogenase-a inhibition induces human glioblastoma multiforme stem cell differentiation and death. *Sci Rep*, 5:15556, 2015.

[232] D. Maciaczyk, D. Picard, L. Zhao, K. Koch, D. Herrera-Rios, G. Li, V. Marquardt, D. Pauck, T. Hoerbelt, W. Zhang, D. M. Ouwens, M. Remke, T. Jiang, H. J. Steiger, J. Maciaczyk, and U. D. Kahlert. Cbf1 is clinically prognostic and serves as a target to block cellular invasion and chemoresistance of emt-like glioblastoma cells. *Br J Cancer*, 117(1):102–112, 2017.

[233] P. Mao, K. Joshi, J. Li, S. H. Kim, P. Li, L. Santana-Santos, S. Luthra, U. R. Chandran, P. V. Benos, L. Smith, M. Wang, B. Hu, S. Y. Cheng, R. W. Sobol, and I. Nakano. Mesenchymal glioma stem cells are maintained by activated glycolytic metabolism involving aldehyde dehydrogenase 1a3. *Proc Natl Acad Sci U S A*, 110(21):8644–9, 2013.

[234] E. Vlashi, C. Lagadec, L. Vergnes, T. Matsutani, K. Masui, M. Poulou, R. Popescu, L. Della Donna, P. Evers, C. Dekmezian, K. Reue, H. Christofk, P. S. Mischel, and F. Pajonk. Metabolic state of glioma stem cells and nontumorigenic cells. *Proc Natl Acad Sci U S A*, 108(38):16062–7, 2011.

[235] C. Choi, S. K. Ganji, R. J. DeBerardinis, I. E. Dimitrov, J. M. Pascual, R. Bachoo, B. E. Mickey, C. R. Malloy, and E. A. Maher. Measurement of glycine in the human brain in vivo by 1h-mrs at 3 t: application in brain tumors. *Magn Reson Med*, 66(3):609–18, 2011.

[236] B. Forstera, O. D. a Dzaye, A. Winkelmann, M. Semtner, B. Benedetti, D. S. Markovic, M. Synowitz, P. Wend, M. Fahling, M. P. Junier, R. Glass, H. Kettenmann, and J. C. Meier. Intracellular glycine receptor function facilitates glioma formation in vivo. *J Cell Sci*, 127(Pt 17):3687–98, 2014.

[237] J. Perez-Escuredo, R. K. Dadhich, S. Dhup, A. Cacace, V. F. Van Hee, C. J. De Saedeleer, M. Sboarina, F. Rodriguez, M. J. Fontenille, L. Brisson, P. E. Porporato, and P. Sonveaux. Lactate promotes glutamine uptake and metabolism in oxidative cancer cells. *Cell Cycle*, 15(1):72–83, 2016.

[238] J. Liao, P. P. Liu, G. Hou, J. Shao, J. Yang, K. Liu, W. Lu, S. Wen, Y. Hu, and P. Huang. Regulation of stem-like cancer cells by glutamine through beta-catenin pathway mediated by redox signaling. *Mol Cancer*, 16(1):51, 2017.

[239] N. Koglin, A. Mueller, M. Berndt, H. Schmitt-Willich, L. Toschi, A. W. Stephens, V. Gekeler, M. Friebe, and L. M. Dinkelborg. Specific pet imaging of xc- transporter activity using a (1)(8)f-labeled glutamate derivative reveals a dominant pathway in tumor metabolism. *Clin Cancer Res*, 17(18):6000–11, 2011.

[240] M. I. Gross, S. D. Demo, J. B. Dennison, L. Chen, T. Chernov-Rogan, B. Goyal, J. R. Janes, G. J. Laidig, E. R. Lewis, J. Li, A. L. Mackinnon, F. Parlati, M. L. Rodriguez, P. J. Shwonek, E. B. Sjogren, T. F. Stanton, T. Wang, J. Yang, F. Zhao, and M. K. Bennett. Antitumor activity of the glutaminase inhibitor cb-839 in triple-negative breast cancer. *Mol Cancer Ther*, 13(4):890–901, 2014.

[241] M. Martin-Rufian, R. Nascimento-Gomes, A. Higuero, A. R. Crisma, J. A. Campos-Sandoval, M. C. Gomez-Garcia, C. Cardona, T. Cheng, C. Lobo, J. A. Segura, F. J. Alonso, M. Szeliga, J. Albrecht, R. Curi, J. Marquez, A. Colquhoun, R. J. Deberardinis, and J. M. Mates. Both gls silencing and gls2 overexpression synergize with oxidative stress against proliferation of glioma cells. *J Mol Med (Berl)*, 92(3):277–90, 2014.

[242] V. I. Sayin, S. E. LeBoeuf, S. X. Singh, S. M. Davidson, D. Biancur, B. S. Guzelhan, S. W. Alvarez, W. L. Wu, T. R. Karakousi, A. M. Zavitsanou, J. Ubriaco, A. Muir, D. Karagiannis, P. J. Morris, C. J. Thomas, R. Possemato, M. G. Vander Heiden, and T. Papagiannakopoulos. Activation of the nrf2 antioxidant program generates an imbalance in central carbon metabolism in cancer. *Elife*, 6, 2017.

[243] U. D. Kahlert, M. Cheng, K. Koch, L. Marchionni, X. Fan, E. H. Raabe, J. Maciaczyk, K. Glunde, and C. G. Eberhart. Alterations in cellular metabolome after pharmacological inhibition of notch in glioblastoma cells. *Int J Cancer*, 138(5):1246–55, 2016.

[244] D. M. Miller, S. D. Thomas, A. Islam, D. Muench, and K. Sedoris. c-myc and cancer metabolism. *Clin Cancer Res*, 18(20):5546–53, 2012.

[245] C. V. Dang. Myc, metabolism, cell growth, and tumorigenesis. *Cold Spring Harb Perspect Med*, 3(8), 2013.

[246] A. Deshmukh, K. Deshpande, F. Arfuso, P. Newsholme, and A. Dharmarajan. Cancer stem cell metabolism: a potential target for cancer therapy. *Mol Cancer*, 15(1):69, 2016.

[247] S. Zhang, W. Wang, G. Liu, S. Xie, Q. Li, Y. Li, and Z. Lin. Long non-coding rna hottip promotes hypoxia-induced epithelial-mesenchymal transition of malignant glioma by regulating the mir-101/zeb1 axis. *Biomed Pharmacother*, 95:711–720, 2017.

[248] W. Zhang, X. Shi, Y. Peng, M. Wu, P. Zhang, R. Xie, Y. Wu, Q. Yan, S. Liu, and J. Wang. Hif-1alpha promotes epithelial-mesenchymal transition and metastasis through direct regulation of zeb1 in colorectal cancer. *PLoS One*, 10(6):e0129603, 2015.

[249] M. Yuneva, N. Zamboni, P. Oefner, R. Sachidanandam, and Y. Lazebnik. Deficiency in glutamine but not glucose induces myc-dependent apoptosis in human cells. *J Cell Biol*, 178(1):93–105, 2007.

# 5 Appendix

## 5.1 Declaration of Author's Contribution

### The effect of neurosphere culture conditions on the cellular metabolism of glioma cells

Ulf D. Kahlert[1,2], Katharina Koch[2], Abigail K. Suwala[2], Rudolf Hartmann[3], Menglin Cheng[4], Donata Maciaczyk[2], Dieter Willbold[3,5], Charles G. Eberhart[1], Kristine Glunde[4], and Jaroslaw Maciaczyk[2,*]

[1]Department of Pathology, Division of Neuropathology, Johns Hopkins Hospital, Baltimore, USA

[2] Department of Neurosurgery, University Medical Center Düsseldorf, Germany

[3] Institute of Complex Systems ICS-6, Research Center Jülich, Germany

[4] Division of Cancer Imaging Research, Russell H. Morgan Department of Radiology and Radiological Science, Johns Hopkins Hospital, Baltimore, USA

[5] Institute of Physical Biology, Heinrich-Heine-University Düsseldorf, Germany

[*] corresponding author, Jaroslaw.Maciaczyk@med.uni-duesseldorf.de

Published in: **Folia Neuropathologica**, Vol. 53, Issue 3, pp. 219-225, 2015 [146]
DOI: 10.5114/fn.2015.54422
Journal Impact Factor (2015): 1.233

**Contribution:** 30 %. Katharina Koch designed the experiments, performed the culture, and performed the $^{1}$H-NMR metabolic analysis of U87 adherent cells and evaluated the data. She further commented on the manuscript.

### Reciprocal regulation of the cholinic phenotype and epithelial-mesenchymal transition in glioblastoma cells

Katharina Koch[1], Rudolf Hartmann[2], Friederike Schröter[3], Abigail K. Suwala[1], Donata Maciaczyk[1], Andrea C. Krüger1[1], Dieter Willbold[2,3], Ulf D. Kahlert[1], and Jaroslaw Maciaczyk[1,*]

[1] Department of Neurosurgery, University Hospital Düsseldorf, Düsseldorf, Germany

[2] Institute of Complex Systems ICS-6, Research Center Jülich, Jülich, Germany

[3] Institute for Stem Cell Research and Regenerative Medicine, Medical Faculty, Heinrich-Heine-University Düsseldorf, Düsseldorf, Germany

[4] Institute fuer Physikalische Biology, Heinrich-Heine-University Düsseldorf, Düsseldorf, Germany

* corresponding author, Jaroslaw.Maciaczyk@med.uni-duesseldorf.de

Published in: **Oncotarget**, Vol. 7, Issue 45, pp. 73414-73431, 2016 [172]
DOI: 10.18632/oncotarget.12337
Journal Impact Factor (2016): 5.17

**Contribution:** 75 %. Jaroslaw Maciaczyk, Ulf Kahlert and Katharina Koch designed the experiments. Katharina Koch performed the experiments and evaluated the data. The LSM microscopy was performed by Friederike Schröter and Katharina Koch. Aquisition of $^{1}$H-NMR spectra was performed by Rudolf Hartmann and Katharina Koch. Abigail Kora Suwala, Andrea Caroline Krüger, and Donata Maciaczyk assisted in data aquisition. KK, JM and UDK wrote the manuscript. All authors commented on the manuscript.

## Glutaminase inhibition targets c-Myc positive, starvation-resistant glioblastoma stem-like cells

Katharina Koch[1], Rudolf Hartmann[2], Abigail K. Suwala[1], Dayana Herrera Rios[1,3], Hans-Jakob Steiger[1], Dieter Willbold[2,4], Ulf D. Kahlert[1,5], and Jaroslaw Maciaczyk[1,*]

[1] Department of Neurosurgery, University Hospital Düsseldorf, Düsseldorf, Germany
[2] Institute of Complex Systems ICS-6, Research Center Jülich, Jülich, Germany
[3] current address: Skin Cancer Unit of the Dermatology Department, West German Cancer Center, University Duisburg-Essen, Essen, Germany
[4] Institute fuer Physikalische Biology, Heinrich-Heine-University Düsseldorf, Düsseldorf, Germany
[5] German Cancer Consortium (DKTK), Germany
* corresponding author, Jaroslaw.Maciaczyk@med.uni-duesseldorf.de

Submitted to: **Cancer Letters**, 05.12.2017.
Journal Impact Factor (2016): 6.37

**Contribution:** 75 %. Jaroslaw Maciaczyk, Ulf Kahlert and Katharina Koch designed the experiments. Katharina Koch performed the experiments and evaluated the data. Aquisition of $^{1}$H-NMR spectra was performed by Rudolf Hartmann and Katharina Koch. Abigail Kora Suwala and Dayana Herrera Rios assisted in data aquisition. KK, JM and UDK wrote the manuscript. All authors commented on the manuscript.

## 5.2 Danksagung

Als erstes möchte ich Jarek Maciaczyk danken, der mir ermöglicht hat meine Doktorarbeit in seiner Arbeitsgruppe zu schreiben. Er konnte mich für die Neuroonkologie begeistern und war in den letzten dreieinhalb Jahren immer für mich da wenn ich Rat brauchte.

Hans-Jakob Steiger möchte ich danken, dass ich die Doktorarbeit in seinem Institut anfertigen durfte.

Des Weiteren gilt mein Dank Ulf Kahlert, der mich durchweg unterstützt hat und mir sehr mit der Projektplanung, der Anfertigung der Manuskripte und organisatorischen Angelegenheiten geholfen hat.

Mein Dank geht auch an Dieter Willbold und Rudolf Hartmann. Dank unserer Kooperation konnte ich erste Erfahrungen mit der $^{1}$H-NMR Spektroskopie machen. Eine Methode welche ich sehr zu schätzen gelernt habe und die mich hoffentlich noch lange Zeit begleiten wird. Dieter Willbold möchte ich weiterhin auch für die Übernahme der Zweitkorrektur danken. Rudolf Hartmann danke ich für die tollen Gespräche und den leckeren Kaffee in den Wartezeiten neben dem 700er.

Abigail Suwala und Donata Maciaczyk möchte ich besonders für die wundervolle Zusammenarbeit über die gesammten dreieinhalb Jahre danken. Ohne euch wäre die Zeit im Labor beiweitem nicht so schön gewesen!

Des Weiteren, möchte ich auch Brigitte Senger, Andrea-Caroline Krüger, Dayana Herrera Rios, Julia Tsiampali, Constanze Uhlmann, Philippe Aretz, Darius Schenk und Andres Vargas Toscano für eine tolle Zeit im Labor, viel gemeinsames Lachen und tolle Gespräche danken.

Ich möchte auch Guido Reifenberger und dem ganzen Institut für Neuropathologie für die vielen Ratschläge und eine tolle Arbeitsatmosphäre auf der Etage danken.

Besonderer Dank geht an meine Eltern und Großeltern die immer für mich da waren, die mich in der Wahl meines Studiums immer unterstützt haben und mir immer geholfen haben meine Ziele zu erreichen. Danke dass man sich immer auf euch verlassen kann.

Ich danke meinen Schulfreunden aus Leverkusen, den Bonner Mädels und Michael Wördehoff und Hannah Rosenbach. Auch in der stressigsten Zeit konntet ihr mich immer zum Lachen bringen. Mein besonderer Dank gilt hier meiner besten Freundin Marina Arcidiacono.

Da das Beste bekanntlich zum Schluss kommt möchte ich zuletzt meinem Freund Julian Victor danken. Danke dass du seit sieben Jahren für mich da bist, immer ein offenes Ohr für mich hast und auch an den stressigsten Tagen nicht an mir verzweifelst ;) .

## 5.3 Abbreviations

| | |
|---|---|
| $^1$H | proton |
| 1p/19p | combined loss of chromosome arms 1p and 19q |
| 2-HG | 2-hydroxyglutarate |
| Ac | acetate |
| Ade | adenine |
| ADP | adenosine diphosphate |
| $\alpha$-KG | alpha-ketoglutarate |
| AKS | Abigail Kora Suwala |
| Akt | RAC-alpha serine/threonine-protein kinase |
| Ala | alanine |
| AMP | adenosine monophosphate |
| AOA | aminooxyacetic acid |
| ATP | adenosine triphosphate |
| Avastin | Bevacizumab |
| BBB | blood brain barrier |
| BCL-2 | B-cell lymphoma 2 |
| BCL-xL | B-cell lymphoma-extra large |
| BCRP1 | breast cancer resistance protein |
| bFGF | basic fibroblast growth factor |
| BTSC | brain tumor stem cell |
| C968 | compound 968 |
| CD133 | prominin-1 |
| CD44 | CD44 molecule |
| CDKN2A | cyclin dependent kinase inhibitor 2A |
| cDNA | complementary desoxyribonucleic acid |
| CDP | cytidine diphosphate |
| CHK$\alpha$ | choline kinase alpha |
| CHK$\beta$ | choline kinase beta |
| CI | combination index |
| CKB | creatine kinase beta |
| CMP | cytidine monophosphate |
| c-Myc | MYC proto-oncogene |
| CNS | central nervous system |
| CpG | cytosine-phosphate-guanine |
| CT | computed tomography |
| CTP | cytidine triphosphate |

| | |
|---|---|
| cXT | cystine/glutamate transporter |
| $D_2O$ | deuterium oxide |
| DAG | diacylglycerol |
| DNA | deoxyribonucleic acid |
| DAPI | 4',6-diamidino-2-phenylindole |
| $ddH_2O$ | double-distilled water |
| DMEM | Dulbecco's Modified Eagle's Medium |
| DMSO | Dimethyl sulfoxide |
| DSS | 4,4-dimethyl-4-silapentane-1-sulfonic acid |
| EGCG | epigallocatechin gallate |
| EGFR | epidermal Growth Factor Receptor |
| EMT | epithelial-mesenchymal transition |
| F12 | Ham's F-12 Nutrient Mixture |
| FACS | fluorescence-activated cell sorting |
| fCho | free choline |
| FCS | fetal calf serum |
| Fig. | figure |
| FLIP | cellular FLICE-like inhibitory protein |
| g | gram |
| G1 phase | gap 1 phase |
| GABRA1 | gamma-aminobutyric acid type A receptor $\alpha$1 subunit |
| GBM | glioblastoma |
| GCL | glutamate-cysteine ligase |
| GDH | glutamatdehydrogenase |
| GFAP | glial fibrillary acidic protein |
| GLS | glutaminase |
| Gly | glycin |
| GMP | guanosine monophosphate |
| GOT1 | glutamic-oxaloacetic transaminase 1 |
| GPC | glycerophosphocholine |
| GPNA | L-$\gamma$-glutamyl-p-nitroanilide |
| GPT2 | glutamic-pyruvic transaminase 2 |
| GS | glutamine synthetase |
| GSC | glioblastoma stem-like cell |
| GSH | glutathione |
| GSI | gamma-secretase inhibitor |
| GTS | glutathione synthetase |

| | |
|---|---|
| h | hour |
| H&E | hematoxylin and eosin |
| H3F3A | H3 histone family member 3A |
| HEK293T | human embryonic kidney cells 293T |
| HHU | Heinrich-Heine University |
| HIF | hypoxia-inducible factor |
| HR | high resolution |
| HRas | HRas proto-oncogene |
| HRE | hypoxia response element |
| Hz | hertz |
| ICS-6 | Institute of Complex Systems 6 |
| IDH | isocitrate dehydrogenase |
| IMP | inosine monophosphate |
| JM | Jaroslaw Maciaczyk |
| K | Kelvin |
| KK | Katharina Koch |
| KRas | KRas proto-oncogene |
| l | litre |
| Lac | lactate |
| LDH | lactate dehydrogenase |
| L-DON | 6-diazo-5-oxo-L-norleucine |
| LSM | laser scanning microscope |
| M | molar |
| m | milli |
| MCT1 | monocarboxylate transporter 1 |
| MGMT | O6-methylguanine DNA methyltransferase |
| min | minutes |
| MRI | magnetic resonance imaging |
| mRNA | messenger ribunucleic acid |
| Musashi-1 | Musashi RNA Binding Protein 1 |
| myo | myo-inositol |
| n | nano |
| NAAG | N-acetylaspartylglutamic acid |
| NaCl | sodium cloride |
| NAD | nicotinamide adenine dinucleotide |
| NADPH | nicotinamide adenine dinucleotide phosphate |
| NBT | nitro blue tetrazolium chloride |

| | |
|---|---|
| NEAA | non-essential amino acid |
| NEFL | neurofilament light polypeptide |
| NF-1 | neurofibromin 1 |
| NMR | nuclear magnetic resonance |
| Oct4 | octamer-binding transcription factor 4 |
| OXPHOS | oxidative phosphorylation |
| PBS | phosphate buffered saline |
| PC | phosphocholine |
| PDGF | platelet-derived growth factor |
| PDGFRA | platelet-derived growth factor receptor A |
| PET | positron-emission tomography |
| PI3K | phosphatidylinositol-4,5-bisphosphate 3-kinase |
| p | pico |
| PSAT1 | phosphoserine aminotransferase 1 |
| PtdCho | phosphatidylcholine |
| PtdEtn | phosphatidylethanolamine |
| qPCR | quantitative polymerase chain reaction |
| RIPA | radioimmunoprecipitation assay buffer |
| ROS | reactive oxygen species |
| RT | room temperature |
| RTK | receptor tyrosine kinase |
| S phase | synthesis phase |
| SFF | Studierendenförderungsfonds |
| shRNA | short hairpin ribonucleic acid |
| SLC12A5 | electroneutral potassium-chloride co-transporter 2 |
| SLC1A5 | neutral amino acid transporter B(0) |
| SLC7A11 | anionic amino acid transporter light chain, Xc- system |
| SNAI | snail family transcriptional repressor 1 |
| SOX2 | SRY-Box 2 |
| STD | standard |
| SYT1 | synaptotagmin 1 |
| T | tesla |
| TBST | Tris-buffered saline plus Tween-20 |
| TCA | tricarboxylic acid cycle |
| tCho | total choline |
| tCre | total creatine |
| Thr | threonine |

| | |
|---|---|
| TMZ | temozolomide |
| TP53 | tumor protein P53 |
| TSP | trimethylsilylpropanoic acid |
| TWIST | twist family BHLH transcription factor 1 |
| UDK | Ulf Dietrich Kahlert |
| UTP | uridine triphosphate |
| Val | valine |
| VEGF | vascular endothelial growth factor |
| VP16 | Etoposid |
| WHO | world health organization |
| xCT | cystine/glutamate transporter subunit xCT |
| ZEB | zinc finger E-box-binding homeobox |